Dinàmica no lineal de sistemes làsers: potencials de Lyapunov i diagrames de bifurcacions

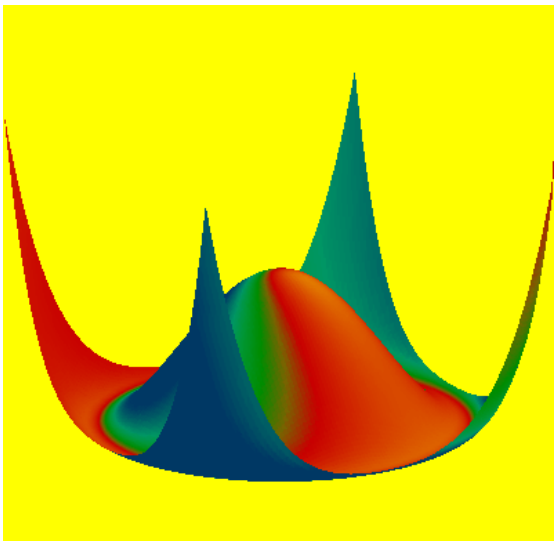

Departament de Física

Universitat de les Illes Balears

Març de 2002

Memòria presentada per Catalina Mayol Serra
per optar al Grau de Doctora en Ciències Físiques
per la Universitat de les Illes Balears.

Raúl Toral Garcés, Catedràtic de la Universitat de les Illes Balears, i Claudio R. Mirasso, Professor Titular de la mateixa Universitat,

CERTIFIQUEN

que la present memòria ha estat realitzada per Catalina Mayol Serra sota la seva direcció en aquest departament i que constitueix la seva Tesi per optar al títol de Doctora en Ciències Físiques.

I, per a què consti, firmen la present en Palma de Mallorca a 23 de gener de 2002.

Raúl Toral Garcés

Claudio R. Mirasso

Als meus pares
Isabel i Mateu,
i a la memòria de
sa meva padrina,
al cel sia.

Agraïments

Amb aquestes línees voldria agrair a totes les persones que m'han ajudat durant els temps que he tardat en l'elaboració dels resultats i redacció d'aquesta memòria.

En primer lloc, tot el suport rebut pels meus dos directors, els professors Raúl Toral i Claudio Mirasso, i tot el que he après durant el temps que he tingut la oportunitat de realitzar investigació amb ells.

Seguidament, al professor Mario Natiello, per la seva hospitalitat i dedicació científica durant les meves dues estades a la Universitat de Lund. De la mateixa manera als professors Luis Pesquera i Sergei I. Turovets, amb els que vaig poder compartir unes setmanes de recerca intensa a la Universidad de Cantabria.

També agrair a tots els professors del Departament de Física de la Universitat de les Illes Balears, la majoria dels quals foren professors meus durant els cursos corresponents a la Llicenciatura; i sobretot als components del Grup de Física No Lineal, amb els quals he compartit cursos de doctorat i molts seminaris.

A continuació, a totes les companyes i companys que he tingut a l'Agència EFE durant aquests anys. N'han passat molts, però amb tots hem disfrutat d'un bon ambient de treball i companyerisme. Així mateix, a totes les persones que he conegut en aquests anys quan he assistit a cursos o congressos, que han fet aquestes estades fora de l'illa molt agradables.

Finalment, als meus pares i germà, per fer–me sempre costat, escoltar–me i donar bons consells.

Contents

Capítol 1

Introducció i estructura de la memòria

En l'estudi de sistemes dinàmics és important calcular els punts fixos de la dinàmica determinista del sistema i determinar la seva estabilitat. Per obtenir aquests resultats es pot fer servir el potencial de Lyapunov, tant en el cas de sistemes mecànics com no mecànics. Aquesta funció dinàmica decreix al llarg de les trajectòries, i és possible calcular els punts fixos com els extrems de la funció de Lyapunov. En alguns casos, l'existència del potencial de Lyapunov permet entendre les trajectòries a l'estat transitori i a l'estacionari. La distribució de probabilitat estacionària en el cas de la dinàmica estocàstica pot, sota determinades condicions, estar també governada pel potencial de Lyapunov. Part del propòsit d'aquest treball és explicar la dinàmica d'alguns sistemes làsers utilitzant aquests potencials.

Físicament, un làser és un dispositiu en què el llum emès s'origina en el procés d'emissió estimulada. Els tres elements bàsics que es requereixen són: un mitjà amb guany, una cavitat òptica i un mecanisme de bombeig. Des del punt de vista dinàmic, els distints tipus de làsers es poden classificar segons el ritme de decaïment de les variables involucrades en les equacions d'evolució: el camp elèctric dins la cavitat, la inversió de població i la polarització material. En els làsers de classe B, la polarització decau cap a l'estat estacionari molt més ràpidament que les altres variables i es pot eliminar adiabàticament. Per als làsers de classe A, una única equació per al camp elèctric és suficient per descriure la dinàmica.

Aquest treball tracta els làsers de classe A i classe B, estudiant la seva dinàmica, en els casos determinista i en presència de renou, fent ús del potencial de Lyapunov.

El control d'un làser a partir de l'aplicació d'un senyal injectat coherent és una àrea important de recerca amb una gran varietat d'aplicacions. Quan als làsers se'ls aplica un senyal injectat, la dinàmica resultant esdevé molt complexa. El comportament del sistema pot ser qualitativament diferent depenent de l'elecció dels paràmetres: estats amb la mateixa freqüència que la d'entrada, polsos, rutes cap al caos, etc. De l'estudi del conjunt invariant d'aquest sistema no lineal, es veu que la bifurcació Hopf–sella–node (HSN) (el camp vectorial linealitzat té un punt fix

degenerat amb dos autovalors imaginaris i un zero) actua com a centre organitzatiu.

La modulació a alta velocitat dels diodes làsers és una àrea en estudi a causa de les seves possibles aplicacions. Els làsers en aquestes circumstàncies poden presentar diversos comportaments no lineals: distorsió harmònica, període doble, biestabilitat, i caos. L'objectiu de part d'aquest treball és el d'obtenir els dominis d'existència de les inestabilitats bàsiques involucrades. Ens restringim a l'estudi de les resonàncies principals: màxima resposta del sistema a una pertorbació externa quan la freqüència de modulació es varia (s'entén com a resposta la intensitat màxima de la potència òptica de sortida).

Aquesta memòria es basa en els següents articles:

[1] C. Mayol, R. Toral i C.R. Mirasso, "Lyapunov–potential description for laser dynamics", Physical Review A **59**, 4690 (1999).

[2] C. Mayol, M.A. Natiello i M. Zimmermann,"Resonance structure in a weakly detuned laser with injected signal". International Journal of Bifurcation and Chaos **11**, 2587 (2001).

[3] C. Mayol, S.I. Turovets, R. Toral, C.R. Mirasso i L. Pesquera, "Main Resonances in Directly Modulated Semiconductor Lasers: Effect of Spontaneous Emission and Gain Saturation". IEE Proc.–Optoelectronics **148**, 41 (2001).

[4] C. Mayol, R. Toral, C.R. Mirasso, S.I. Turovets i L. Pesquera, "Theory of Main Resonances in Directly Modulated Diode Lasers". Acceptat a IEEE Journal of Quantum Electronics, a publicar–se el març de 2002.

[5] C. Mayol, R. Toral, C.R. Mirasso i M.A. Natiello, "Class A lasers with injected signal: bifurcation set and Lyapunov potential function". Enviat a Physical Review E (2002).

A la part I de la memòria es resum els elements bàsics que s'utilitzen a la resta del treball. En el capítol 2, es presenta la relació entre els potencials de Lyapunov i les equacions dinàmiques; en el capítol 3, es fa un resum d'anàlisi de bifurcacions; i en el capítol 4, apareixen les característiques del làser com a sistema dinàmic.

La part II es destina a l'estudi dels làsers de classe A. En el capítol 5, basat en [1], es descriu la dinàmica d'aquests làsers mitjançant el potencial de Lyapunov. En el capítol 6, basat en [5], els làsers de classe A amb senyal injectat s'estudien, obtenint el conjunt de bifurcacions a l'estacionari i estudiant la dinàmica amb el potencial de Lyapunov quan és possible.

La part III tracta de la dinàmica dels làsers de classe B. En el capítol 7, basat en [1], la dinàmica de les equacions de balanç per a aquests làsers s'analitza en termes del potencial, incloent els termes de saturació de guany i d'emissió espontània. El capítol 8, basat en [2], tracta dels làsers de classe B amb senyal injectat. El treball que es presenta completa la sèrie d'estudis anteriors de bifurcacions de làsers amb senyal injectat a prop de la singularitat Hopf–sella–node; s'analitza el rang de paràmetres on el tipus *II* Hopf–sella–node s'espera. En el capítol 9, basat en [3] i [4], s'estudia les resonàncies principals, i l'impacte que els termes de saturació de guany i emissió espontània tenen en ells, en els làsers directament modulats.

Chapter 1

Introduction

In the study of a dynamical system, it is important to obtain its invariant sets, being the fixed points the simplest ones. In some systems, either mechanical or non–mechanical, it is possible to construct a dynamical function (called Lyapunov potential) that decreases along trajectories. The usefulness of Lyapunov functions lies on that they allow an easy calculation of the fixed points of a dynamical (deterministic) system as the extrema of the Lyapunov function as well as determining the stability of these fixed points. In some cases, the existence of a Lyapunov potential gives an intuitive understanding of the transient and stationary trajectories as movements of test particles in the potential landscape. In the case of nondeterministic dynamics, i.e. in the presence of noise terms, and under some general conditions, the stationary probability distribution can also be governed by the Lyapunov potential and averages can be performed with respect to a known probability density function. Part of the aim of this work is to explain the dynamics of some laser systems by using Lyapunov potentials.

1.1 Lasers: Classification

Physically, a laser is a device in which the emitted light is originated in a process of stimulated emission. For obtaining laser action three basic ingredients are necessary: a gain medium (that amplifies the electromagnetic radiation inside the cavity), an optical cavity (that provides the necessary feedback) and a pumping mechanism. Lasers are classified depending on the material which constitutes the gain medium. For example, semiconductor lasers are those for which the gain medium is a semiconductor material. A complete understanding of a laser is based on a fully quantum–mechanical description [Haug, 1969; Sargent *et al.*, 1974]. However, a simpler description can be given in terms of evolution equations for the electric field inside the cavity, the population inversion and the material polarization. Different types of lasers can be classified according to the decay rate of the variables involved in the equations. In class C lasers, the material polarization, the population inversion and the electric field decay within comparable time scales. For

class B lasers, the material polarization decays towards the steady state much faster than the other variables and it can be adiabatically eliminated. Finally, in class A lasers, the population inversion and the material polarization decay much faster than the electric field and only one complex equation is required to describe the dynamics.

In this work we will deal with class A and class B lasers. Both lasers decay to their steady states when their thresholds are crossed. However, this simple dynamics becomes richer when an injected signal is applied or some of the parameters are modulated. During this thesis these effects will be discussed with some detail.

1.2 Laser with injected signal

The control of a laser via an injected coherent signal is an active area of research with a great variety of applications. Experiments and numerical analysis with this special arrangement have been performed leading to different kinds of behaviours (locked lasers, pulses, etc.) [Braza and Erneux, 1990; Gavrielides *et al.*, 1997; Simpson *et al.*, 1997; Nizette and Erneux, 1999]. The behaviour of the system can be qualitatively different depending on the choice of parameters and numerical simulations in three–dimensional models of lasers with injected signal, revealed multistability [Wieczorek *et al.*, 2000b] and different "routes to chaos" for different parameter regions [Tredicce *et al.*, 1985a; Solari and Oppo, 1994; Krauskpof *et al.*, 2000; Wieczorek *et al.*, 2000a; Wieczorek *et al.*, 2000c].

A good theoretical understanding of the underlying mechanisms governing the great variety of possible behaviours was required. An early attempt in this direction, [Solari and Oppo, 1994] aimed to approximate the three–dimensional rate equations for a class B laser in the vicinity of the parameter region, where this system becomes a Hamiltonian system, by a more tractable two–dimensional averaged system [Guckenheimer and Holmes, 1983]. A detailed study of the invariant sets revealed that at the heart of this nonlinear system, the Hopf–saddle–node bifurcation played the role of an organizing center. This local bifurcation arises when the linearization of the vector field has a degenerate fixed point with two purely imaginary and a simple zero eigenvalue. The unfolding of this bifurcation requires two parameters (the amplitude injection rate β and the detuning η of the injected signal to the unperturbed laser operating frequency), and four different variants known as type (*I–IV*) have been studied [Guckenheimer and Holmes, 1983; Wiggins, 1991]. All of these types display curves of saddle–node and Hopf bifurcations of fixed points in parameter space, which are tangent at one point. For increasing cavity detuning $\theta > 0$, Solari and Oppo [Solari and Oppo, 1994] found that type *II*, *I* and *III* may be visited (in that order).

The interest in a physical (and testable) application displaying the above qualitative changes close to the Hopf–saddle–node bifurcation, is not restricted to the determination of the well known invariant sets which result from normal form analysis (saddle–node, primary and secondary Hopf bifurcations). Global behaviour not present in the usual unfolding of Hopf–saddle–node singularity has recently been

studied as a primary source for chaotic behaviour in lasers with injected signal. For example, in the large cavity detuning regime (corresponding to type *III* of Hopf–saddle–node) Zimmermann *et al.* [Zimmermann *et al.*, 1997] showed the occurrence of Sil'nikov homoclinic orbits [Šil'nikov, 1965] to any of the saddle–focus fixed points (locked solutions). Furthermore, as the detuning is decreased the transition from type *III* to type *I* showed that the homoclinic orbits to a fixed point, at the critical θ where the Hopf–saddle–node type changes turns to a homoclinic tangency to the periodic orbit of Hopf–saddle–node [Zimmermann *et al.*, 2001]. This novel behaviour opens the possibility that this physical system may become an ideal test–bench for new global bifurcation scenarios.

In the previous studies on the global bifurcations in laser with injected signal, a combination of the Hopf–saddle–node singularity together with a global reinjection resulted in a proper framework for understanding the laser dynamics. However, in type *II*, which is the interesting case for our work, we find a new possible complication which involves a heteroclinic cycle with the off state.

1.3 Directly modulated lasers

High–speed modulation of laser diodes is an important area of study due to the possible applications of these devices. Diode lasers clearly exhibit in such circumstances various kinds of nonlinear behaviour, i.e., harmonic distortion, multi–pulse response on the time scale of one modulation period, period doubling, amplitude and/or pulse position bistability, and chaos [Kawaguchi, 1994]. Usually, these complicated dynamical phenomena are considered as harmful to the practical application and should be avoided. Nevertheless, there have been some experimental demonstrations of feasibility of using a resonance period doubling regime and pulse position bistability for realizing high speed optical logic elements [Gallagher *et al.*, 1985]. Also, large capacity information transmission and ultrafast optical processing systems [Liu and Ngai, 1993; Mirasso *et al.*, 1993; Breuer and Petermann, 1997] are representative of the possible applications of these systems. Recently, a great deal of interest has been generated by the potential of using lasers running in a chaotic regime as the carriers of information in secure chaotic communication schemes [Mirasso *et al.*, 1996; Goedgebuer *et al.*, 1998; Fisher *et al.*, 2000]. In addition to the optical feedback and saturable absorption effects, chaos in laser diodes induced by modulation in the pump current is another option for building transmitters and receivers for encoded optical communications.

Before Liu and Ngai [Liu and Ngai, 1993] succeeded in observing chaos in a 1.55 μm InGaAsP distributed feedback bulk laser, followed by the report on a similar observation in 1.55 μm multiple quantum well lasers [Matsui *et al.*, 1998], there had been some controversy in earlier theoretical predictions [Tang *et al.*, 1963] and experimental results [Hemery *et al.*, 1990; Kao and Lin, 1993]. Specifically, chaotic and high periodic regimes had not been experimentally observed in contrast to numerical predictions based on the rate equations. It is well known [Agrawal, 1986] that the

gain saturation factor contributes to the damping of relaxation oscillations and it might be the reason for eliminating chaos. The presence of spontaneous emission in the cavity and the Auger recombination factor have also been numerically examined as being one cause of the suppression of chaos [Tang and Wang, 1987]. The importance of noise terms is again under consideration [Lim *et al.*, 2000]. Finally, the gain sharing among multi–longitudinal oscillating modes was identified as an effective gain compression factor and therefore leading to suppression of chaos [Wada *et al.*, 1998]. Now, it is largely accepted that a single mode laser diode with relatively small gain saturation and spontaneous emission parameters might undergo a period doubling route to chaos under current modulation. From the analytical side, such an impact of these parameters was explained in the framework of the small signal analysis showing an increase of the system damping with the increase of the above mentioned parameters [Yoon *et al.*, 1989]. In addition, Hori *et al.* [Hori *et al.*, 1988] suggested that in the large signal modulation regime, the spontaneous emission term, besides contributing to a linear damping of the system, leads to an additional nonlinear damping. This effect would change the representation of the typical Toda oscillator potential topology for the laser and would be also responsible for suppression of chaos. Nevertheless, specific mechanisms of these effects in the large signal regime are not yet fully understood. To the best of our knowledge, a detailed study of the role of spontaneous emission and gain saturation on nonlinear dynamics in the large signal regime is still lacking even in the framework of the simple rate equation model.

Part of this work aims to clarify the parameter domains of the basic instabilities involved. We will restrict ourselves to the study of main resonances to which little attention has been paid in previous works. Defining the response variable as maximum intensity in the optical–power output, a main resonance is understood as the maximum response of the system to the external perturbation when the modulation frequency of the external perturbation is varied. Although main resonances were considered theoretically and numerically [Erneux *et al.*, 1987; Samson and Turovets, 1987; Schwartz, 1988; Samson *et al.*, 1990; Schwartz and Erneux, 1994] and also experimentally [Samson *et al.*, 1992; Chizhevsky and Turovets, 1993; Bennett *et al.*, 1997; Chizhevsky, 2000], for conventional class B lasers the impact of large gain saturation and spontaneous emission terms, which are typical for laser diodes, is not fully understood yet. By using the asymptotic quasi–conservative theory [Katz, 1955; Drozdov, 1955; Erneux *et al.*, 1987; Samson and Turovets, 1987] with an appropriate Lyapunov potential describing the laser dynamics, we compute the domains of existence for the resonance nT periodic responses in arbitrarily large amplitude modulated laser diodes. For this particular kind of nonlinearity, these resonant curves are associated to the so–called primary saddle–node bifurcations and are often confused in experiments with the multiperiodic windows in chaos. When considering gain saturation and spontaneous emission terms on the dynamics we find that, besides increasing the damping of relaxation oscillations, these parameters change the topology of the Lyapunov potential, increasing the thresholds of instabilities in the system. The theory is substantiated by numerical results. The

estimations for primary saddle–node bifurcations in strongly modulated laser diodes create the basis for a systematic search for a priori wanted regimes in simulations or experiment and also naturally explain pulse position multistability [Gallagher *et al.*, 1985; Chizhevsky and Turovets, 1993].

Another way of obtaining nonlinear effects in lasers is by modulating their losses. Cavity loss can be modulated in practise by using a variable reflector or in a two–section laser when modulating periodically the passive section.

1.4 Structure of the work

This manuscript is based on the following papers:

[1] C. Mayol, R. Toral and C.R. Mirasso, "Lyapunov–potential description for laser dynamics", Physical Review A **59** (6), 4690–4698 (1999).

[2] C. Mayol, M.A. Natiello, and M.G. Zimmermann, "Resonance structure in a weakly detuned laser with injected signal". International Journal of Bifurcation and Chaos **11** (10), 2587–2605 (2001).

[3] C. Mayol, S.I. Turovets, R. Toral, C.R. Mirasso, and L. Pesquera, "Main Resonances in Directly Modulated Semiconductor Lasers: Effect of Spontaneous Emission and Gain Saturation". IEE Proc.–Optoelectronics **148** (1), 41–45 (2001).

[4] C. Mayol, R. Toral, C.R. Mirasso, S.I. Turovets, and L. Pesquera, "Theory of Main Resonances in Directly Modulated Diode Lasers". Accepted in IEEE Journal of Quantum Electronics, to appear in March 2002.

[5] C. Mayol, R. Toral, C.R. Mirasso, and M.A. Natiello, "Class *A* lasers with injected signal: bifurcation set and Lyapunov potential function". Submitted to Physical Review E (2002).

and it is structured as follows.

In part I some basic concepts are given:

- In chapter 2, a brief review of the relation between Lyapunov potentials and the dynamical equations and the splitting of the latter into conservative and dissipative parts is given. We also present some results on Fokker–Plank equations and numerical integration of stochastic equations, which are used in the following chapters.
- In chapter 3, a review of bifurcation analysis is done.
- In chapter 4, the main features of the laser as a dynamical system are reviewed.

Part II is devoted to the study of class A lasers:

- In chapter 5, based on [1], the Lyapunov potential gives an intuitive understanding of the dynamics observed in the numerical simulations for class A lasers. In the presence of noise, the probability density function obtained from the potential allows the calculation of stationary mean values of interest as, for example, the mean value of the number of photons. We will show that the mean value of the phase of the electric field in the steady state varies linearly with time only when noise is present, in a phenomenon reminiscent of noise–sustained flows.

- In chapter 6, based on [5], class A lasers with injected signal are studied. The dynamical behaviour in the steady state is more complex than the non–injected signal case due to the introduction of new degrees of freedom. The bifurcation set is obtained in terms of the amplitude and phase of the injected signal by using the tools introduced in chapter 3. Moreover, this complex dynamical system is studied in terms of a Lypunov potential function whenever it is possible. In particular, noise–sustained flows are also obtained and mean values calculated by using the Lyapunov potential in the case of a injected signal without detuning.
  The bifurcation set obtained reveals the complexity of the system and the importance of the parameter choice in experiments. Class A lasers with injected signal are the simplest example one can consider. A more complex situation arises considering class B lasers with injected signal (chapter 8). From the dynamical point of view the main difference between class A and class B lasers is the number of variables that one works with. For class A lasers, two variables suffice and the full bifurcation set can be described. For class B lasers, three variables, a more complex variety of phenomena can appear and the system can also show chaotic behaviour when injecting an external signal. Although part of the bifurcation structure of class B lasers is already present in class A lasers, the overall dynamics of the former becomes extremely complicated.

Part III deals with the dynamics of class B lasers:

- In chapter 7, based on [1], the dynamics of rate equations for class B lasers is presented in terms of the intensity and the carriers number (we will restrict ourselves to the semiconductor laser). In this case we obtain a potential which helps us to analyse the corresponding dynamics in the absence of noise fluctuations. By using the conservative part of the equations, we obtain an expression for the period of the oscillations in the transient regime following the laser switch–on. This expression extends a simpler one that identifies the laser dynamics with a Toda oscillator, by adding in the expression for the period the corresponding modifications due to gain saturation and spontaneous emission noise terms.

- Chapter 8, based on [2], deals with class B lasers with injected signal. The work presented here completes the above series of studies of bifurcations of the laser with injected signal in the neighbourhood of the Hopf–saddle–node singularity, see Sec. 1.2. We analyse a range of parameters where type *II* Hopf–saddle–node is expected by using the tools of chapter 3. The main bifurcation structure consists of a (secondary) Hopf bifurcation on the periodic orbit associated to the Hopf–saddle–node bifurcation. We have analysed in detail the resonance structure which reveals a rich interaction with other bifurcations *not* present in the usual Hopf–saddle–node scenario. We find that the Arnold tongues are truncated by another (secondary) Hopf bifurcations of periodic orbits. These in turn originate in an Andronov global bifurcation at the saddle–node of fixed points (saddle–node infinite period bifurcation) [Kuznetsov, 1997]. Another particular behaviour is that inside the Arnold tongues we also find homoclinic bifurcations to a saddle fixed point corresponding to the off state of the laser. Finally we show how the Arnold tongues of increasing winding number, together with all their associated bifurcations, *accumulate* towards the Hopf–saddle–node bifurcation point.

- In chapter 9, based on [3] and [4], we have undertaken analytical and numerical calculations in the framework of the single mode rate equation model with direct modulation with the aim of clarifying the parameter domains of the basic instabilities involved and relating them to the reported experiments using $1.55\mu m$ InGaAs distributed feedback lasers [Liu and Ngai, 1993]. We study main resonances and the impact that large gain saturation and spontaneous emission terms have on them. By using the asymptotic quasi–conservative theory with an appropriate Lyapunov potential describing the laser dynamics, the one presented in chapter 7, we have computed the domains of existence of resonances in arbitrarily large amplitude modulated laser diodes, and compared them to the numerical results.

In the final chapter, we summarize the main results obtained as well as some possible extensions and other problems.

Part I

Conceptes bàsics

Capítol 2

Resum de sistemes dinàmics

En aquest capítol, es resumeixen alguns resultats bàsics en sistemes dinàmics que seran utilitzats en capítols posteriors. En primer lloc, es revisa la forma de tractar equacions diferencials estocàstiques. Llavors, s'introdueix la definició de potencial de Lyapunov i les diferents maneres que aquest potencial es relaciona amb les equacions dinàmiques per a sistemes determinístics. Per acabar, les relacions entre processos estocàstics i potencials de Lyapunov es presenten en els casos on la funció densitat de probabilitat estacionària per a un procés estocàstic es pot obtenir a partir del potencial de Lyapunov.

Per descriure els sistemes dinàmics, s'utilitzen equacions diferencials que modelitzen el sistema. En el cas de sistemes determinístics, s'empren equacions diferencials ordinàries o equacions diferencials en derivades parcials. El tractament d'aquest tipus d'equacions està ben establert, i es pot fer analíticament o emprant mètodes numèrics.

Alguns sistemes tenen alguna de les seves parts modelada de forma aleatòria, ja que el coneixement d'aquestes parts no és prou detallat o és massa complex per poder ésser tractat de manera determinista. Aquestes parts aleatòries són les que contenen els *processos aleatoris*, o també coneguts com *termes de renou*. Les equacions diferencials que contenen els termes aleatoris són les *equacions diferencials estocàstiques*. Les equacions estocàstiques on els termes aleatoris apareixen linealment s'anomenen *equacions de Langevin*. Segons que la funció que multiplica el terme de renou en l'equació de Langevin sigui constant o no, tendrem, respectivament, renou additiu o multiplicatiu. Dels diferents termes de renou que poden ésser considerats, es restringeix l'estudi al *renou blanc*, que es caracteritza per ser un procés gaussià Markovià de mitja zero i delta–correlacionat (2.2). L'equació diferencial estocàstica de Langevin no està completament definida a menys que es digui quina interpretació s'agafa per realitzar integrals que involucren el procés aleatori, les interpretacions sovint més emprades són la de Itô i la de Stratonovich. La generació numèrica de les trajectòries que defineix l'equació diferencial estocàstica de Langevin ve donada per la generalització dels mètodes utilitzats amb equacions diferencials ordinàries, com el de Runge–Kutta o el de Euler. En aquest cas, les equacions recurrents que

s'obtenen al afegir els termes de renou donen lloc als mètodes de Milshtein i de Heun. Aquests mètodes són els que s'utilitzen per obtenir molts dels resultats que es presenten en les parts II i III de la memòria.

L'evolució d'un sistema dinàmic es pot classificar en diferents categories depenent de la relació del *potencial de Lyapunov* amb les equacions de moviment. El teorema d'estabilitat de Lyapunov diu que si es coneix una funció de les variables del sistema que sigui una funció decreixent en l'evolució temporal, els mínims de l'esmentada funció en termes de les variables són els punts fixos estables de la dinàmica del sistema. L'evolució del sistema és cap al mínims de la funció de Lyapunov, i a més, el sistema queda a prop d'aquests mínims quan hi actuen petites pertorbacions. El potencial de Lyapunov dóna informació de l'estabilitat global del sistema: dels possibles mínims, el més estable és aquell que té el valor del potencial més baix. Els sistemes per als quals existeix un potencial de Lyapunov s'anomenen *sistemes potencials*, mentre que els altres són *sistemes no potencials*. Dins els sistemes potencials es pot fer una subdivisió depenent de com es relacionen les derivades de la funció de Lyapunov amb les equacions del moviment. El tipus més general, i que serà del nostre interès en els capítols posteriors, és l'anomenat *flux potencial no relaxacional* (2.26, 2.28): les trajectòries van cap al mínim del potencial sense necessitat de seguir les línies de màxim pendent, i pot haver–hi una dinàmica residual una vegada que s'ha arribat al mínim. Perquè el potencial que s'obté sigui un bon potencial de Lyapunov, una condició suficient és que verifiqui la *condició d'ortogonalitat* (2.30), que relaciona els termes residuals amb les derivades del potencial.

El potencial de Lyapunov introduït per a sistemes determinístics pot ser també d'utilitat en el cas de considerar sistemes amb renou. Les equacions diferencials estocàstiques es tracten amb la seva funció densitat de probabilitat, que verifica l'equació de Fokker–Planck (2.33). Quan la part determinista de les equacions estocàstiques és un flux potencial, es pot obtenir una expressió per a la funció densitat de probabilitat estacionària en termes del potencial (2.38). Ara bé, algunes restriccions addicionals s'han de satisfer per a la matriu que relaciona el potencial i les equacions del moviment i els termes residuals, com la *condició de fluctuació–dissipació* (2.35) i la condició de divergència nul·la per als termes residuals (2.37). En tot cas, existeix un resultat més general, indicant que es pot obtenir la funció densitat de probabilitat a partir del potencial de Lyapunov sempre i quan la intensitat del renou sigui molt petita. La utilitat de la funció densitat de probabilitat apareix a l'hora de calcular valors mitjos de les variables d'interès (2.39).

Als capítols 5, 6 i 7 s'estudia la dinàmica de làsers de classe A i classe B mitjançant els potencials de Lyapunov.

Chapter 2

Summary of Dynamical Systems

In this chapter, we summarize some results on dynamical systems that will be used subsequently. First, a way of dealing with stochastic differential equations is given. Then, we introduce the definition of Lyapunov potential and the different forms in which the potential is related to the dynamical equations for deterministic systems. Finally, the relationships between stochastic processes and Lyapunov potentials are presented in the cases where the stationary probability distribution function for an stochastic process can be obtained from the Lyapunov potential.

2.1 Brief review on Stochastic Processes

The aim of this section is to give a brief introduction to the basic techniques of stochastic processes that will be used during the rest of this work. We follow closely Ref. [San Miguel and Toral, 1997].

Dynamical systems can be described by a set of differential equations, usually derived after considering certain approximations. Deterministic systems can be well described either by ordinary differential equations or partial differential equations. There is a well established literature to deal with this kind of equations either analytically or numerically, although in some cases the results obtained can be quite complicated due to nonlinear terms appearing in the equations. Furthermore, there are some systems for which certain parts of their behaviour are modelled as random, because the knowledge of these parts is not detailed enough or it is too complex to be treated deterministically. Random parts are those containing a *random process* usually referred to as a *noise term*, $\xi(t)$. The differential equations containing a random process are referred to as *stochastic differential equations*.

Stochastic equations in which the random processes appear linearly are known as *Langevin equations*. For a real variable x, the Langevin equation has the general form

$$\frac{dx}{dt} = q(x,t) + g(x,t)\,\xi(t). \tag{2.1}$$

If the function $g(x,t)$ is a constant, the noise is called *additive*, otherwise, it is a

multiplicative noise.

There are different noise terms that can be considered, all of them defined by their moments and their correlation functions. We will restrict our study to the *white noise*, characterized as a Markovian[1] Gaussian process of mean value and correlations given by

$$\begin{aligned} \langle \xi(t) \rangle &= 0, \\ \langle \xi(t_1)\, \xi(t_2) \rangle &= \delta(t_1 - t_2). \end{aligned} \tag{2.2}$$

The white noise term can be considered as the derivative of the Wiener process, $W(t)$, which has a Gaussian, time dependent, probability density function

$$f(W;t) = \frac{1}{\sqrt{2\,\pi\,t}} \exp\left(-\frac{W^2}{2\,t}\right), \tag{2.3}$$

with one–time moments and two–times correlation function

$$\langle W(t) \rangle = 0, \tag{2.4}$$

$$\langle W(t)^2 \rangle = t, \tag{2.5}$$

$$\langle W(t_1) W(t_2) \rangle = \min(t_1, t_2). \tag{2.6}$$

The derivative of the Wiener process has lack of mathematical rigor and can lead to different possible interpretations [van Kampen, 1981; Gardiner, 1985]. The stochastic integral

$$\int_{t_0}^{t} G(t') dW(t'), \tag{2.7}$$

is interpreted as the limit of partial sums

$$S_n = \sum_{i=1}^{n} G_i [W(t_i) - W(t_{i-1})], \tag{2.8}$$

where t_i corresponds to the partition of the time interval

$$(t_0, t) = (t_0, t_1) \bigcup (t_1, t_2) \bigcup \ldots \bigcup (t_{n-1}, t_n = t). \tag{2.9}$$

The arbitrariness in the definition is related to the problem of which G_i one takes in order to evaluate the integral. Amongst all possible interpretations, the most widely used are those of Itô and Stratonovich. In the Itô interpretation $G_i = G(t_{i-1})$, while for the Stratonovich interpretation $G_i = \frac{1}{2}[G(t_i) + G(t_{i-1})]$.

The Langevin stochastic differential equation is not completely defined unless one chooses one of the previous interpretations. However, there is a simple relationship between the results of these most common interpretations. The rule is that the stochastic differential equation in the Itô sense

$$\frac{dx}{dt} = q(x) + g(x)\, \xi(t), \tag{2.10}$$

[1] In a Markovian process the probability of a future event depends only on the present state of the system and not on the way it reached its present situation.

is equivalent to the stochastic differential equation in the Stratonovich sense

$$\frac{dx}{dt} = q(x) - \frac{1}{2}\, g(x)\, g'(x) + g(x)\, \xi(t). \tag{2.11}$$

In the Itô interpretation $\langle G(t)\xi_w(t)\rangle = 0$, for any non–anticipating function $G(t)$ of $\xi_w(t)$ [Gardiner, 1985]. However, this result is not true in the Stratonovich interpretation, where the Novikov's theorem [Novikov, 1964; Novikov, 1965] should be applied. The Stratonovich interpretation enables the use of the rules of ordinary calculus. However, this is not possible in the Itô interpretation, although it is the most mathematically and technically satisfactory.

Since in most of the cases, it is not possible to integrate the differential equations analytically, one will be interested in obtaining the numerical values for the variables as time evolves. In the next subsection, numerical algorithms for the generation of trajectories are reviewed.

Numerical generation of trajectories

For an ordinary (non–stochastic) differential equation of the form

$$\frac{dx(t)}{dt} = q(t, x), \tag{2.12}$$

the second order Runge–Kutta method gives an approximation to $x(t+h)$ of order $O[h^3]$

$$x(t+h) = x(t) + \frac{h}{2}\,[q(t, x(t)) + q(t+h, x(t) + h\, q(t, x(t)))] + O[h^3]. \tag{2.13}$$

This is an improved algorithm upon the Euler method

$$x(t+h) = x(t) + h\, q(t, x(t)) + O[h^2]. \tag{2.14}$$

In the presence of a Langevin equation as (2.1), one is interested in generating trajectories $x(t)$ for different values of the random process. There are different numerical algorithms to solve this problem [Sancho *et al.*, 1982; Gard, 1987; Greiner *et al.*, 1988; Kloeden and Platen, 1992].

For the stochastic differential equation (2.1), in the Stratonovich sense, we can derive the recurrence relation

$$x(t+h) = x(t) + h^{1/2}\, g(x(t))\, u(t) + h\, \left[q(x(t)) + \frac{1}{2}\, g(x(t))\, g'(x(t))\, u(t)^2\right] + O[h^{3/2}], \tag{2.15}$$

which is known as Milshtein method [Milshtein, 1974; Milshtein, 1978; Sancho *et al.*, 1982]. $u(t)$ are a set of independent Gaussian random variables defined only for the discrete set of recurrence times, $t = 0, h, 2\,h, \ldots$, of zero mean and variance one

$$\begin{aligned} \langle u(t) \rangle &= 0, \\ \langle u(t)^2 \rangle &= 1, \\ \langle u(t)\, u(t') \rangle &= 0,\ t \neq t'. \end{aligned}$$

There are different numerical methods for generating the independent Gaussian random variables, based on random numbers uniformly distributed in the interval $(0, 1)$. We follow here the one developed in [Toral and Chakrabarti, 1993].

A modification of (2.15) is the "Euler algorithm"

$$x(t+h) = x(t) + h^{1/2}\, g(x(t))\, u(t) + h\, \left[q(x(t)) + \frac{1}{2}\, g(x(t)) g'(x(t)) \right] + O[h^{3/2}]. \quad (2.16)$$

This algorithm appears naturally when considering the numerical integration of the equivalent stochastic differential equation (2.10) in the Itô formalism.

The same idea of the Runge–Kutta method applied to ordinary differential equations can be applied to stochastic differential equation. By modifying the Euler method (2.16) one obtains the Heun method [Gard, 1987]

$$\begin{aligned} k &= h\, q(t, x(t)), \\ l &= h^{1/2}\, u(t)\, g(t, x(t)), \\ x(t+h) &= x(t) + \frac{h}{2}\, [q(t, x(t)) + q(t+h, x(t)+k+l)] + \\ &\quad \frac{h^{1/2}\, u(t)}{2}\, [g(t, x(t)) + g(t+h, x(t)+k+l)]\,. \end{aligned} \quad (2.17)$$

In this work, we are interested in the numerical solution of a set of coupled ordinary differential equations with *diagonal noise* of the form

$$\frac{dA_i(t)}{dt} = q_i([A]) + g_i(A_i)\, \xi_i(t), \quad i = 1, \ldots, N. \quad (2.18)$$

In this case, the Milshtein method reads

$$\begin{aligned} A_i(t+h) &= A_i(t) + g_i(A_i(t))\, h^{1/2}\, u_i(t) + \\ &\quad h\, \left[q_i([A(t)]) + \frac{1}{2}\, g_i(A_i(t))\, g_i'(A_i(t))\, u_i(t)^2 \right]. \end{aligned} \quad (2.19)$$

While the Heun method is

$$\begin{aligned} k_i &= h\, q_i([A(t)]), \\ l_i &= h^{1/2}\, u_i(t)\, g_i([A(t)]), \\ A_i(t+h) &= A_i(t) + \frac{h}{2}\, [q_i([A(t)]) + q_i([A(t)+k+l])] + \\ &\quad \frac{h^{1/2}\, u_i(t)}{2}\, [g_i(A_i(t)) + g_i(A_i(t)+k_i+l_i)]\,. \end{aligned} \quad (2.20)$$

2.2 Potentials and Lyapunov Functions

The evolution of a system (dynamical flow) can be classified into different categories according to the relationship of the Lyapunov[2] potential to the actual equations of motion [Montagne *et al.*, 1996; San Miguel *et al.*, 1996].

Classification of Dynamical Systems

Consider a deterministic dynamical flow where the real variables $\mathbf{x} \equiv (x_1, \ldots, x_N)$ satisfy the general evolution equations

$$\frac{dx_i}{dt} = f_i(\mathbf{x}), \qquad i = 1, \ldots, N. \tag{2.21}$$

One is usually interested in finding the fixed points $\bar{\mathbf{x}}$ of the dynamical system, i.e. those having a zero time derivative. The knowledge of the fixed points and their stability is usually the first step in the study of a dynamical system. A fixed point $\bar{\mathbf{x}}$ is said to be stable if for any initial condition sufficiently close to $\bar{\mathbf{x}}$, the system remains in the neighbourhood of $\bar{\mathbf{x}}$ as the time evolves. The fixed point is asymptotically stable if for any initial condition, sufficiently close to $\bar{\mathbf{x}}$, the system tends to $\bar{\mathbf{x}}$ with time.

Lyapunov's stability theorem is useful to determine the stability of a fixed point [Guckenheimer and Holmes, 1983]. The theorem states that if a function $V(\bar{\mathbf{x}}) = V(x_1, ..., x_N)$ exists, such that V is bounded from below and $dV/dt \leq 0$, then the minima $\bar{\mathbf{x}}$ of V are stable fixed points of the dynamics. In this case, V is called a *Lyapunov potential* or, simply, the potential.

The description of the behaviour of a dynamical system is greatly simplified if the Lyapunov potential is known: the system evolves towards the minima of the Lyapunov and once there it stays nearby when small perturbations act upon the system. The Lyapunov potential not only tells us about local stability, but also gives information about global stability. In the case of the comparison between only two fixed points $\bar{\mathbf{x}}^{(1)}$ and $\bar{\mathbf{x}}^{(2)}$ such that $V(\bar{\mathbf{x}}^{(1)}) > V(\bar{\mathbf{x}}^{(2)})$, then we can infer that $\bar{\mathbf{x}}^{(2)}$ is the stable fixed point and that $\bar{\mathbf{x}}^{(1)}$ is a metastable fixed point. This means that a sufficiently strong perturbation might take the system out from $\bar{\mathbf{x}}^{(1)}$ to $\bar{\mathbf{x}}^{(2)}$. Therefore, to understand the asymptotic dynamics it is of great importance to find out whether a Lyapunov potential can be found for the dynamical system under study.

The systems for which a Lyapunov function exists are called in the literature *potential systems* and the name *non–potential systems* is reserved for those systems which do not have a Lyapunov function. According to these definitions, the following classification of dynamical systems can be established.

[2] Some details of the biography of the Russian mathematician Aleksandr Mikhailovich Lyapunov (1857-1918) can be found in [Lyapunov, 1992].

(1) Relaxational gradient potential flow

In this case, there exists a function (the *potential*) $V(\mathbf{x}) = V(x_1, ..., x_N)$ in terms of which the evolution equations are written as

$$\frac{dx_i}{dt} = -\frac{\partial V}{\partial x_i}, \quad i = 1, \ldots, N. \tag{2.22}$$

The fixed points of this dynamical system are the extrema of the potential $V(\mathbf{x})$. The trajectories lead to any of the minimum values of $V(\mathbf{x})$ following the lines of maximum slope (steepest descent). In this case the potential $V(\mathbf{x})$ is a Lyapunov function (with the additional condition that $V(\mathbf{x})$ is bounded from bellow). The proof of this statement is very simple indeed

$$\frac{dV}{dt} = \sum_{i=1}^{N} \frac{\partial V}{\partial x_i}\frac{dx_i}{dt} = -\sum_{i=1}^{N}\left(\frac{\partial V}{\partial x_i}\right)^2 \leq 0. \tag{2.23}$$

(2) Relaxational non–gradient potential flow

There exists again a potential function, $V(\mathbf{x})$, but in this case the dynamics is not governed just by $V(\mathbf{x})$, but is given by

$$\frac{dx_i}{dt} = -\sum_{j=1}^{N} S_{ij}\frac{\partial V}{\partial x_j}, \quad i = 1, \ldots, N, \tag{2.24}$$

where $S_{ij}(\mathbf{x})$ is a real, symmetric and positive definite matrix. The fixed points of the dynamics are still given by the extrema of $V(\mathbf{x})$, however the trajectories lead to the minima of $V(\mathbf{x})$ but not necessarily through the lines of maximum slope but instead they can have an orthogonal component due to the fact that the matrix S is not necessarily diagonal. In this sense, we can say that the transient dynamics is not governed only by the potential. However, $V(\mathbf{x})$ is still a Lyapunov functional

$$\frac{dV}{dt} = \sum_{i=1}^{N} \frac{\partial V}{\partial x_i}\frac{dx_i}{dt} = -\sum_{i,j=1}^{N} S_{ij}\frac{\partial V}{\partial x_i}\frac{\partial V}{\partial x_j} \leq 0, \tag{2.25}$$

since, by definition, $S(\mathbf{x})$ is a positive definite matrix.

(3) Non–relaxational potential flow

In these systems the asymptotic behaviour is not determined simply by the minima of the potential, but there exists a residual dynamics once the minima have been reached. A first category within this class is given by

$$\frac{dx_i}{dt} = -\sum_{j=1}^{N} D_{ij}\frac{\partial V}{\partial x_j}, \quad i = 1, \ldots, N. \tag{2.26}$$

Here, $D_{ij}(\mathbf{x})$ is an arbitrary matrix. When $D_{ij}(\mathbf{x})$ is split into a symmetric and an antisymmetric part $D(\mathbf{x}) = S(\mathbf{x}) + A(\mathbf{x})$, $S(\mathbf{x})$ is a positive definite matrix. Again,

the fixed points of the dynamics are determined by the extrema of the potential $V(\mathbf{x})$. $V(\mathbf{x})$ is a Lyapunov potential, i.e.

$$\frac{dV}{dt} = -\sum_{i,j=1}^{N} S_{ij}\frac{\partial V}{\partial x_i}\frac{\partial V}{\partial x_j} - \sum_{i,j=1}^{N} A_{ij}\frac{\partial V}{\partial x_i}\frac{\partial V}{\partial x_j} \leq 0, \tag{2.27}$$

where the second sum of this expression is zero due to the antisymmetry of the matrix $A(\mathbf{x})$.

The second, and more general, category of non–relaxational potential flow is one in which the dynamical equations can be split into two parts, namely

$$f_i = -\sum_{j=1}^{N} S_{ij}\frac{\partial V}{\partial x_j} + v_i, \quad i = 1, \ldots, N. \tag{2.28}$$

Here $S(\mathbf{x})$ is a symmetric, positive definite matrix and $v_i(\mathbf{x})$ represents the residual dynamics after the relaxational part has acted. Since we demand $V(\mathbf{x})$ to be a Lyapunov potential the residual dynamics must not contribute to its decay

$$\frac{dV}{dt} = -\sum_{i,j=1}^{N} S_{ij}\frac{\partial V}{\partial x_i}\frac{\partial V}{\partial x_j} - \sum_{i=1}^{N} v_i\frac{\partial V}{\partial x_i} \leq 0 \tag{2.29}$$

or, since the first term of the r.h.s. is always negative, a sufficient condition is

$$\sum_{i=1}^{N} v_i\frac{\partial V}{\partial x_i} = 0. \tag{2.30}$$

This is the so–called *orthogonality condition.*

Since the above (sufficient) conditions for a potential flow lead to $dV/dt \leq 0$, one concludes that $V(\mathbf{x})$ (when it satisfies the additional condition of being bounded from below) is a Lyapunov potential for the dynamical system. In this case, one can get an intuitive understanding of the dynamics: the fixed points are given by the extremes of $V(\mathbf{x})$ and the trajectories relax asymptotically towards the surface of minima of $V(\mathbf{x})$. This decay is produced by the only effect of the terms containing the matrix $S(\mathbf{x})$ in Eq. (2.28), since the dynamics induced by $v_i(\mathbf{x})$ conserves the potential, and $v_i(\mathbf{x})$ represents the residual dynamics on this minima surface.

(4) Non–potential flow

For non–potential flows, the splitting (2.28) satisfying (2.30) admits only the trivial solution $V(\mathbf{x}) = 0$, $v_i(\mathbf{x}) = f_i(\mathbf{x})$. Notice that for a system to be classified as non–potential, we have to prove the non–existence of nontrivial solutions of (2.30) which, of course, is different from not being able to find nontrivial solutions of (2.30).

There are different examples in the literature of systems that can be classified as above. We only give here the references in order to show the great variety of fields that can be treated with this formalism. The real Ginzburg–Landau equation

(also known in the theory of critical dynamics as model A in the classification of [Hohenberg and Halperin, 1977]) is a relaxational gradient flow. A typical example of relaxational non–gradient flow is the Cahn–Hilliard model [Cahn and Hilliard, 1958] for spinodal decomposition [Gunton *et al.*, 1983] or model B in the context of critical dynamics [Hohenberg and Halperin, 1977]. As examples of non–relaxational potential flows, the nematodynamics equations commonly used to describe the dynamics of liquid crystals in the nematic phase [San Miguel and Sagues, 1987] and the complex Ginzburg–Landau equation [Descalzi and Graham, 1992; Descalzi and Graham, 1994; Montagne *et al.*, 1996] (the classification given above can also be applied in the case of complex variables, the extension is trivial, and it is presented in [San Miguel *et al.*, 1996]).

Potentials and Stationary Distributions

We now consider dynamical systems where noise is included. We will develop the relationship between stochastic equations and Lyapunov potentials introduced in the previous subsection. Consider the dynamical system described by the stochastic equations (Itô sense) of the form

$$\frac{dx_i}{dt} = f_i(\mathbf{x}) + \sum_{j=1}^{N} g_{ij}(\mathbf{x})\, \xi_j(t), \tag{2.31}$$

where $g_{ij}(\mathbf{x})$ are given functions and $\xi_j(t)$ are white noise sources: Gaussian random processes of zero mean and correlations

$$\langle \xi_i(t)\xi_j(t')\rangle = 2\,\epsilon\,\delta_{ij}\,\delta(t-t'), \tag{2.32}$$

where ϵ is the intensity of the noise.

In this case, it is not adequate to talk about fixed points of the dynamics, but consider instead the maxima of the probability density function $P(\mathbf{x},t)$, which satisfies the multivariate Fokker–Planck equation [Risken, 1989; San Miguel and Toral, 1997]

$$\frac{\partial P(\mathbf{x},t)}{\partial t} = \sum_{i=1}^{N} \frac{\partial}{\partial x_i}\left[-f_i P + \epsilon \sum_{j=1}^{N} \frac{\partial}{\partial x_j}(G_{ij}P)\right], \tag{2.33}$$

where the matrix $G(\mathbf{x})$ is

$$G = g\, g^T, \tag{2.34}$$

and whose general solution is unknown. When the deterministic part of (2.31) is a potential flow, a closed form for the stationary distribution $P_{st}(\mathbf{x})$ can be given in terms of the potential $V(\mathbf{x})$ if the following (sufficient) conditions are satisfied

1. The *fluctuation–dissipation* condition, relating the symmetric matrix $S(\mathbf{x})$ to the noise matrix $g(\mathbf{x})$,

$$S_{ij} = \sum_{k=1}^{N} g_{ik}\, g_{jk}, \qquad S = g \cdot g^T. \tag{2.35}$$

2. S_{ij} satisfies

$$\sum_{j=1}^{N} \frac{\partial S_{ij}}{\partial x_j} = 0, \qquad \forall i. \tag{2.36}$$

This condition is satisfied, for instance, for a constant matrix $S(\mathbf{x})$.

3. $v_i(\mathbf{x})$ is divergence free,

$$\sum_{i=1}^{N} \frac{\partial v_i}{\partial x_i} = 0. \tag{2.37}$$

This third condition is automatically satisfied for potential flows of the form (2.26) with a constant matrix $A(\mathbf{x})$.

Under these circumstances, the stationary probability density function is

$$P_{st}(\mathbf{x}) = Z^{-1} \exp\left(-\frac{V(\mathbf{x})}{\epsilon}\right), \tag{2.38}$$

where Z is a normalization constant, such that $\int P_{st}(\mathbf{x}) d\mathbf{x} = \mathbf{1}$. Conditions (2.35), (2.36) and (2.37) appear naturally when one substitutes expression (2.38) into the Fokker–Planck equation (2.33) and imposes that the derivative with respect to time of $P(\mathbf{x}, t)$ is zero. In some sense, the stationary distribution is still governed by the minima of the potential, since the maxima of this stationary distribution will be centered around these minima. The effect of the noise terms on the asymptotic dynamics is to introduce fluctuations (governed by the Gibbs type distribution (2.38)) in the remaining dynamics which occurs in the attractors identified by the minima of $V(\mathbf{x})$.

A more general result, [Graham, 1987; Graham, 1991], states that if conditions (2.36) and (2.37) are not satisfied, then the above expression (2.38) for $P_{st}(\mathbf{x})$ is still valid in the limit $\epsilon \to 0$.

By using (2.38), the mean value in the steady state of a given function $f(\mathbf{x})$ can be calculated as

$$\langle f(\mathbf{x}) \rangle_{st} = \int f(\mathbf{x})\, P_{st}(\mathbf{x}) d\mathbf{x}. \tag{2.39}$$

This is an useful expression because in the presence of noise terms, one can be more interested in calculating the mean values for different values of the noise terms than in one single realization of the process.

In chapters 5, 6 and 7 we discuss the dynamics of lasers by means of Lyapunov potential functions.

Capítol 3

Bifurcacions

En aquest capítol es fa un resum d'anàlisi de bifurcacions que serà utilitzat en els capítols 6 i 8.

Es considera un sistema dinàmic del tipus $\dot{\mathbf{x}} = \mathbf{f}(\mathbf{x})$, on $\mathbf{x} = (x_1, \ldots, x_n)$ i $\mathbf{f} = (f_1, \ldots, f_n)$. Les seves solucions es poden visualitzar com a *trajectòries* en un espai n–dimensional anomenat *retrat de fases*. L'aparièncía de les trajectòries d'aquest retrat de fases és controlada pels *punts fixos*, $f_i(x_1^*, \ldots, x_n^*) = 0$. És possible analitzar l'estabilitat d'un punt fix a partir de linealitzar les equacions al voltant del punt. Un punt fix es diu *estable* quan tots els autovalors de la matriu linealitzada són negatius; és absolutament *inestable* quan tots els autovalors són positius; i *sella*, quan alguns autovalors són positius i d'altres negatius.

L'estructura qualitativa del flux pot canviar quan es varien el paràmetres del sistema. Aquests canvis qualitatius s'anomenen *bifurcacions*. La representació dels punts o línees on apareixen les bifurcacions en l'espai de paràmetres dóna lloc al *conjunt de bifurcacions*.

Hi ha tipus de bifurcacions que apareixen repetidament en molts problemes. Una possible classificació de les bifurcacions es basa en conceptes que tenen el seu origen en la teoria de transversalitat en topologia diferencial. La *codimensió* d'una bifurcació és la menor dimensió en l'espai de paràmetres que conté la bifurcació.

El *teorema de la varietat central* indica una manera per reduir sistemàticament la dimensió de l'espai d'estats que són necessaris quan s'analitzen bifurcacions d'un cert tipus. Aquest mètode aïlla el comportament asimptòtic més complex a partir de localitzar la varietat invariant tangent al subespai generalitzat d'autovectors amb autovalors imaginaris purs.

Una vegada que s'ha aplicat aquest teorema, s'intenta obtenir transformacions de coordenades addicionals que simplifiquen les expressions analítiques del camp vectorial a la varietat central. Els camps vectorials simplificats són les *formes normals*. La dinàmica a prop d'una bifurcació típicament apareix representada per la seva forma normal.

Algunes bifurcacions de codimensió un són les següents. Una bifurcació *sella–node* és el mecanisme bàsic per el qual dos punts fixos són creats o destruïts, com es veu a la figura 3.1. En una bifurcació *transcrítica*, figura 3.2, dos punts fixos canvien la seva estabilitat en el punt de bifurcació. En una bifurcació tipus *forca*, figura 3.3, dos punts fixos apareixen (destrueixen) simètricament amb l'estabilitat d'un punt fix que existia abans del punt de bifurcació i aquest canvia la seva estabilitat.

A més de punts fixos, poden existir altres conjunts invariants en el sistema dinàmic. Un *cicle límit* és una trajectòria tancada aïllada: les trajectòries properes van cap al cicle límit o es fan enfora d'ell en forma d'espiral.

En una bifurcació de *Hopf*, tal com apareix a la figura 3.6, un punt fix canvia la seva estabilitat i apareix o desapareix un cicle límit amb la mateixa estabilitat que la del punt fix abans del punt de bifurcació. En el punt de bifurcació existeixen un parell d'autovalors imaginaris purs.

Existeixen altres formes amb les quals els cicles límits es poden crear o destruir. En una bifurcació *sella–node de cicles*, dos cicles límits es junten i s'aniquilen. En una bifurcació de *període infinit*, el període d'oscil·lació del cicle límit augmenta fins a fer–se infinit en el punt de bifurcació, i dos punts fixos (un sella i un estable/inestable) hi apareixen. En una bifurcació *homoclínica*, part del cicle límit s'apropa cada vegada més a un punt sella, fins que en el punt de bifurcació el cicle toca el punt sella i es forma una òrbita homoclínica.

A més de les bifurcacions indicades fins ara, és possible obtenir bifurcacions locals de codimensió dos. Un dels l'exemples més típics d'aquest tipus de bifurcació és el cas en què apareixen un parell d'autovalors imaginaris i un autovalor zero (bifurcació Hopf–sella–node). De l'anàlisi de la seva forma normal, es veu que quatre diferents tipus de bifurcacions es poden obtenir depenent del valor dels paràmetres del sistema. A les figures 3.7 a 3.10 apareixen el conjunt de bifurcacions i el retrats de fases per cada un dels tipus que sorgeixen.

Un espai de fases bidimensional important és el *torus*. A damunt aquest torus poden existir òrbites tancades (resonàncies), o la trajectòria pot donar voltes al voltant del torus sense fi, flux *quasiperiòdic*.

Les *projeccions de Poincaré* ens poden servir per a estudiar el flux a prop d'òrbites periòdiques. Si es considera un sistema n–dimensional $\dot{\mathbf{x}} = \mathbf{f}(\mathbf{x})$ i S_n una superfície transversa al flux $n-1$–dimensional. La projecció de Poincaré, $\mathbf{x_{k+1}} = \mathbf{P}(\mathbf{x_k})$, és una relació de S_n amb ella mateixa, obtinguda a partir d'obtenir les interseccions de les trajectòries amb S_n: $\mathbf{x_k} \in S_n$. Es pot establir un criteri en termes dels autovalors λ_j de la projecció de Poincaré linealitzada: L'òrbita tancada serà estable si i només si $|\lambda_j| < 1$ per a tots $j = 1, \ldots, n-1$. Contrariament, si $|\lambda_j| > 1$ per a algun j, les pertorbacions al llarg de la direcció j creixen i l'òrbita és inestable. Un cas límit ocorr quan l'autovalor més gran té magnitud $|\lambda_j| = 1$; això passa en bifurcacions d'òrbites periòdiques i cal un anàlisi nolineal d'estabilitat. Els valors λ_j s'anomenen multiplicadors de *Floquet* de l'òrbita periòdica i generalment només es poden obtenir mitjançant integració numèrica.

Chapter 3

Bifurcations

In this chapter, we summarize some results on bifurcation analysis that will be used in chapters 6 and 8. We follow closely Refs. [Guckenheimer and Holmes, 1983; Hilborn, 1994; Strogatz, 1994; Solari *et al.*, 1996].

Let us consider the general dynamical system

$$\dot{\mathbf{x}} \;=\; \mathbf{f}(\mathbf{x}),$$

where $\mathbf{x} = (x_1, \ldots, x_n)$ and $\mathbf{f} = (f_1, \ldots, f_n)$. Its solutions can be visualized as *trajectories* flowing through an n–dimensional phase space with coordinates $(x_1, \ldots, x_n)$. A picture which shows all the qualitatively different trajectories of the system is called a *phase portrait*. The appearance of the phase portrait is controlled by the *fixed points* $f_i(x_1^*, \ldots, x_n^*) = 0$, for $i = 1, \ldots, n$, which represent equilibrium solutions. An equilibrium point is defined to be *stable* if all sufficiently small perturbations away from it damp out in time. Conversely, in *unstable* fixed points, peturbations grow in time. For a *saddle* fixed point some perturbations grow in time whereas others damp out, depending on the direction chosen near the fixed point. It is possible to perform a quantitative measure of the stability of a fixed point by linearizing about it. The eigenvalues of the linearized matrix give information of the stability of the fixed point: for positive eigenvalues perturbations grow in time, for negative eigenvalues perturbations damp out.

The qualitative structure of the flow can change when parameters of the system are varied. In particular, fixed points can be created or destroyed, or their stability change. These qualitative changes in the dynamics are called *bifurcations*, and the parameter values at which they occur are called *bifurcation points*. The representation of the bifurcation points (or lines) in the parameter space will give rise to the *bifurcation set*.

What is of particular interest is that there are some kinds of bifurcations which appear repeatedly in many problems. It would be interesting to have a classification of bifurcations which produces a specific list of possibilities for each example, starting with only general considerations such as the number of parameters in the problem,

the dimension of the phase space, and any symmetries or other special properties of the system. The classification schemes are based upon concepts of differential topology. The *codimension* of a bifurcation is the smallest dimension of a parameter space which contains the bifurcation, and an *unfolding* of a bifurcation is a set of equations which contains the bifurcation in a persistent way.

The *center manifold theorem* provides a mean for systematically reducing the dimension of the state space which needs to be considered when analysing bifurcations of a given type. This theorem states that it is possible to define manifolds tangent to the eigenspaces associated to the eigenvalues of a flow. The center manifold is defined as a manifold tangent to the center eigenspace. The local dynamical behaviour transverse to the center manifold is relatively simple, since it is controlled by the exponentially contracting (and expanding) flows in the local stable (and unstable) manifolds. Then, the center manifold method isolates the complicated asymptotic behaviour by locating an invariant manifold tangent to the subspace spanned by the (generalized) eigenspace of eigenvalues on the imaginary axis.

Once the center manifold theorem has been applied to a system, it is useful to find additional coordinate transformations which simplify the analytical expression of the vector field on the center manifold. The resulting simplified vector fields are called *normal forms*. The dynamics close to a bifurcation typically look like the one represented by its normal form. Moreover, the analysis of the dynamics of the normal forms yields a qualitative picture of the flows of each bifurcation type.

In real physical systems, the explosive instabilities that can appear when analysing the normal forms are compensated by the stabilization influence of higher–order terms.

In the following we will describe some of the bifurcations that will appear in later chapters.

The *saddle–node* bifurcation is the basic mechanism by which fixed points are created or destroyed. As a parameter is varied, two fixed points move toward each other, collide, and mutually annihilate. The prototypical example of a saddle–node bifurcation is the first–order system (normal form)

$$\dot{x} = -r - x^2,$$

where r is a real parameter. In figure 3.1 one can observe a representation of this bifurcation. When $r < 0$, there are two fixed points, one stable and one unstable. When $r = 0$ (bifurcation point), the fixed points coalesce into a half–stable fixed point at $x^* = 0$. For $r > 0$, there are no fixed points at all.

In a *transcritical* bifurcation, with normal form

$$\dot{x} = rx - x^2,$$

the two fixed points switch their stability at the bifurcation point $r = 0$, see Fig. 3.2.

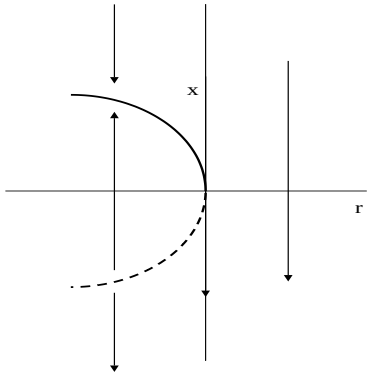

Figure 3.1: Saddle–node bifurcation.

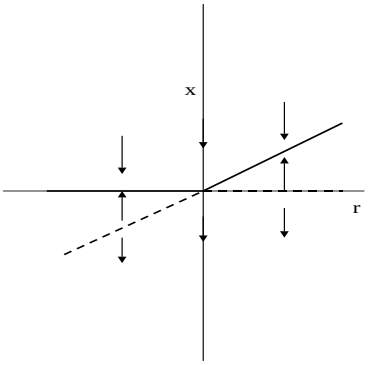

Figure 3.2: Transcritical bifurcation.

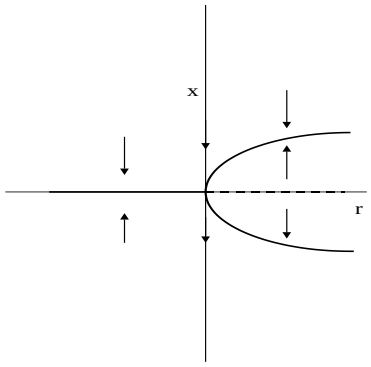

Figure 3.3: Pitchfork bifurcation (supercritical).

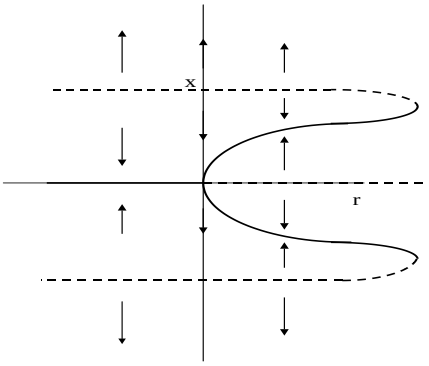

Figure 3.4: Pitchfork bifurcation (supercritical), including a high order term.

The normal form of a *supercritical pitchfork* bifurcation is

$$\dot{x} = rx - x^3.$$

For $r < 0$ the origin is the only fixed point, and it is stable while for $r > 0$, two new stable fixed points appear symmetrically located $x^* = \pm\sqrt{r}$ and the origin becomes unstable, see Fig. 3.3. A more completed form of the supercritical pitchfork bifurcation includes a higher order term

$$\dot{x} = rx - x^3 + x^5,$$

and its representation is the one appearing in Fig. 3.4.

In a *subcritical pitchfork* bifurcation, with normal form

$$\dot{x} = rx + x^3,$$

the nonzero fixed points $x^* = \pm\sqrt{-r}$ are unstable, and exist only below the bifurcation ($r < 0$). The origin is stable for $r < 0$ and unstable for $r > 0$, see Fig. 3.5.

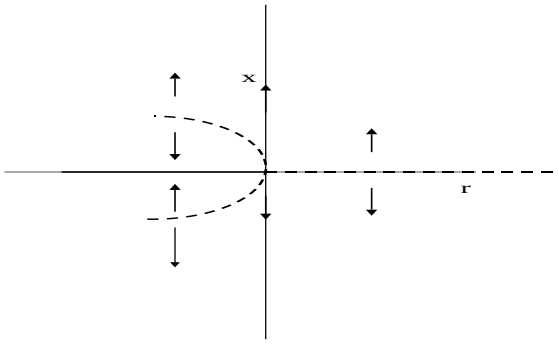

Figure 3.5: Pitchfork bifurcation (subcritical).

Apart from the fixed points, there can appear other invariant sets in the dynamical system. A *limit cycle* is an isolated closed trajectory: neighbouring trajectories are not closed, they spiral toward or away from the limit cycle. If all neighbouring trajectories approach to the limit cycle, the limit cycle is stable or attracting. Otherwise, the limit cycle is unstable, or in exceptional cases, saddle.

In a *Hopf* bifurcation, see Fig. 3.6, a stable (unstable) fixed point changes its stability and an stable (unstable) limit cycle appears or disappears. The normal form is

$$\begin{aligned} \dot{x} &= \mu x - y - (x^2 + y^2)x, \\ \dot{y} &= x + \mu y - (x^2 + y^2)y. \end{aligned}$$

At the bifurcation point, there exist a pair of purely imaginary eigenvalues.

There exist other ways in which limit cycles are created or destroyed. They are harder to detect because they involve large regions of the phase plane than just the neighbourhood of a single fixed point. Hence they are called *global bifurcations*. For each of the bifurcations, there are characteristic *scaling laws* that govern the amplitude and period of the limit cycle as the bifurcation is approached.

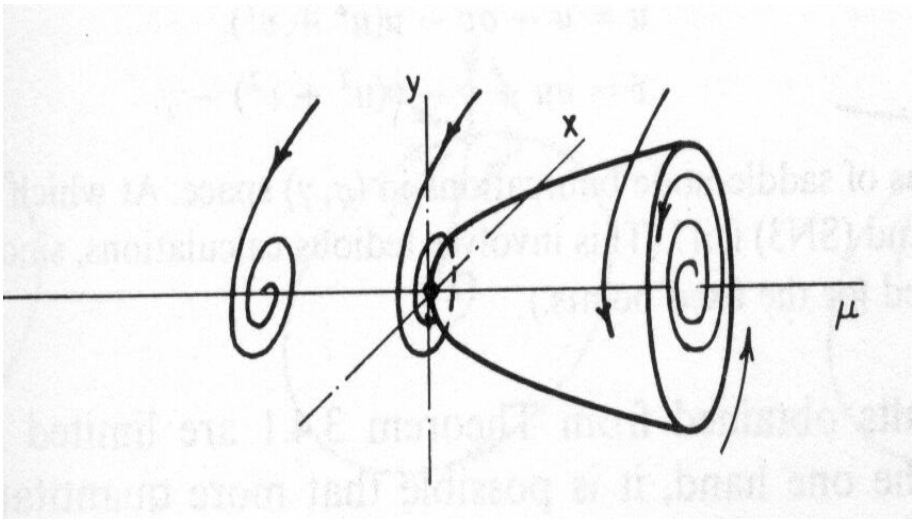

Figure 3.6: Hopf bifurcation.

A bifurcation in which two limit cycles coalesce and annihilate is called a *saddle–node bifurcation of cycles*.

In a *infinite–period bifurcation* (also called Andronov–Leontovich bifurcation), the oscillation period of a limit cycle lengthens and finally becomes infinity, when a fixed point appears on the cycle, at the bifurcation point. Varying the bifurcation parameter, μ, the fixed point splits into a saddle and a node. As the bifurcation is approached, the amplitude of the oscillation stays $O(1)$ but the period of the cycle increases like $O(\mu^{-1/2})$.

The *homoclinic bifurcation* is a kind of infinite–period bifurcation. In this scenario, part of a limit cycle moves closer and closer to a saddle point. At the bifurcation the cycle touches the saddle point and becomes a homoclinic orbit.

Apart from the local codimension–one bifurcation of flows (as saddle–node, pitchfork, transcritical and Hopf bifurcations), it is possible to obtain local codimension–two bifurcations. These will be found in the bifurcation set as intersection of two codimension–one bifurcations.

One of the typical examples of codimension–2 bifurcations is the case in which a pure imaginary pair and a simple zero eigenvalue appear. This is the basis of the analysis of chapter 8, where it is refereed as Hopf–saddle–node bifurcation. The normal form in the reduced planar system is

$$\begin{aligned} \dot{x} &= \mu_1 x + a\, x\, y, \\ \dot{y} &= \mu_2 + b\, x^2 - y^2. \end{aligned} \tag{3.1}$$

The fixed points of the system are given in terms of μ_1, μ_2, a and b. However, the qualitative features (the stability of the invariant sets in different regions) will be different depending on the sign of a and b. Consequently, four types of this bifurcation can be encountered. For a more detailed study of the different types,

the reader can reference to [Guckenheimer and Holmes, 1983] where the parameter region (μ_1, μ_2) is detailed for each part. From that book we have extracted Figs. 3.7 - 3.10, were the bifurcation set and the phase portraits for each case are shown.

An important two–dimensional phase space is the *torus* (this appears when a periodic orbit suffers a Hopf bifurcation changing its stability). We will illustrate some general features of flows on the torus. One could imagine a single point tracing out a trajectory on a torus with coordinates θ_1, θ_2. There are two different cases. The trajectories are closed orbits on the torus, because θ_1 completes p revolutions in the same time than θ_2 completes q revolutions. The resulting curves are called $p : q$ knots (resonances in chapter 8). The second possibility is that every trajectory winds around endlessly on the torus, never intersecting itself and yet never quite close. Each trajectory is dense in the torus and in this case the flow is said to be *quasiperiodic*.

Poincaré maps are useful for studying swirling flows, such as the flow near a periodic orbit. We consider a n–dimensional system $\dot{\mathbf{x}} = \mathbf{f}(\mathbf{x})$ and let S_n be a $n-1$–dimensional surface transverse to the flow. The Poincaré map P is a mapping from S_n to itself, obtained by following trajectories from one intersection with S_n to the next. If $\mathbf{x_k} \in \mathbf{S_n}$ denotes the k intersection, the Poincaré map is $\mathbf{x_{k+1}} = \mathbf{P}(\mathbf{x_k})$. In supposing a fixed point of P, $\mathbf{x}^*$, a trajectory starting at $\mathbf{x}^*$ returns to $\mathbf{x}^*$ after some time T, and it is therefore a closed orbit for the original system. Moreover, by looking at the behaviour of P near this fixed point, we can determine the stability of the closed orbit. The desired stability criterion is expressed in terms of the eigenvalues λ_j of the linearized Poincaré map: The closed orbit will be linearly stable if and only if $|\lambda_j| < 1$ for all $j = 1, \ldots, n-1$. Conversely, if $|\lambda_j| > 1$ for some j, perturbations along the j direction grow and $\mathbf{x}^*$ is unstable. A borderline case occurs when the largest eigenvalue has magnitude $|\lambda_j| = 1$; this occurs at bifurcations of periodic orbits, and a nonlinear stability analysis is required. The λ_j are called the *characteristic* or *Floquet* multipliers of the periodic orbit and they can only be found by numerical integration.

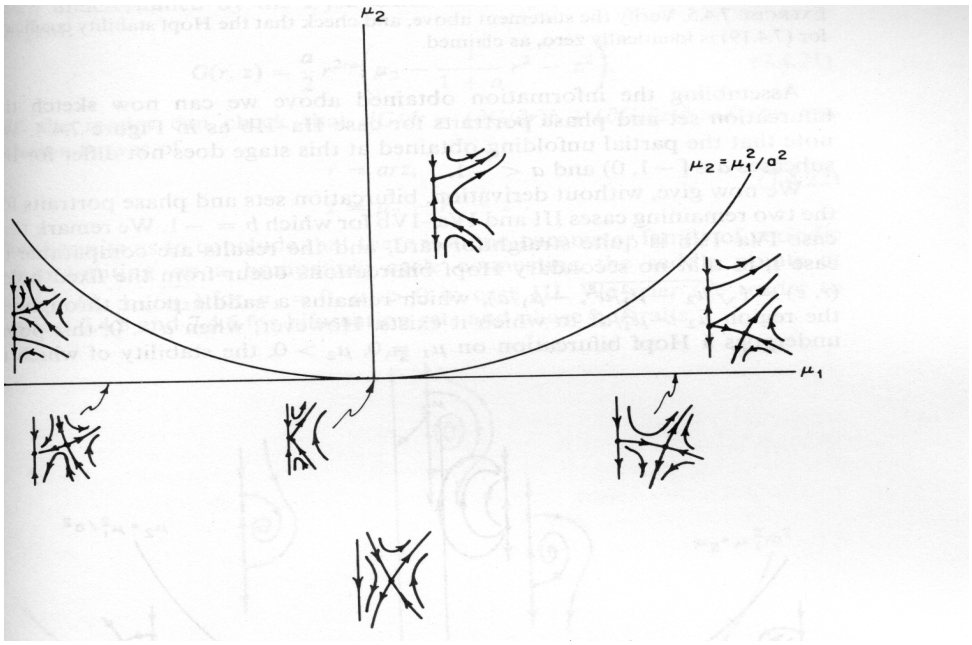

Figure 3.7: Bifurcation set and phase portraits for the unfolding case of a Hopf–saddle–node bifurcation for the type *I* case: $b = +1$, $a > 0$.

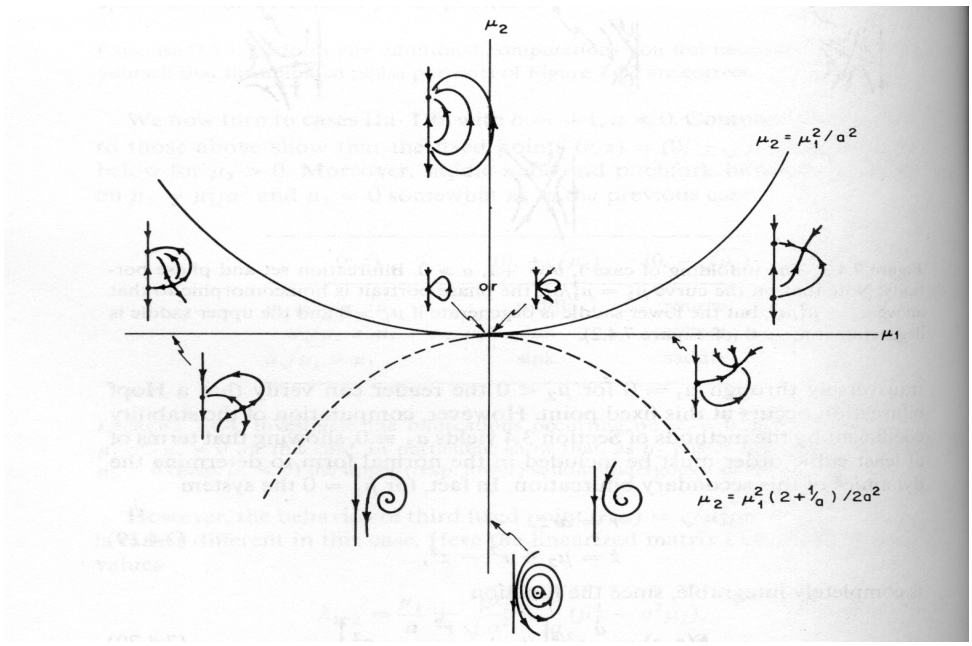

Figure 3.8: Bifurcation set and phase portraits for the unfolding case of a Hopf–saddle–node bifurcation for the type *II* case: $b = +1$, $a < 0$.

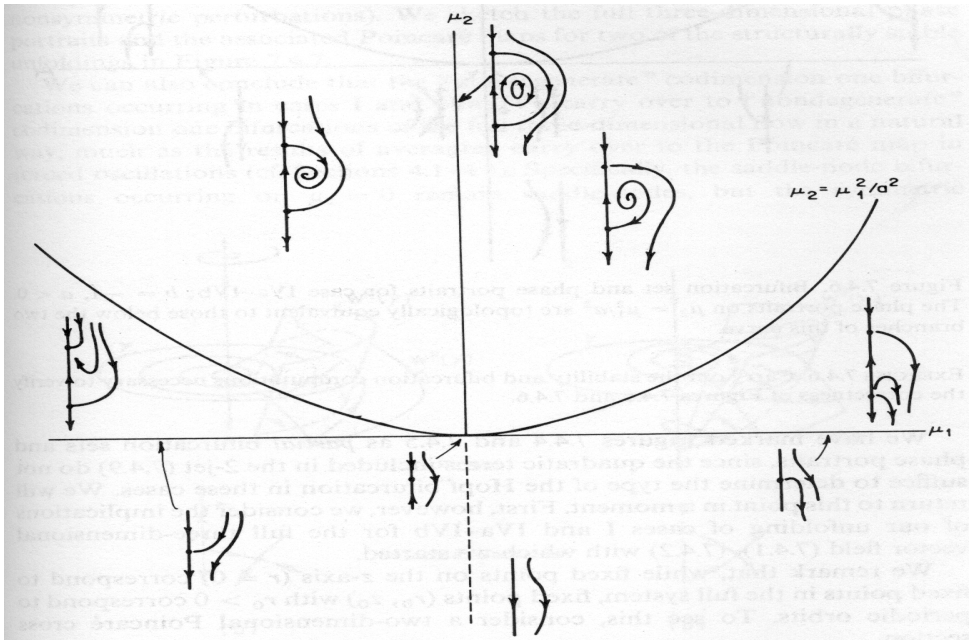

Figure 3.9: Bifurcation set and phase portraits for the unfolding case of a Hopf–saddle–node bifurcation for the type *III* case: $b = -1$, $a > 0$.

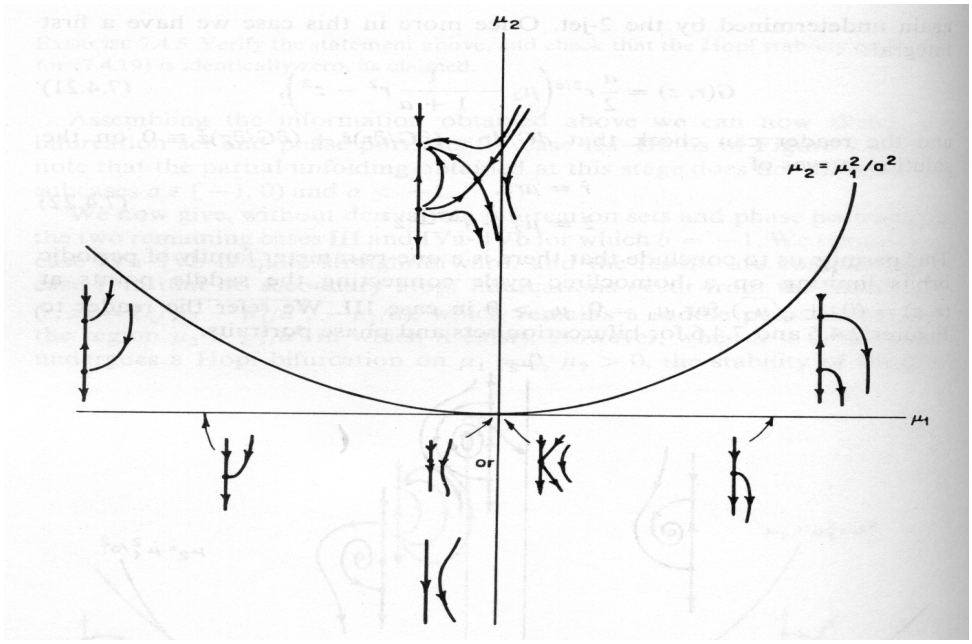

Figure 3.10: Bifurcation set and phase portraits for the unfolding case of a Hopf–saddle–node bifurcation for the type *IV* case: $b = -1$, $a < 0$.

Capítol 4

Làsers: Fenòmens físics i models

En aquest capítol es presenta un breu resum dels fenòmens físics involucrats en els sistemes làser, així com els models que s'utilitzen per descriure el seu comportament.

En un sistema làser una ona electromagnètica interacciona amb el material, i hi poden ocórrer tres processos: emissió espontània, emissió estimulada i absorció. En condicions normals el material es comporta com un absorbent. En condicions de no–equilibri (la població d'un nivell d'energia és major que la població d'un nivell amb energia més baixa), el material actua com un amplificador i la situació és d'*inversió de població*. Un *material actiu* és aquell amb inversió de població.

Per poder convertir l'amplificador en un làser cal a més un terme de realimentació. Aquest efecte es pot obtenir col·locant el material actiu entre dos miralls altament reflectants, de manera que l'ona electromagnètica sigui amplificada a cada viatge dins el material actiu. Per poder haver–hi amplificació es necessita que es verifiqui un cert llindar: l'oscil·lació (inicialitzada pels fotons emesos espontàniament) comença quan el guany del material actiu compensa les pèrdues dins el làser. Per extraure un feix útil del sistema làser es fa un dels dos miralls parcialment transparent.

Així que els tres elements bàsics en un làser són: a) un medi de guany capaç d'amplificar la radiació electromagnètica que es propaga dins la cavitat, b) una cavitat òptica que proporciona la realimentació necessària, i c) un mecanisme de bombeig. Les propietats que caracteritzen els làsers (alta monocromaticitat, coherència temporal i espacial, direccionalitat, ...) han fet que els làsers tinguin un gran ventall d'aplicacions.

La modelització dels sistemes làsers inclou el tractament de processos d'alta complexitat. Una descripció completa de la seva dinàmica es basa en una descripció mecànico–quàntica de la interacció radiació–matèria dins la cavitat làser. No obstant, normalment es fa una descripció en termes de la teoria semiclàssica. Aquesta teoria ignora la naturalesa mecànico–quàntica del camp electromagnètic (perquè el nombre de fotons dins un sistema làser és molt més gran que un) utilitzant les equacions de Maxwell, mentre que el medi amplificador sí que es modela quànticament com una col·lecció d'àtoms de dos nivells a través de les equacions

de Bloch. Les equacions resultants són les de Maxwell–Bloch (4.5 - 4.7), que descriuen les variacions temporals de les variables involucrades en el procés: amplitud complexa lentament variable del camp elèctric que es propaga dins la cavitat, polarització material i inversió de població.

Els làsers es poden classificar segons el ritme de decaïment de les tres variables del sistema. Els làsers de classe C tenen els ritmes de decaïment dels fotons, portadors i polarització material del mateix ordre, i es requereix el conjunt complet de les equacions de Maxwell–Bloch per a la seva descripció. En els làsers de classe B, la polarització material decau cap a l'estacionari molt més ràpidament que les altres dues variables, i es pot realitzar una eliminació adiabàtica d'aquesta variable. D'aquesta manera, els làsers de classe B es descriuen mitjançant dues equacions de balanç, una per a la inversió de població (o nombre de portadors) i una altra per al camp elèctric. Dels distints làsers de classe B existents, es restringeix l'estudi als làsers de semiconductor, on les transicions es produeixen entre bandes d'electrons i forats en comptes d'entre nivells d'energia atòmics o moleculars. Per finalitzar, en els làsers de classe A, tant la inversió de població com la polarització material decauen a l'estacionari molt més ràpidament que el camp elèctric, es pot fer una eliminació adiabàtica d'ambdues variables i, és suficient amb l'equació pel camp elèctric per descriure l'evolució d'aquests làsers.

Una descripció més senzilla de les equacions de Maxwell–Bloch es pot fer promitjant en la direcció de propagació i considerant emissió en un únic mode. Les equacions resultants són les equacions de balanç, que en el cas dels làsers de classe B són les equacions (4.8, 4.9). A l'equació per a la variació de l'amplitud lentament variable del camp elèctric hi ha una competició entre els termes de guany i de pèrdues; a més, s'introdueix el factor d'increment d'amplada de línia o terme de disintonia (α) que considera que en els làsers de semiconductor les transicions ocorren entre bandes d'energia i per tant l'espectre de guany és antisimètric. L'equació per al nombre de portadors consta de tres termes: el bombeig extern, el terme de pèrdues degut a emissió espontània o transicions no radiatives, i el terme d'emissió espontània. L'efecte de l'emissió espontània com una font radiativa es pot incloure en les equacions de balanç amb la inclusió de termes de renou blanc (4.11, 4.12). Quan les equacions s'escriuen en termes de les variables intensitat i fase del camp elèctric (4.14 - 4.16), a l'equació per la intensitat apareix (en la interpretació de Itô) un terme de renou d'emissió espontània promig. El terme de disintonia només apareix en l'equació per la fase del camp elèctric. A partir d'aquestes equacions es poden obtenir les equacions per als làsers de classe A realitzant una eliminació adiabàtica dels portadors.

Els capítols de la part II són dedicats a l'estudi dels làsers de classe A, mentre que els làsers de classe B es tracten al llarg de la part III de la memòria.

Chapter 4

Lasers: Physical phenomena and models

In this chapter we present a brief review of lasers, the physical phenomena involved in these systems and some models used to describe their behaviour. There exist in the literature a huge amount of papers and books related to this subject. Some references that we follow in this section are [Svelto, 1982; Hecht and Zajac, 1986; Petermann, 1988; Homar, 1996].

Laser[1] is the acronym of light amplification by stimulated emission of radiation accounting for the basic mechanism by which a laser works.

Some pioneer works by Einstein in 1917 already described the stimulated emission process. However, it was not until 1954 when Town succeded with the first experiment with the maser (microwave amplification by stimulated emission of radiation). In 1958, Schawlow and Townes predict theoretically the existence of laser systems and in 1960, Theodore H. Maiman announced the first operation of a laser, namely a ruby laser. Since then, a lot of different lasers have been studied, both experimentally and theoretically.

4.1 Physical phenomena in lasers

In a laser system an electromagnetic wave interacts with a material and three processes can occur: a photon can be absorbed by the material or it can be emitted either spontaneously or by stimulated emission. The simplest way to sketch this situation is as follows.

Consider a material whose atoms (or molecules) have two energy levels, 1 and 2, with energies E_1 and E_2 ($E_2 > E_1$). An atom (or molecule) of the given material which is initially in level 2 tends to decay *spontaneously* to level 1 emitting a photon of frequency ν (Planck's law)

$$\nu = \frac{E_2 - E_1}{h}, \tag{4.1}$$

[1] Laser was also a plant with miraculous properties which grew wild over a large area around Cyrene (in present-day Libya) [Svelto, 1982].

where h is the Planck's constant. In this process, the photon is emitted in any direction and with no definite phase relation with that emitted by another atom (or molecule). However, it may happen that an atom initially in level 2 decays to the level 1 forced by an incoming photon. This phenomenon is the basis of the laser operation and it is called *stimulated emission*. Since the process is forced by the incident photon, the emitted photon adds in phase to the incoming one and in the same direction. Finally, an atom in level 1 can undergo a transition from this energy level to level 2 by *absorbing* an incident photon.

Once the basic concepts have been given, we can use them to explain the mechanisms for the operation of a laser. Let us consider two energy levels as above and let N_1 and N_2 be their respective populations. If a plane wave is travelling along the material, the three processes explained before (spontaneous emission, stimulated emission and absorption) can be present. Considering only stimulated emission and absorption processes, the material behaves as an amplifier if $N_2 > N_1$ and it behaves as an absorber if $N_2 < N_1$. Under ordinary conditions the material behaves as an absorber [e.g., in the case of thermal equilibrium for which $N_2/N_1 = \exp\left(-\frac{(E_2-E_1)}{k_B T}\right)$]. If a nonequilibrium condition is reached for which $N_2 > N_1$, the material will act as an amplifier and *population inversion* can be achieved. An *active material* is a material with population inversion.

To turn an amplifier into a laser, a suitable positive feedback has to be introduced. In a laser, the feedback is obtained by placing the active material between two highly reflecting mirrors (e.g., plane–parallel mirrors), such that an electromagnetic wave traveling in a direction orthogonal to the mirrors bounces back and forth between the two mirrors and is amplified on each passage through the active material. By making one of the two mirrors partially transparent, an useful output beam can be extracted. A certain threshold condition must be satisfied: the oscillation (built up from the spontaneous emission) starts when the gain of the active material compensates the losses in the laser. The photons spontaneously emitted along the cavity axis initiate the amplification process.

Summarizing, a laser has three basic ingredients: i) a gain medium capable of amplifying the electromagnetic radiation propagating inside the cavity (typically gas, liquid, solid state or semiconductor materials), ii) an optical cavity that provides the necessary feedback (Fabry–Perot or ring cavities, distributed feedback structures or distributed Bragg reflectors), and iii) a pumping mechanism (electrical discharge, current injection or optical pump). Laser radiation has very useful properties: a high degree of monochromaticity, temporal and spatial coherence, directionality, brightness and it can be produced (using different systems) in a broad range of wavelengths. Likewise, there is a large variety of laser applications. Since its discovery, lasers have been used in metrology, industrial and medical applications, trapping and cooling of atoms, detection of gravitational waves, cutting materials, optical communications, CD players and recorders, printers, etc.

4.2 Modelling lasers

A complete understanding of laser dynamics is based on a fully quantum-mechanical description of matter–radiation interaction within the laser cavity. However, the laser is a system where the number of photons is much larger than one, thus allowing a semiclassical treatment of the electromagnetic field inside the cavity through the Maxwell equations. This fact was introduced in the semiclassical laser theory, developed by Lamb [Lamb, 1964; Sargent *et al.*, 1974] and independently by Haken [Haken and Sauermann, 1963; Haken, 1983; Haken, 1984; Haken, 1985]. The model for the laser dynamics was constructed from the Maxwell–Bloch equations for a single–mode field interacting with a two–level medium. The semiclassical laser theory ignores the quantum–mechanical nature of the electromagnetic field, while the amplifying medium is modelled quantum–mechanically as a collection of two–level atoms through the Bloch equations. The evolution of the wave electric field $\vec{\mathcal{E}}(\vec{x},t)$ can be obtained from the wave equation of the electromagnetic theory

$$\triangle\vec{\mathcal{E}} - \frac{1}{c^2}\ddot{\vec{\mathcal{E}}} - \mu_0\sigma_0\dot{\vec{\mathcal{E}}} = \mu_0\ddot{\vec{\mathcal{P}}} \tag{4.2}$$

where $\triangle$ represents the Laplace operation, c is the velocity of light in vacuum, μ_0 is the vacuum magnetic permeability, σ_0 is the electric conductivity of the medium, and $\vec{\mathcal{P}}(\vec{x},t)$ is the electric polarization of the medium. By assuming a plane–wave structure, $\vec{\mathcal{E}}(\vec{x},t)$ and $\vec{\mathcal{P}}(\vec{x},t)$ can be expressed as

$$\vec{\mathcal{E}}(\vec{x},t) = \frac{1}{2}\left[\vec{e}E(t)e^{i(kz-\Omega_0 t)} + c.c.\right], \tag{4.3}$$

$$\vec{\mathcal{P}}(\vec{x},t) = \frac{1}{2}\left[\vec{e}'P(t)e^{i(kz-\Omega_0 t)} + c.c.\right], \tag{4.4}$$

where k is the resonator wave vector (it has been taken in the z–direction), $\vec{e}$ and $\vec{e}'$ are unit vectors and Ω_0 is the laser frequency.

By using these definitions, the Maxwell–Bloch equations, after appropriate rescaling, are

$$\partial_t E + \frac{c}{\eta_g}\partial_z E = -\frac{\gamma}{2}E + \frac{P}{2}, \tag{4.5}$$

$$\partial_t P = -\gamma_p(1 - i\,\alpha)\,P + \gamma_p\,g_N\,(1+\alpha^2)\,(N - N_o)\,E, \tag{4.6}$$

$$\partial_t N = C - \gamma_N\,N - \frac{1}{2}\,(E\,P^* + E^*\,P). \tag{4.7}$$

E is the slowly–varying complex amplitude of the electric field propagating in the z direction, P is the slowly–varying complex amplitude of the material polarization and N gives the population inversion.

Eq. (4.5) is obtained from the Maxwell's equations by considering an isotropic non–magnetic dielectric medium and a single transversal electrically polarized mode at a given frequency. The other equations are the matter equations that are developed from quantum mechanics. It is assumed two energy levels for the atoms that

participate in the interaction with the laser field. The parameters appearing in the equations are: η_g is the group refractive index of the mode such that c/η_g is the group velocity; γ is the inverse of the photon lifetime or cavity decay rate and it accounts for internal and mirror losses. In (4.6) γ_p is the polarization decay rate, and it accounts for the collision with other atoms or the interaction with lattice vibrations; α is the normalized detuning, which takes into account the difference between the frequency of the transition of the two energy levels and the cavity resonant frequency; g_N is the differential gain at the lasing frequency (in the simplest approximation, g_N is considered to be constant, but a more realistic model includes gain saturation through a nonlinear dependence on the modulus of the electric field, as will be considered later); N_o is the population inversion at transparency (value of the population inversion at which the material is transparent to radiation).

In (4.7), C is the rate at which the carriers, electrons and holes are injected into the active layer due to the external pumping. The second term of this equation, stands for carrier losses due to spontaneous emission or non–radiative transitions. In this work, γ_N (population relaxation parameter due to spontaneous recombinations) is considered as a constant, although a more general form can be also considered [Olshansky *et al.*, 1984]. The third term accounts for the stimulated emission.

Different types of lasers can be classified according to the decay rate of the photons, carriers and material polarization. Arecchi et al. [Arecchi *et al.*, 1984; Tredicce *et al.*, 1985a] were the first to give a classification scheme: class C lasers have all the decay rates of the same order, and therefore the full set of three nonlinear differential equations is required for a satisfactory description of the electric field, the population inversion and the material polarization. For class B lasers, the polarization decays towards the steady state much faster than the other two variables, and it can be adiabatically eliminated. Class B lasers, of which semiconductor lasers [Agrawal and Dutta, 1986] are an example, are then described by two rate equations for the atomic population inversion (or carriers number) and the electric field. Other examples of class B lasers are CO_2 lasers and solid state lasers [Weiss and Vilaseca, 1991]. From now on, when studying class B lasers, we will restrict ourselves to semiconductor lasers. The main characteristic of these lasers is that the transitions occur between electron and hole bands instead of atomic or molecular energy levels [Agrawal and Dutta, 1986; Petermann, 1988; Wilson and Hawkes, 1989; Saleh and Teich, 1991]. Finally, in class A lasers population inversion and material polarization decay much faster than the electric field. Both material variables can be adiabatically eliminated, and the equation for the electric field is enough to describe the dynamical evolution of the system. Some properties of class A lasers, like a dye laser, are studied in [Hernández-García *et al.*, 1990; Ciuchi *et al.*, 1991].

A description simpler than (4.5 - 4.7) can still be obtained when averaging over the z direction and considering single–mode emission (longitudinal, lateral and transversal mode emission). This simple set of equations is called *rate equations* [Statz and deMars, 1960; Tang *et al.*, 1963]. As already pointed out, in semicon-

ductor lasers, and after eliminating the polarization, one ends up with only two equations that describe the slowly varying amplitude of the electric E and the number of carriers N. By taking $\frac{dP}{dt} = 0$ in (4.6) and changing $E \rightarrow E \exp(i\alpha\gamma t/2)$, Eqs. (4.5) and (4.7) become

$$\dot{E} = \frac{(1 + i\,\alpha)}{2}\,[G - \gamma]\,E, \tag{4.8}$$

$$\dot{N} = \frac{J}{e} - \gamma_N\,N - G\,|E|^2, \tag{4.9}$$

where $G = G(N) = g_N\,(N - N_o)$, J accounts for the injection current, and e is the electronic charge ($e = 1.6 \times 10^{-19} C$).

In Eq. (4.8), there is a competition between the gain, G, and the losses, γ, terms. However, the previous expression for G is incomplete since it does not account for some effects as the spectral and spatial hole burning [Agrawal, 1987] or carrier heating [Kressel and Ippen, 1987]. A more general expression for G considering these factors yields [Agrawal and Dutta, 1986]

$$G = G(N, |E|^2) = g_N\,\frac{N - N_o}{1 + s|E|^2}, \tag{4.10}$$

where s is the saturation coefficient and g_N is a constant.

For semiconductor lasers, α is called the linewidth enhancement factor and is defined as the ratio between the derivatives of the real and imaginary parts of the carrier–dependent susceptibility with respect to the carrier density [Henry, 1982]. It considers the fact that, in semiconductor lasers, the lasing transitions occur between energy bands instead of energy levels, giving an asymmetry in the gain spectrum.

In Eqs. (4.8) and (4.9), the effect of spontaneous emission, as a source of radiation, has to be included. This can be treated quantum mechanically, via quantum Langevin equations, or via the density matrix equations. In previous works [Henry, 1982; Henry, 1983] the effect of spontaneous emission was incorporated in the rate equations in the form of noise terms and the resulting equations, interpreted in the Itô sense, are

$$\dot{E} = \frac{(1 + i\,\alpha)}{2}\,[G(N, |E|^2) - \gamma]\,E + \sqrt{2\,\varepsilon\,N}\,\xi_E(t), \tag{4.11}$$

$$\dot{N} = \frac{J}{e} - \gamma_N\,N - G(N, |E|^2)\,|E|^2 - \sqrt{2\,\varepsilon\,N}\,(E^*\,\xi_E(t) + E\,\xi_E^*(t)) + \sqrt{2\,\gamma_N\,N}\,\xi_N(t). \tag{4.12}$$

ε is the spontaneous emission rate. $\xi_E(t)$ is a complex Langevin noise term accounting for the stochastic nature of spontaneous emission and $\xi_N(t)$ describes random non–radiative carrier recombination due to thermal fluctuations. They are considered as Gaussian noise terms of zero mean and correlations

$$\langle \xi_i(t)\,\xi_j(t') \rangle = \delta_{ij}\,\delta(t - t'), \tag{4.13}$$

where ξ_i, ξ_j denote $Re(\xi_E)$, $Im(\xi_E)$ and ξ_N.

Equations (4.11) and (4.12) can be written in terms of the intensity and phase, $E = \sqrt{I}\,\exp(i\phi)$ such that

$$\dot{I} = [G(N,I) - \gamma]\, I + 4\varepsilon\, N + \sqrt{8\,\varepsilon\, N\, I}\,\xi_I(t), \tag{4.14}$$

$$\dot{\phi} = \frac{1}{2}\,\alpha\,[G(N,I) - \gamma] + \sqrt{\frac{2\,\varepsilon\, N}{I}}\,\xi_\phi(t), \tag{4.15}$$

$$\dot{N} = \frac{J}{e} - \gamma_N\, N - G(N,I)\, I - \sqrt{8\,\varepsilon\, N\, I}\,\xi_I(t) + \sqrt{2\gamma_N\, N}\,\xi_N(t), \tag{4.16}$$

where $\xi_I(t)$, $\xi_\phi(t)$ and $\xi_N(t)$ are real gaussian noise terms of zero mean and correlations

$$\langle \xi_i(t)\, \xi_j(t') \rangle = \delta_{ij}\, \delta(t - t'), \tag{4.17}$$

where i, j denote I, ϕ and N. $4\varepsilon N$ represents the mean power spontaneously emitted in the lasing mode.

The equations we have described are for semiconductor lasers (class B lasers). To obtain a set of equations for a class A laser, we can adiabatically eliminate N by setting $\dot{N} = 0$ in (4.9) and obtain N as a function of E. The resulting equation for the electric field after replacing in Eq. (4.8) is

$$\dot{E} = (1 + i\alpha) \left[\frac{g_N(J/e - \gamma_N N_o)/(2\gamma_N)}{1 + (\gamma_N s + g_N)|E|^2/\gamma_N} - \frac{\gamma}{2} \right] E. \tag{4.18}$$

We will devote the chapters of part II to the study of class A lasers. In part III we will study class B lasers.

Part II

Làsers de Classe A

Capítol 5

Làsers de Classe A: Potencial de Lyapunov

En aquest capítol es presenta un exemple d'utilització del potencial de Lyapunov (introduït en el capítol 2) en un sistema dinàmic. El sistema que es considera és el d'un làser de classe A (capítol 4).

La dinàmica del làser de classe A es descriu en termes de l'amplitud complexa lentament variable del camp elèctric, que es pot descompondre en les seves parts real i imaginària. Les equacions resultants són les (5.3) i (5.4), que es tracten en aquest capítol.

En primer lloc es considera el sistema determinista, menyspreant els termes de renou. El resultat de les simulacions es pot veure a les figures 5.1 i 5.2. Començant d'una condició inicial a prop de l'estat apagat, la intensitat es va atracant al seu estat estacionari, mentre que les parts real i imaginària del camp elèctric oscil·len en el temps fins també arribar a un valor constant. En el pla definit per les parts real i imaginària del camp, els sistema realitza una oscil·lació en forma d'espiral. El valor camp elèctric no depèn del paràmetre de disintonia (α), i l'única dependència amb el paràmetre α apareix en la velocitat angular (o equivalentment en la fase del camp elèctric).

Les equacions del làser de classe A constitueixen un flux potencial (5.10), on el paràmetre de disintonia no hi és inclòs. La matriu que relaciona les derivades del potencial amb les equacions de la dinàmica es designa com D, (5.11). Els punts fixos de la dinàmica determinista són els extrems del potencial. Per a un valor del guany fixat de manera que el làser estigui encès, la forma del potencial és del tipus *capell mexicà* (Fig. 5.5), té un màxim central i una corba de mínims que l'envolten. En la dinàmica transitòria, la part simètrica de D és la responsable de dur el sistema cap als mínims del potencial, seguint les línies de màxim pendent. La part antisimètrica (que és proporcional a α) indueix el moviment ortogonal a la direcció de variació màxima del potencial. Aquests dos efectes combinats (corresponents a les parts simètrica i antisimètrica del camp vectorial) produeixen la trajectòria espiral, abans esmentada, en el pla definit per les parts real i imaginària del camp elèctric, amb

una velocitat angular proporcional a α, Fig. 5.6. A partir del camp vectorial dels làsers de classe A, Figs. 5.7 i 5.9, es pot observar que la direcció de rotació (per a un α donat) és diferent entre la part interna i la part externa de les línies de potencial mínim.

La dinàmica de les equacions en presència de renou és tal que les característiques qualitatives de la dinàmica transitòria (a part de petites oscil·lacions degudes al renou) són les mateixes que el cas determinista. Ara bé, les diferències més importants apareixen a prop de la situació estacionària, a causa que l'estat final no té un valor constant per a la fase, sinó que la fase varia amb el temps, Figs. 5.10 i 5.11. En el cas de considerar les equacions amb renou és de gran utilitat considerar valors mitjos. El valor mig de la fase del camp elèctric varia, per a $\alpha \neq 0$, linealment amb el temps en l'estat estacionari, Fig. 5.13, efecte que anomenam *flux sostingut per renou*.

Aquestes característiques de la dinàmica amb renou es poden explicar mitjançant el potencial de Lyapunov, que s'havia obtingut per a la dinàmica determinista. La funció densitat de probabilitat estacionària ve donada a partir del potencial, Eq. (2.38), ja que la matriu D verifica les condicions corresponents. En termes de les variables intensitat i fase del camp elèctric, aquesta funció es pot escriure com a funcions independents de cadascuna de les variables. La funció densitat de probabilitat de la intensitat (5.17), té el seu màxim al valor mínim del potencial, que coincideix amb el valor estacionari de la dinàmica determinista (Fig. 5.14), i és asimètrica al voltant d'aquest màxim, Fig. 5.15. Amb aquesta funció densitat es poden calcular valors mitjos de les variables a l'estacionari. El valor mig de la intensitat a l'estacionari, que no depèn del paràmetre α, es pot calcular analíticament (5.19), el seu valor augmenta així com s'incrementa el valor del paràmetre de renou, Fig. 5.16.

El fet que la fase del camp elèctric fluctuï al voltant d'un valor mig que canvia linealment amb el temps també es pot explicar amb el potencial de Lyapunov. L'origen d'aquest flux sostingut per renou es pot entendre de la següent manera: els termes que indueixen rotació, els proporcionals a α, són zero a la línia de mínims de potencial, i per tant no actuaven a l'estat estacionari determinista. No obstant, les fluctuacions, que ara s'inclouen, permeten que el sistema explori regions de l'espai definit per les parts real i imaginària del camp elèctric on el potencial ja no té el seu valor mínim. La part antisimètrica de D (que conté el paràmetre α) és la responsable de la rotació a l'espai de fases. A causa que el valor mig de la intensitat és més gran que el valor determinístic de l'estat estacionari, el sistema passa més temps, en valor mig, en la part externa del mínim del potencial que en la part interna, i és per aquest motiu que hi ha una contribució distinta de zero al termes rotacionals produint la velocitat de fase observada. El valor mig de la velocitat de rotació es pot calcular a partir de la funció densitat de probabilitat (5.23). La rotació mitja és zero quan el terme de disintonia és zero o en el cas determinista; i a més, aquesta rotació té un sentit oposat al que es tenia en la dinàmica transitòria quan es partia de l'estat apagat. El canvi d'aquest valor mig de la freqüència amb el renou es veu en la figura 5.17.

Chapter 5

Class A Lasers: Lyapunov Potential

In this chapter, a first example of the use of Lyapunov potentials in a dynamical system is presented. The system we consider is a class A laser.

5.1 Model

For class A lasers, such as He-Ne laser, the dynamics of can be described in terms of the slowly varying complex amplitude E of the electric field [Haken, 1984], Eq. (4.18). The noise term is simply additive, as it is usually taken in this kind of lasers. The resulting equation is

$$\dot{E} = (1 + i\,\alpha)\left(\frac{\Gamma}{1 + \vartheta|E|^2} - \kappa\right) E + \zeta(t), \tag{5.1}$$

where α, ϑ, Γ and κ are real parameters. κ is the cavity decay rate; Γ the gain parameter; ϑ the saturation–intensity parameter, and α is the detuning parameter. Their relationship with the variables of class B lasers (4.8) and (4.9) are:

$$\Gamma = g_N\left(\frac{J}{e} - \gamma_N N_o\right)/(2\gamma_N), \quad \kappa = \gamma/2, \quad \vartheta = (g_N + s\gamma_N)/\gamma_N.$$

Another widely used model expands the nonlinear term to give a cubic dependence on the field (third order Lamb theory [Sargent *et al.*, 1974]), but this is not necessary here. Eq. (5.1) is written in a reference frame in which the frequency of the *on* steady state is zero (and the trivial solution has frequency $(\Gamma - \kappa)\alpha$ [Ciuchi *et al.*, 1991]). $\zeta(t)$ is a complex Langevin source term accounting for the stochastic nature of spontaneous emission. It is taken as a Gaussian white noise of zero mean and correlations

$$\langle \zeta(t)\,\zeta^*(t')\rangle = 4\,\Delta\,\delta(t - t'), \tag{5.2}$$

where Δ measures the strength of the noise.

By writing the complex variable E as $E = x_1 + i\,x_2$ and introducing a new dimensionless time such that $t \to \kappa\, t$, the evolution equations become

$$\dot{x}_1 = \left(\frac{a}{b + x_1^2 + x_2^2} - 1\right)\,(x_1 - \alpha\, x_2) + \xi_1(t), \tag{5.3}$$

$$\dot{x}_2 = \left(\frac{a}{b + x_1^2 + x_2^2} - 1\right)\,(\alpha\, x_1 + x_2) + \xi_2(t), \tag{5.4}$$

where $a = \Gamma/(\kappa\vartheta)$ and $b = 1/\vartheta$. $\xi_1(t)$ and $\xi_2(t)$ are white noise terms with zero mean and correlations given by equation (2.32) with $\epsilon = \Delta/\kappa$.

5.2 Class A lasers: Deterministic case

In this section, we consider the reduced equations for a class A laser in the absence of noise, i.e. in the case $\epsilon = 0$,

$$\dot{x}_1 = \left(\frac{a}{b + x_1^2 + x_2^2} - 1\right)\,(x_1 - \alpha\, x_2), \tag{5.5}$$

$$\dot{x}_2 = \left(\frac{a}{b + x_1^2 + x_2^2} - 1\right)\,(\alpha\, x_1 + x_2). \tag{5.6}$$

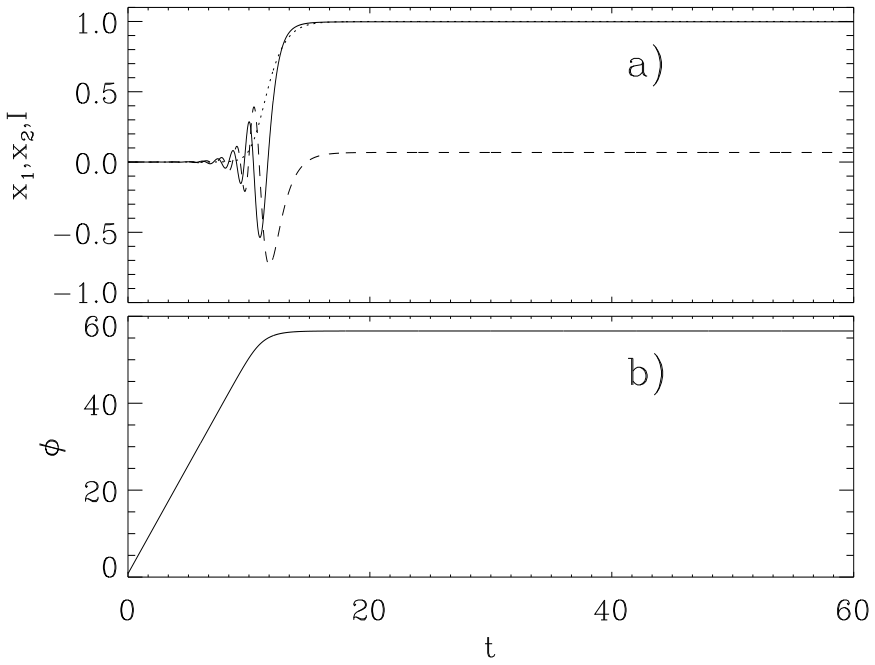

Figure 5.1: Simulation of Eqs. (5.5) and (5.6). (a) Dynamical evolution of x_1 (solid line), x_2 (dashed line) and $x_1^2 + x_2^2$ (dotted line) with time. (b) Phase evolution with time. Parameters: $a = 2$, $b = 1$, $\alpha = 5$. Initial conditions: $x_1 = 10^{-5}$, $x_2 = 10^{-5}$. Dimensionless units.

Performing the change of variables

$$I = x_1^2 + x_2^2 \quad \text{and} \quad \phi = \arctan\left(x_2/x_1\right), \tag{5.7}$$

one obtains a set of equations

$$\dot{I} = 2\left(\frac{a}{b+I} - 1\right) I, \tag{5.8}$$

$$\dot{\phi} = \left(\frac{a}{b+I} - 1\right) \alpha. \tag{5.9}$$

The steady state solutions of (5.8) and (5.9) give rise to two fixed points, one corresponding to the laser *off* ($I = 0$), and the other to the steady state of the system: $I_{st} = a - b$ and $\dot{\phi} = 0$ (fixed intensity and arbitrary phase).

Numerical simulations have been performed using a Runge–Kutta method (explained in chapter 2). When starting with an initial condition close to the *off* state, the intensity I monotonically approaches the steady state value I_{st} while the real and imaginary parts of the electric field (x_1 and x_2) oscillate in time until they reach a constant value, see Fig. 5.1 (a). In Fig. 5.1 (b), it can be seen that the continuous phase (defined between $-\infty$ and ∞) increases until it arrives to a constant value. Fig. 5.2 shows that the imaginary part versus the real part of the field spirals to the fixed point.

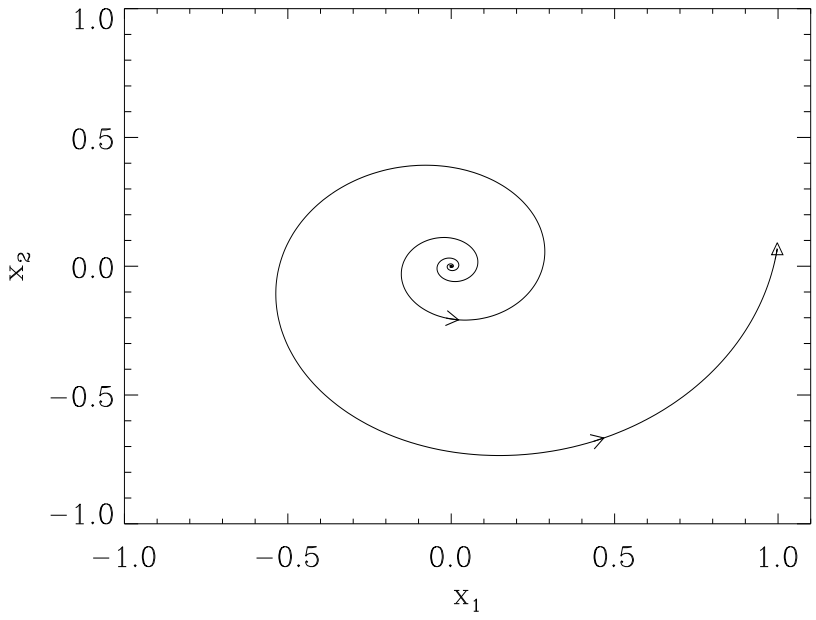

Figure 5.2: x_2 versus x_1 for Eqs. (5.5) and (5.6). Parameters: $a = 2$, $b = 1$, $\alpha = 5$. Initial conditions: $x_1 = 10^{-5}$, $x_2 = 10^{-5}$. Dimensionless units.

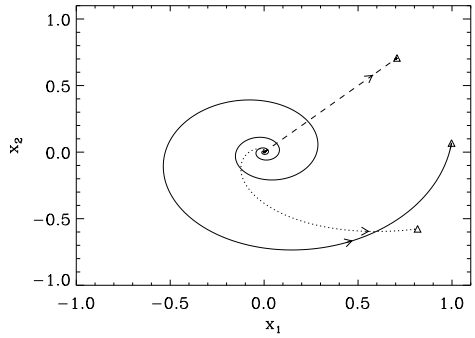

Figure 5.3: x_2 versus x_1 for Eqs. (5.5) and (5.6). Parameters: $a = 2$, $b = 1$. $\alpha = 5$ (solid line), $\alpha = 1$ (dotted line), $\alpha = 0$ (dashed line). Initial conditions: $x_1 = 10^{-5}$, $x_2 = 10^{-5}$. Dimensionless units.

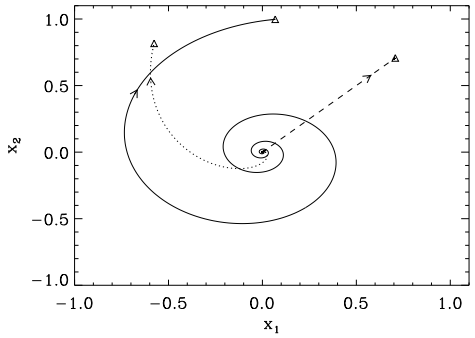

Figure 5.4: x_2 versus x_1 for Eqs. (5.5) and (5.6). Parameters: $a = 2$, $b = 1$. $\alpha = 0$ (dashed line), $\alpha = -1$ (dotted line), $\alpha = -5$ (solid line). Initial conditions: $x_1 = 10^{-5}$, $x_2 = 10^{-5}$. Dimensionless units.

It is worth noting that the final value I_{st} does not depend on α, and the only dependence on α appears in the angular velocity (or equivalently in the phase), as it is shown in Figs. 5.3 and 5.4. In these figures, it can be seen that when α increases the rotation speed increases in the (x_1, x_2) plane, and when the sign of α changes, the rotation sense inverts. Here we have used large values of the parameter α. With these values of α, the influence of this parameter in the dynamical equations can be clearly seen.

Equations (5.5) and (5.6) constitute a potential flow of the form (2.26) where the potential $V(\mathbf{x})$ is given by ([Haken, 1983])

$$V(x_1, x_2) = \frac{1}{2}\left[x_1^2 + x_2^2 - a\,\ln(b + x_1^2 + x_2^2)\right] \tag{5.10}$$

and the matrix $D(\mathbf{x})$ (split into symmetric and antisymmetric parts)

$$D = S + A = \begin{pmatrix} 1 & 0 \\ 0 & 1 \end{pmatrix} + \begin{pmatrix} 0 & -\alpha \\ \alpha & 0 \end{pmatrix}. \tag{5.11}$$

A simpler expression for the potential is given in [Risken, 1989] and [Haken, 1984] valid for the case in which the gain term is expanded in Taylor series.

When writing the potential in terms of I and ϕ, it appears to be independent of the phase (rotational symmetry in the plane (x_1, x_2)),

$$V(I, \phi) = \frac{1}{2}\left[I - a\,\ln(b + I)\right]. \tag{5.12}$$

By using this potential, one can obtain the fixed points of the set of equations and also the transient dynamics.

According to our discussion of chapter 2, the fixed points of the deterministic dynamics are the extrema of the potential $V(\mathbf{x})$: for $a > b$ there is a maximum at

$(x_1, x_2) = 0$ (corresponding to the laser in the *off* state) and a curve of minima given by $x_1^2 + x_2^2 = a - b$ (see Fig. 5.5). The asymptotic stable situation, then, is that the laser switches to the *on* state reaching an intensity $I \equiv |E|^2 = x_1^2 + x_2^2 = a - b$. For $a < b$ the only (stable) fixed point is the *off* state $I = 0$. In this case, the shape of the potential is not the one appearing in Fig. 5.5 but V is paraboloidal.

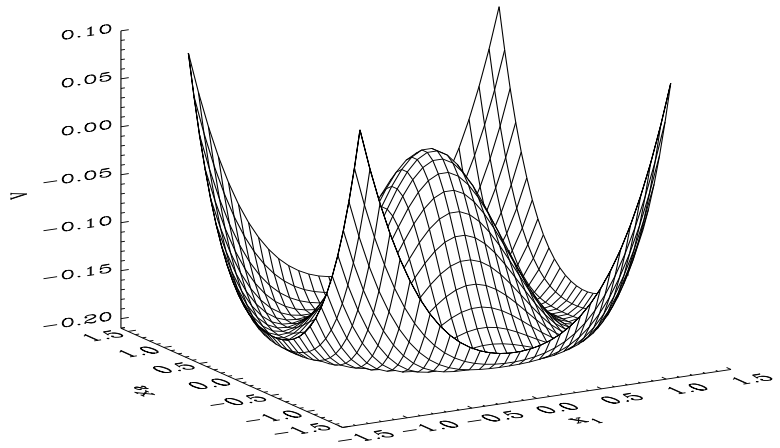

Figure 5.5: Potential for a class A laser, Eq. (5.10) with the parameters: $a = 2$, $b = 1$. Dimensionless units.

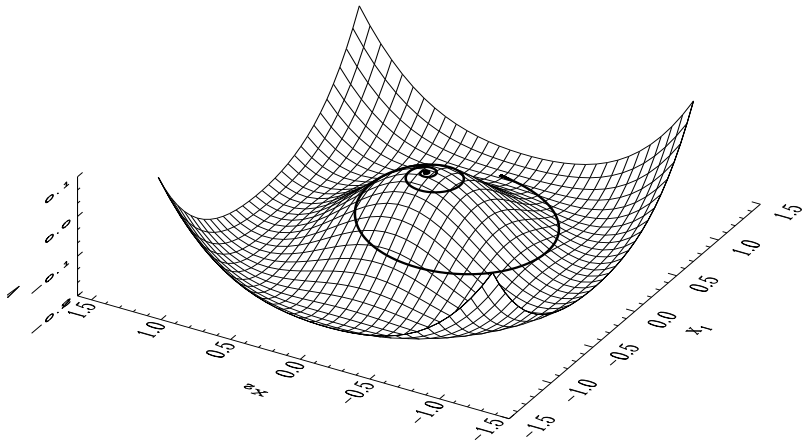

Figure 5.6: Potential for a class A laser, Eq. (5.10) with the parameters: $a = 2$, $b = 1$. Solid line: simulation of Eqs. (5.5) and (5.6) (same as in Figs. 5.1 and 5.2, $\alpha = 5$). Initial conditions: $x_1 = 10^{-5}$, $x_2 = 10^{-5}$. Dimensionless units.

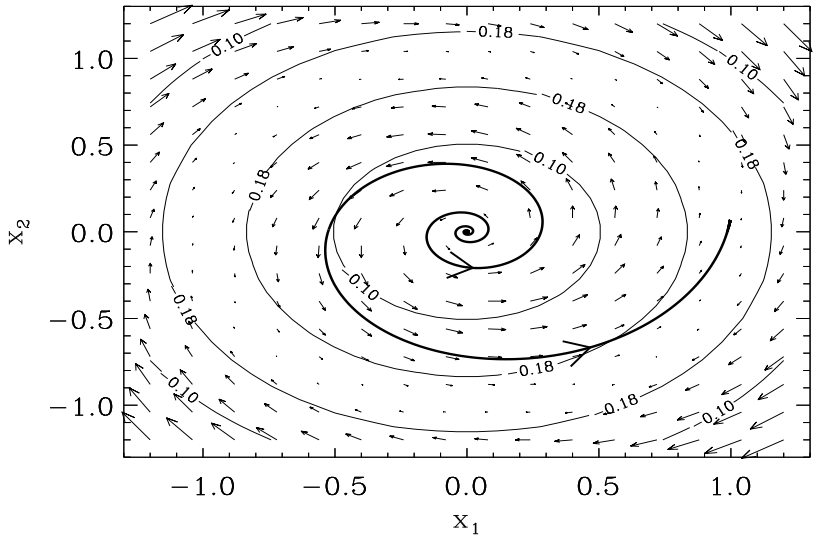

Figure 5.7: Vector field for a class A laser. Thick solid line: simulation of Eqs. (5.5) and (5.6). Thin lines are the equipotential curves of Eq. (5.10) and the arrows indicate the sense of the flow. Parameters: $a = 2$, $b = 1$, $\alpha = 5$. Initial conditions: $x_1 = 10^{-5}$, $x_2 = 10^{-5}$. Dimensionless units.

In the transient dynamics, the symmetric matrix S is responsible for driving the system towards the minima of V following the lines of maximum slope of V. The antisymmetric part A (which is proportional to α) induces a movement orthogonal to the direction of maximum variation of $V(\mathbf{x})$. The combined effects of S and A produce a spiraling trajectory in the (x_1, x_2) plane, with an angular velocity proportional to α, see Figs. 5.6 and 5.7.

Asymptotically, the system tends to one of the minima in the line $I = a - b$, the exact location depending on the initial conditions. The potential decreases in time until it arrives at its minimum value: $V(x_1^2 + x_2^2 = a - b) = \frac{1}{2}[a - b - a \ln(a)]$ (see Fig. 5.8).

The different rotation speeds and directions that one could observe in Figs. 5.3 and 5.4 can be explained with the antisymmetric part of the equations. This can be seen by comparing Figs. 5.7 and 5.9 where we have taken different signs of the value of α. In the case of $\alpha = 0$ the antisymmetric part is zero, and there is no rotation in the plane (x_1, x_2) (Fig. 5.12).

Another interesting feature that has to be mentioned here is that the direction of rotation for a given α is different for the internal part of the lines of minimal potential and the external part, see Figs. 5.7 and 5.9. This implies, for $\alpha > 0$, that the trajectories starting near the *off* state will rotate counterclockwise, while those starting with an intensity larger than the equilibrium value, $I > I_{st}$, will rotate clockwise. This difference in the direction of rotation will have an interesting effect in the presence of noise, as discussed in the next section.

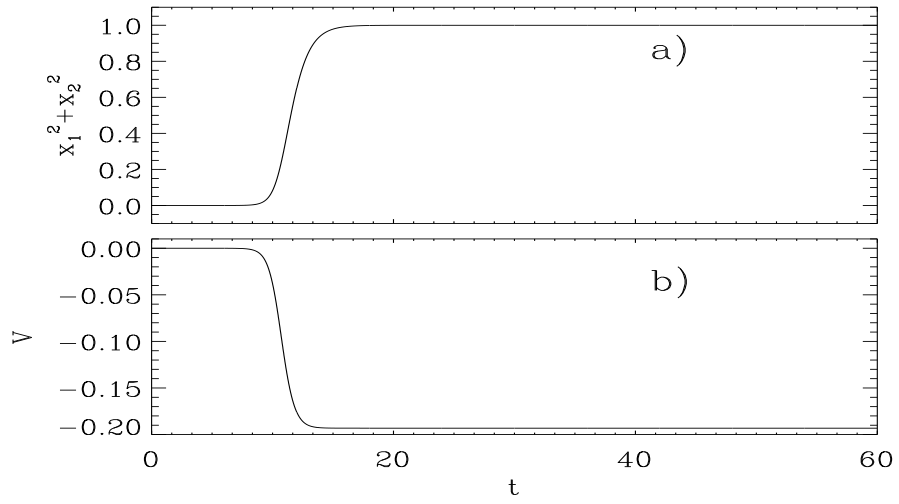

Figure 5.8: Simulation of Eqs. (5.5) and (5.6). (a) Dynamical evolution of the intensity $x_1^2 + x_2^2$ with time. (b) Evolution of the potential given by Eq. (5.10) with time. Parameters: $a = 2$, $b = 1$, $\alpha = 5$. Initial conditions: $x_1 = 10^{-5}$, $x_2 = 10^{-5}$. Dimensionless units.

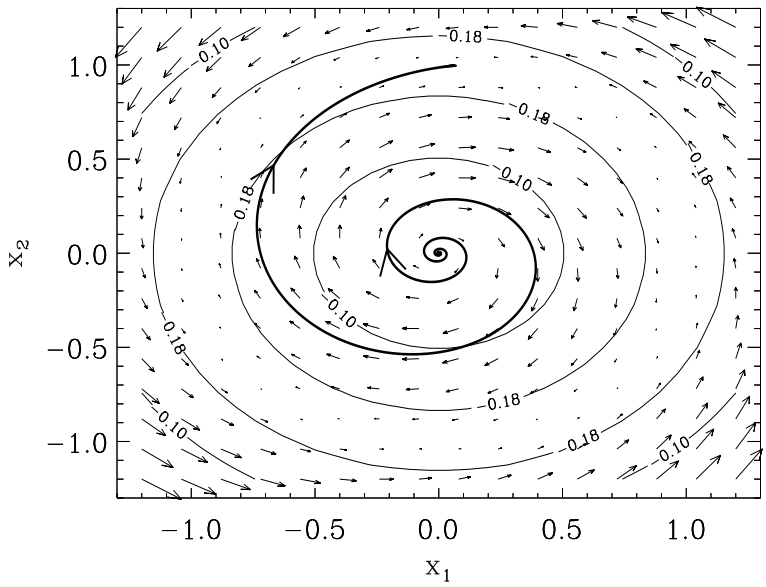

Figure 5.9: Vector field for a class A laser. Thick solid line: simulation of Eqs. (5.5) and (5.6). Thin lines are the equipotential curves of Eq. (5.10) and the arrows indicate the sense of the flow. Parameters: $a = 2$, $b = 1$, $\alpha = -5$. Initial conditions: $x_1 = 10^{-5}$, $x_2 = 10^{-5}$. Dimensionless units.

5.3 Class A lasers with noise

In this section, we consider the set of equations for class A laser in the presence of noise:

$$\dot{x}_1 = \left(\frac{a}{b + x_1^2 + x_2^2} - 1\right)(x_1 - \alpha\, x_2) + \xi_1(t), \tag{5.13}$$

$$\dot{x}_2 = \left(\frac{a}{b + x_1^2 + x_2^2} - 1\right)(\alpha\, x_1 + x_2) + \xi_2(t). \tag{5.14}$$

In the presence of moderate levels of noise, the qualitative features of the transient dynamics remain the same as in the deterministic case. The most important differences appear near the stationary situation.

We have performed simulations of Eqs. (5.13) and (5.14) using the Heun method (2.20) explained in chapter 2. In this case, one can take initial conditions in ($x_1 = 0, x_2 = 0$) and the small fluctuations, induced by noise terms, take the system away from the "off" state. The transient dynamics, see Fig. 5.10, is quite similar to that in the deterministic case (compare with Fig. 5.7). However, the final state does not have a constant phase but it changes in time. The direction in which the phase changes is not constant but varies in time, see Fig. 5.11.

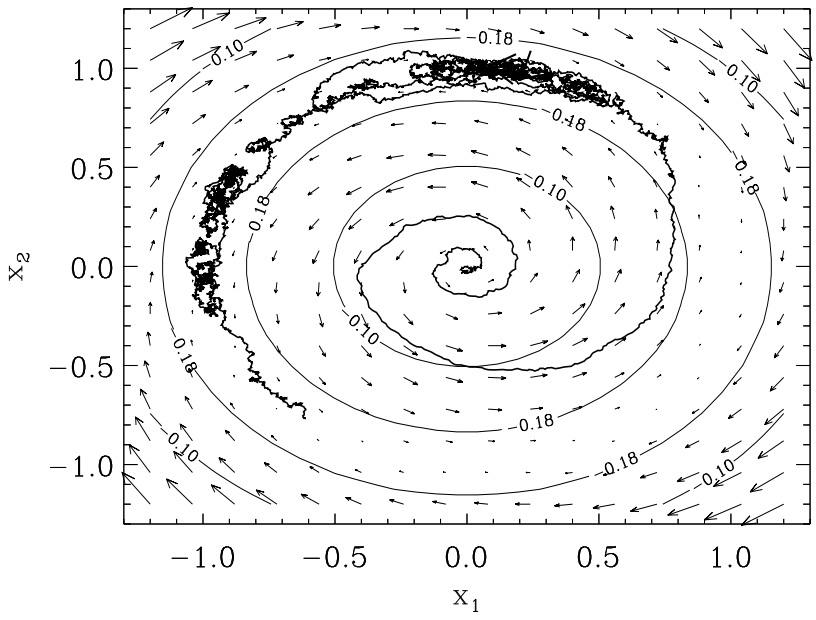

Figure 5.10: Vector field for a class A lasers. Thick solid line: simulation of Eqs. (5.13) and (5.14). Thin lines are the equipotential curves of Eq. (5.10) and the arrows indicate the sense of the flow. Parameters: $a = 2$, $b = 1$, $\alpha = 5$, $\epsilon = 0.001$. Initial conditions: $x_1 = 0$, $x_2 = 0$. Dimensionless units.

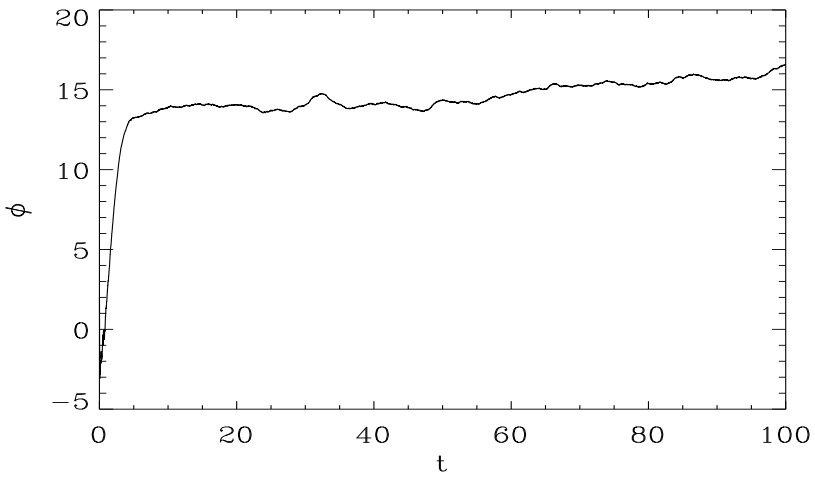

Figure 5.11: Phase evolution with time from the simulation of Eqs. (5.13) and (5.14). Parameters: $a = 2$, $b = 1$, $\alpha = 5$, $\epsilon = 0.001$. Initial conditions: $x_1 = 0$, $x_2 = 0$. Dimensionless units.

Therefore, for $\alpha \neq 0$ the real and imaginary parts of E oscillate not only in the transient dynamics but also in the steady state. The frequency of the oscillations still depends on α (as well as ϵ), while the amplitude of the oscillations depends on the noise strength ϵ.

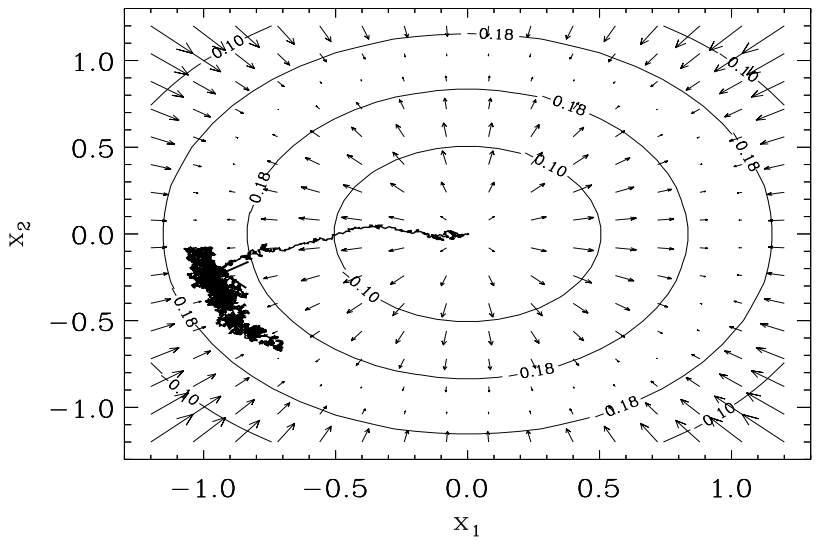

Figure 5.12: Vector field for a class A lasers. Thick solid line: simulation of Eqs. (5.13) and (5.14). Thin lines are the equipotential curves of Eq. (5.10) and the arrows indicate the sense of the flow. Parameters: $a = 2$, $b = 1$, $\alpha = 0$, $\epsilon = 0.001$. Initial conditions: $x_1 = 0$, $x_2 = 0$. Dimensionless units.

For $\alpha = 0$ there is only phase diffusion around the circumference $x_1^2 + x_2^2 = a - b$ that represents the set of all possible deterministic equilibrium states [Ciuchi *et al.*, 1991] (compare Figs. 5.10 and 5.12 which cover the same simulation time).

A small value of the parameter ϵ has been considered in these figures, allowing only a small deviation of the dynamical evolution in the plane (x_1, x_2) around the deterministic steady state (intensity is almost constant). When ϵ increases, the range of values available around the steady state also increases. As the final value of the intensity is approached, and for $\alpha \neq 0$, the phase rotation speed slows down and the mean value of the phase ϕ, of the electric field E, changes linearly with time also in the steady state, see Fig. 5.13.

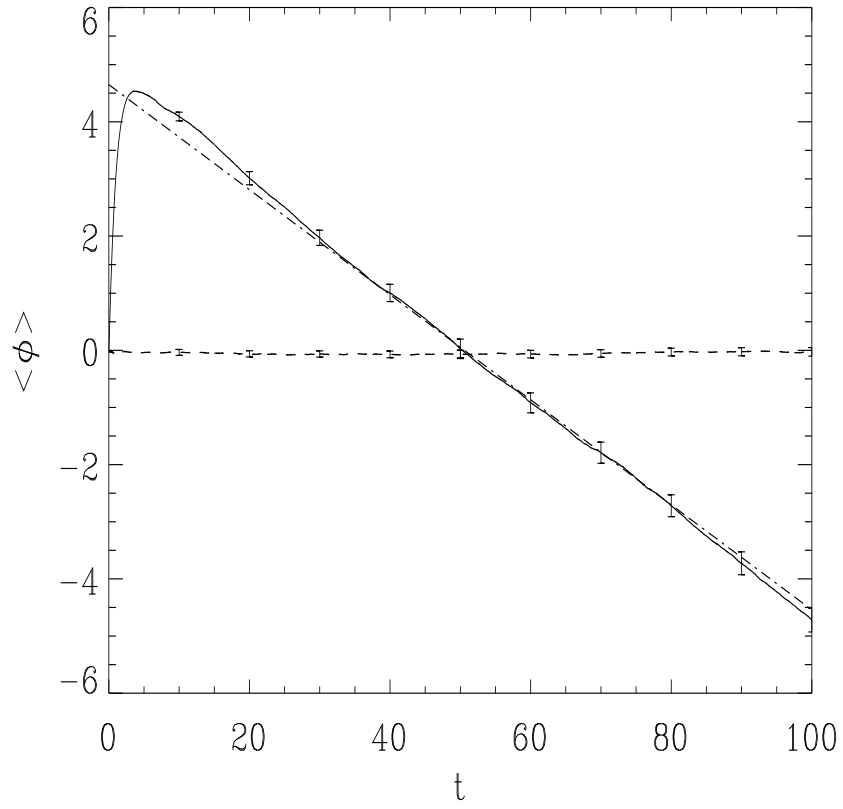

Figure 5.13: Time evolution of the mean value of the phase ϕ in a class A laser, in the case $a = 2$, $b = 1$, $\epsilon = 0.1$. For $\alpha = 0$ (dashed line) there is only phase diffusion and the average value is 0 for all times. When $\alpha = 5$ (solid line) there is a linear variation of the mean value of the phase. Error bars are included for some values. The dot–dashed line has the slope given by the theoretical prediction Eq. (5.23). The initial condition is taken as $x_1 = x_2 = 0$ and the results were averaged over 10000 trajectories with different realizations of the noise. Initial conditions: $x_1 = 0$, $x_2 = 0$. Dimensionless units.

We can understand these aforementioned features of the noisy dynamics using the deterministic Lyapunov potential $V(x_1, x_2)$. Since conditions (2.35), (2.36) and (2.37) are satisfied, the stationary probability distribution is given by (2.38) with $V(x_1, x_2)$ given by (5.10). By changing variables to intensity and phase, we find that the probability density functions for I and ϕ are independent functions (due to the form of the potential (5.12))

$$P_{st}(I, \phi) = P_{st}(I)\, P_{st}(\phi), \tag{5.15}$$

where

$$P_{st}(\phi) = \frac{1}{2\pi} \tag{5.16}$$

is a constant and

$$P_{st}(I) = Z^{-1}\, \mathrm{e}^{-I/(2\,\epsilon)}\, (b + I)^{a/(2\,\epsilon)}, \tag{5.17}$$

where the normalization constant is given by

$$Z = (2\epsilon)^{\frac{a}{2\,\epsilon}+1}\, \mathrm{e}^{\frac{b}{2\,\epsilon}}\, \Gamma\left(\frac{a}{2\,\epsilon} + 1, \frac{b}{2\,\epsilon}\right), \tag{5.18}$$

and $\Gamma(x, y)$ is the incomplete Gamma function. From this expression, we see that, independently of the value of ϵ, $P_{st}(I)$ has its maximum at the deterministic stationary value $I_m = a - b$, and by increasing ϵ the shape of the distribution becomes more asymmetric, see Figs. 5.14 and 5.15.

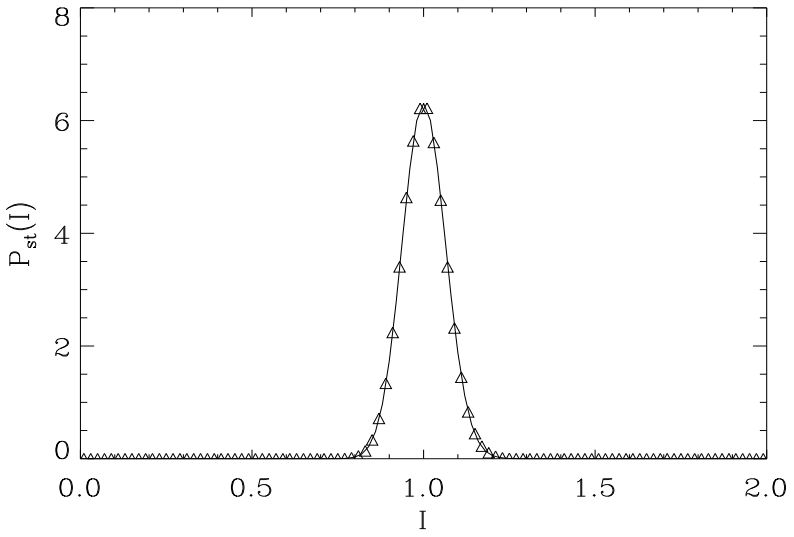

Figure 5.14: Probability distribution function for $I = x_1^2 + x_2^2$ in a class A laser, in the case $a = 2$, $b = 1$, $\epsilon = 0.001$. Dots correspond to the histogram obtained with the simulation of Eqs. (5.13) and (5.14). The solid line correspond to Eq. (5.17). Dimensionless units.

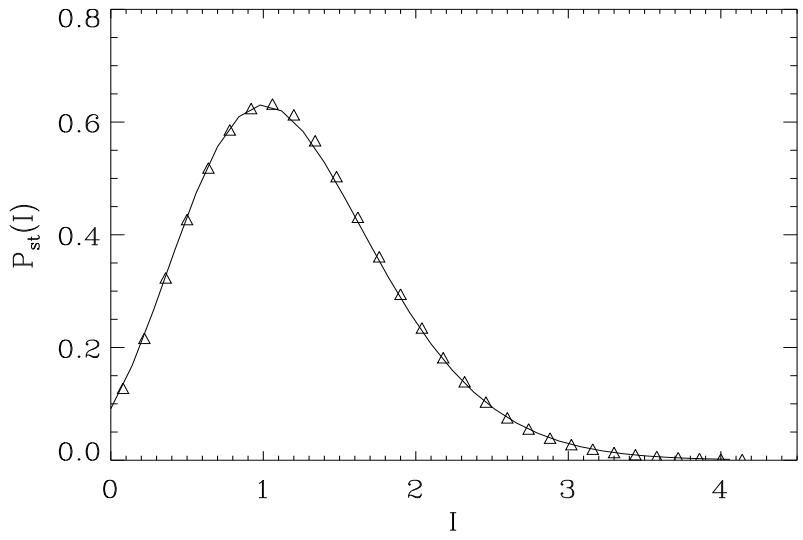

Figure 5.15: Probability distribution function for $I = x_1^2 + x_2^2$ in a class A laser, in the case $a = 2$, $b = 1$, $\epsilon = 0.1$. Dots correspond to the histogram obtained with the simulation of Eqs. (5.13) and (5.14). The solid line correspond to Eq. (5.17). Dimensionless units.

Starting from a given initial condition corresponding, for instance, to the laser in the *off* state, the intensity fluctuates around a mean value that increases monotonically with time. In the stationary state, the intensity fluctuates around the deterministic value $I_m = a - b$ but, since the distribution (5.17) is not symmetric around I_m, the mean value $\langle I \rangle_{st}$ is larger than the deterministic value. By using (5.17) and (2.39) one can easily find that

$$\langle I \rangle_{st} = (a - b) + 2\,\epsilon \left[1 + \frac{\exp(-b/2\,\epsilon)\,(b/2\,\epsilon)^{\frac{a}{2\epsilon}+1}}{\Gamma\left(\frac{a}{2\,\epsilon}+1, \frac{b}{2\,\epsilon}\right)} \right]. \tag{5.19}$$

The evolution of this mean value in terms of the parameter ϵ is plotted in Fig. 5.16. The mean value of I_{st} increases as the noise strength increases. In the deterministic case one obtains the value corresponding to the minimum of the potential.

An expression for the mean value of the intensity in the steady state was also given in [Risken, 1989], valid for the case in which the saturation terms in the dynamical equations are expanded to third order in the field amplitude.

As mentioned before, in the steady state of the stochastic dynamics, the phase ϕ of the electric field fluctuates around a mean value that changes linearly with time. Since any value of ϕ can be mapped into the interval $[0, 2\pi)$, this is consistent with the fact that the stationary distribution for ϕ is uniform, Eq. (5.16). We can easily understand the origin of this *noise sustained flow*: the rotation inducing terms, proportional to α in the equations of motion, are zero at the line of minima of the potential V and, hence, do not act in the deterministic steady state. Fluctuations

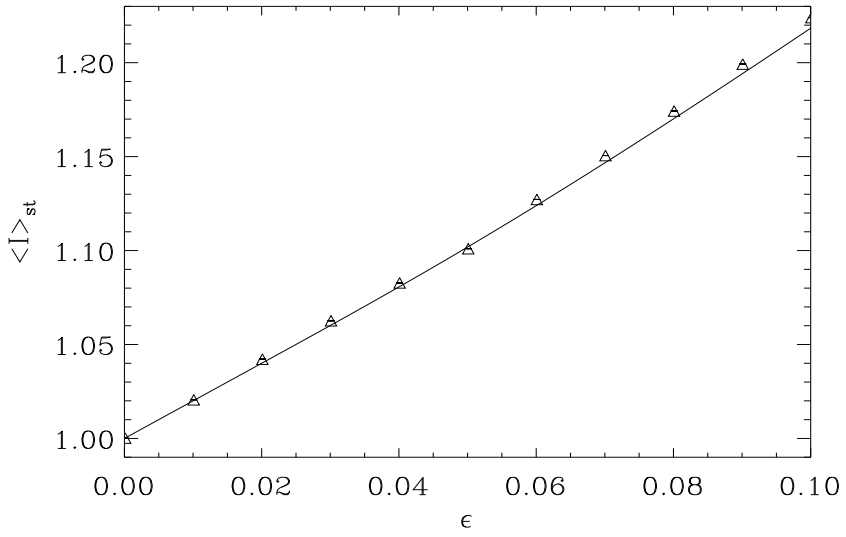

Figure 5.16: Evolution of $< I >_{st}$ with ϵ. Solid line, with Eq. (5.19). Points correspond to the mean values obtained by different simulations of Eqs. (5.13) and (5.14). $a = 2$ and $b = 1$.

allow the system to explore regions of the configuration space (x_1, x_2) where the potential is not at its minimum value. The antisymmetric part of the matrix D (which contains the parameter α) is then the responsible for the rotation in the plane (x_1, x_2). According to Eq. (5.19) the mean value of I is not at the minimum of the potential because there is, on average, a nonzero contribution of the rotational terms producing the observed phase drift.

The rotation speed can be calculated by writing the evolution equation for the phase of the electric field. After a change of variables in Eqs. (5.13 – 5.14) to intensity and phase, $x_1 + ix_2 = \sqrt{I}e^{i\phi}$, the evolution equations become (Itô sense)

$$\dot{I} = \left(\frac{a}{b+I} - 1\right) 2\,I + 4\,\epsilon + 2\sqrt{I}\,\xi(t), \tag{5.20}$$

$$\dot{\phi} = \left(\frac{a}{b+I} - 1\right) \alpha + \frac{1}{\sqrt{I}}\,\xi(t), \tag{5.21}$$

where $\xi(t)$ is a white noise term with zero mean value and correlations given by (2.32). In these equations one can see that apart from the stochastic noise terms, in the first equation it appears an extra term corresponding to the mean number of photons spontaneously emitted. Hence, the steady state is not $\langle I \rangle_{st} = a - b$ but it has a corrective term depending on ϵ as shown in (5.19).

By taking the average value of (5.21) and using the rules of the Itô calculus (the mean value of the last term of that equation is zero), one gets

$$\langle \dot{\phi} \rangle = \alpha \left\langle \frac{a}{b+I} - 1 \right\rangle. \tag{5.22}$$

By using the distribution (5.17) and the expression (2.39), one obtains the stochastic frequency shift

$$\langle \dot{\phi} \rangle_{st} = -\alpha \, \frac{\exp(-b/2\,\epsilon)\,(b/2\,\epsilon)^{\frac{a}{2\epsilon}}}{\Gamma\left(\frac{a}{2\,\epsilon}+1, \frac{b}{2\,\epsilon}\right)}. \tag{5.23}$$

Notice that this average rotation speed is zero in the case of no detuning ($\alpha = 0$) or for the deterministic dynamics ($\epsilon = 0$) and that, due to the minus sign, the rotation speed is opposite to that of the deterministic transient dynamics when starting from the *off* state. These results are in excellent agreement with numerical simulations of the rate equations in the presence of noise (see Fig. 5.13). The evolution of the mean value of the frequency with ϵ is plotted in Fig. 5.17. One can see the phase drift is negligible for a small values of ϵ.

The noise sustained flow we have obtained in this laser system implies that the laser frequency will be shifted with respect to the deterministic one in the presence of noise. It would be interesting to check experimentally the existence of this noise induce phase drift. However, according to our results, the noise intensity required for an observable phase drift is much larger than the typical noise intensity in experiments. Nevertheless, this necessary extra noise could be externally induced.

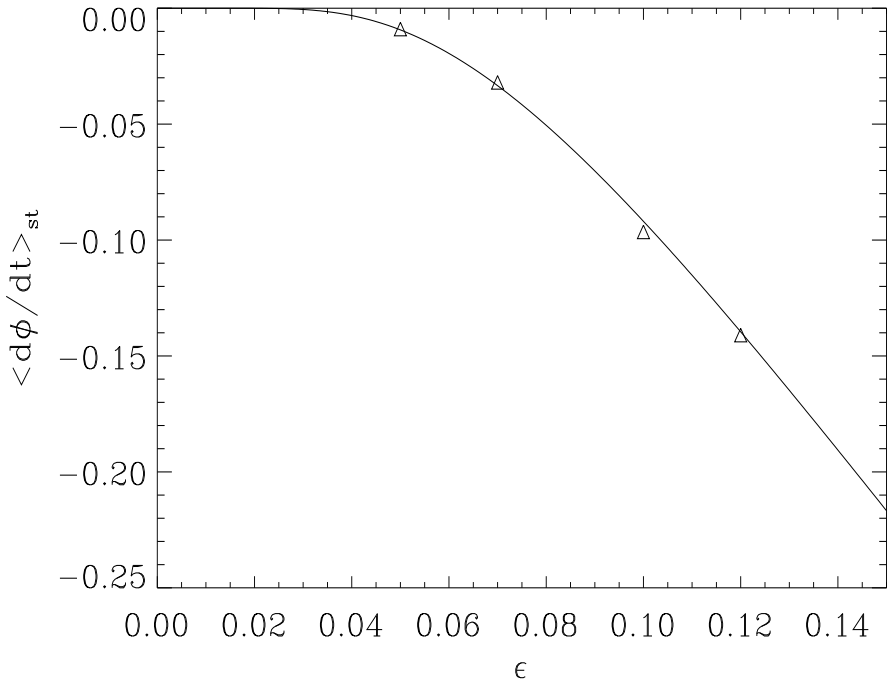

Figure 5.17: $< \dot{\phi} >_{st}$ versus ϵ as given by (5.23). Points correspond to the mean values obtained by simulating Eqs. (5.13) and (5.14). $a = 2$, $b = 1$ and $\alpha = 5$.

Capítol 6

Làsers de Classe A amb senyal injectat: Conjunt de bifurcacions i potencial de Lyapunov

En aquest capítol es descriu el conjunt de bifurcacions (capítol 3) per a un làser de classe A amb senyal injectat, en termes de l'amplitud, ρ, i freqüència, η, del senyal que s'aplica. A més, s'explica el comportament dinàmic d'aquests tipus de làsers, en els casos que es possible, en termes del potencial de Lyapunov (capítol 2).

El sistema que es considera és el d'un làser de classe A (capítol 4) amb un camp òptic monocromàtic aplicat. La dinàmica del sistema ve donada per la variació temporal del camp elèctric, Eq. (6.1). Escrivint les equacions en el sistema de referència que rota amb la freqüència del camp aplicat, les equacions que s'obtenen per a les parts real i imaginària del camp elèctric són les que es tracten en aquest treball, (6.3 – 6.4) (Els punts fixos d'aquestes equacions corresponen, en el sistema de referència inicial (6.1), a una solució per a les variables que oscil·la a la mateixa freqüència del camp aplicat).

La dinàmica del sistema és tal que, per a valors petits de η el sistema oscil·la en el pla definit per les parts real i imaginària del camp elèctric fins arribar a un punt fix. Quan s'augmenta el valor de la freqüència per damunt d'un cert valor, η_L, la intensitat del camp elèctric té un valor aproximadament constant, però la fase evoluciona linealment amb el temps.

Per a valors més grans de η i depenent del valor de ρ, la dinàmica és més complexa i apareixen distints possibles estats estacionaris. En la secció 6.2, es descriu el conjunt de bifurcacions complet, format per les distintes regions de l'espai de paràmetres (ρ, η), amb diferent comportament qualitatiu a l'estat estacionari. El conjunt de bifurcacions obtingut és el que apareix a la figura 6.2, i les distintes regions senyalades tenen punts fixos i òrbites periòdiques amb l'estabilitat que apareix a la Taula 6.1. En la bifurcació sella–node, línea sòlida, dos punts fixos col·lapsen a l'espai de fases i desapareixen (per exemple de la regió 5 a la 1). A la bifurcació de Hopf, línees a trossos curts, un punt fix canvia la seva estabilitat i es crea una

òrbita periòdica (com passant de la regió 2 a la 3). En les òrbites homoclíniques (línees de punts), l'òrbita periòdica va augmentant el seu període fins arribar a infinit en la corba homoclínica i allà desapareix, per exemple acostant–se de la regió 3 cap a la 4. La intersecció entre les bifurcacions sella–node, Hopf i homoclínica és una singularitat Takens–Bogdanov [els dos punts gruixuts de la figura 6.2 (a)]. Les zones de coincidència entre les corbes sella–node i òrbites homoclíniques, corresponen a bifurcacions Andronov–Leontovich: una òrbita periòdica en la regió on no hi ha punts fixos col·lisiona a l'òrbita homoclínica amb el punt fix sella–node. Cal notar que hi existeixen aquest tipus de bifurcacions a cada una de les branques de la bifurcació sella–node. En línies a trossos llargs apareix la bifurcació sella–node d'òrbites periòdiques: passant de la regió 6 a la 7 dues òrbites periòdiques de distinta estabilitat col·lisionen i es destrueixen.

En la secció 6.3, apareix el potencial (6.25) en el cas de considerar un camp real, $\eta = 0$. Té la forma de *capell mexicà* inclinat, Fig. 6.9. La dinàmica transitòria del sistema va cap a l'estacionari seguint una trajectòria espiral, igual que en el cas $\rho = 0$, capítol 5. A causa de la inclinació del potencial, es romp la simetria de fase pel sistema, i l'estat final és fixat per a la intensitat i la fase. La bifurcació sella–node en la línia $\eta = 0$ es pot obtenir partint que el potencial és més inclinat per a valors més grans de ρ, i en aquesta bifurcació els punts fixos sella i inestable desapareixen.

En el cas $\rho = 0$, $\eta \neq 0$, el sistema es pot escriure en termes d'un flux potencial, (2.26). El potencial és el mateix que en el cas sense injecció (5.10), i el terme residual (6.27) conté el terme de la freqüència. El cas determinista es pot entendre com el moviment damunt la superfície del potencial cap al mínim. En el mínim, la part residual actua donant el moviment harmònic de freqüència la d'injecció.

La forma qualitativa del potencial en alguna regió del cas general ($\rho \neq 0$, $\eta \neq 0$) es pot inferir a partir del potencial en els dos casos límits descrits. Per a un valor de $\rho \neq 0$, es va augmentant η partint de $\eta = 0$. Inicialment el potencial té la forma del potencial inclinat en una direcció; quan s'augmenta η, el potencial es deforma de manera que els punts mínim i sella es van apropant, fins a desaparèixer en la bifurcació sella–node. Apareixeria un conjunt de mínims en forma d'el·lipse, on els termes residuals serien els responsables del moviment periòdic en l'estat estacionari. L'el·lipse de mínims es deformaria contínuament en la regió 9 fins arribar a ser, quan es va disminuint ρ, el capell mexica en la línia $\rho = 0$.

En presència de renou, la funció densitat de probabilitat estacionària es pot obtenir a partir del potencial (en el cas $\rho\eta = 0$), (6.33). La intensitat fluctua al voltant del valor determinista, però com la funció densitat de probabilitat no és simètrica, el valor mig de la intensitat és major que el valor determinista, Fig. 6.11. La fase del camp elèctric també fluctua al voltant de un valor mig que canvia linealment en el temps, Fig. 6.12. Les fluctuacions permeten que el sistema explori regions fora del mínim i, després, els termes rotacionals (proporcionals a α) actuen. El valor mig es pot calcular a partir de l'expressió (6.35), i aquest *flux sostingut per renou* depèn del camp aplicat i del valor del renou, Fig. 6.13.

Chapter 6

Class A lasers with injected signal: Bifurcation set and Lyapunov–potential function

In this chapter, we describe the bifurcation set for a class A laser with an injected signal in terms of the amplitude and the frequency of the applied field by using the concepts introduced in chapter 3. We explain the dynamical behaviour of this kind of lasers in terms of a Lyapunov potential (chapter 2) in the case where such a description is possible. In particular, a full description for the deterministic and nondeterministic dynamics can be given by using the Lyapunov potential for some particular values of the external parameters. This represents an extension of the work performed in chapter 5 for class A lasers without injection. Depending also on the value of these parameters, the phase of the electric fields drifts also with time in the stochastic case, as it was found in the non–injected laser (section 5.3).

The chapter is organized as follows. In Sec. 6.1, we present the model equations for a class A laser with injected signal used in remaining sections. In Sec. 6.2, the bifurcation set in terms of the amplitude and frequency of the injected signal is determined. While a portion of the lines presented in this bifurcation set can be analytically calculated, the rest of the bifurcation set has been numerically computed. In Sec. 6.3, we describe the laser dynamics in terms of a potential function, valid for the case of a zero–detuning injected signal, and discuss its relevance both in the deterministic and stochastic dynamics.

6.1 Model

We consider a class A laser [Haken, 1985] whose dynamics can be described in terms of the slowly varying complex amplitude E of the electric field (5.1). The physical electric field is given by $\mathcal{E}(t) = [E(t)e^{i\Omega_0 t} + c.c.]/2$. The laser is injected with a monochromatic optical field $E_x e^{i\Omega t}$ of amplitude E_x and frequency Ω. The

resulting evolution equation is [Haken, 1984; van der Graaf, 1997]

$$\dot{E}(t) = (1+i\alpha)\left(\frac{\Gamma}{1+\vartheta|E|^2} - \kappa\right) E + \sigma E_x e^{-i\bar{\eta}t} + \zeta(t), \tag{6.1}$$

where $\bar{\eta} = \Omega_0 - \Omega$ is the detuning between the external field and the free running laser frequency Ω_0. κ, Γ, ϑ and α are (real) intrinsic parameters defined in Sec. 5.1. σ is the injection coupling, proportional to the inverse of the round–trip time τ_{in}. $\zeta(t)$ is a complex Langevin source term accounting for the stochastic nature of spontaneous emission. It is taken as a Gaussian white noise of zero mean and correlations

$$\langle \zeta(t)\zeta^*(t')\rangle = 4\Delta\delta(t-t'), \tag{6.2}$$

where Δ measures the strength of the noise.

By writing the complex variable E as $E = (x_1 + ix_2)e^{-i\bar{\eta}t}$ (i.e. (x_1, x_2) are the real and imaginary parts of the electric field E in the reference system that rotates with frequency $-\bar{\eta}$), and introducing a new dimensionless time $\kappa t \to t$, the evolution equations become

$$\begin{aligned}
\dot{x}_1 &= \left(\frac{a}{b+x_1^2+x_2^2} - 1\right)(x_1 - \alpha x_2) + \rho - \eta x_2 + \xi_1(t)\cos(\eta t) - \xi_2(t)\sin(\eta t), \\
\dot{x}_2 &= \left(\frac{a}{b+x_1^2+x_2^2} - 1\right)(\alpha x_1 + x_2) + \eta x_1 + \xi_1(t)\sin(\eta t) + \xi_2(t)\cos(\eta t),
\end{aligned}$$

where $a = \Gamma/(\kappa\beta)$, $b = 1/\beta$, $\rho = \sigma E_x/\kappa$ and $\eta = \bar{\eta}/\kappa$, and $\zeta(t) = \xi_1(t) + i\xi_2(t)$ introduces real white noise processes, ξ_1 and ξ_2, with zero mean and correlations given by (2.32) with $\epsilon = \Delta/\kappa$. The statistical properties that follow from this set of equations are contained in the Fokker–Planck equation (2.33) for the time evolution of the probability density function [Risken, 1989]. A simpler, yet equivalent set of equations, in the sense that they give rise to the same Fokker–Planck equation, is [Hernández-García *et al.*, 1990]

$$\dot{x}_1 = \left(\frac{a}{b+x_1^2+x_2^2} - 1\right)(x_1 - \alpha x_2) + \rho - \eta x_2 + \xi_1(t), \tag{6.3}$$

$$\dot{x}_2 = \left(\frac{a}{b+x_1^2+x_2^2} - 1\right)(\alpha x_1 + x_2) + \eta x_1 + \xi_2(t). \tag{6.4}$$

These equations can be written in terms of the intensity I and phase ϕ, by making the change of variables $x_1 = \sqrt{I}\cos(\phi)$ and $x_2 = \sqrt{I}\sin(\phi)$,

$$\frac{dI}{dt} = 2\left[\frac{a}{b+I} - 1\right] I + 2\rho\sqrt{I}\cos(\phi) + 2\sqrt{I}\,\xi_I(t), \tag{6.5}$$

$$\frac{d\phi}{dt} = \alpha\left[\frac{a}{b+I} - 1\right] - \frac{\rho}{\sqrt{I}}\sin(\phi) + \eta + \frac{1}{\sqrt{I}}\,\xi_\phi(t), \tag{6.6}$$

where $\xi_I(t)$ and $\xi_\theta(t)$ are white noise processes of mean zero and correlations (2.32). The multiplicative terms of these equations have to be understood in the Stratonovich sense [Risken, 1989].

In the next sections, the system of equations (6.3 – 6.4) is studied. For convenience, we will switch between the descriptions (6.3 – 6.4) and (6.5 – 6.6) whenever it simplifies the discussion.

6.2 Bifurcation set

We consider throughout this section the deterministic version of Eqs. (6.3) and (6.4), i.e. the case $\epsilon = 0$. It is easy to observe that any trajectory remains bounded in the (x_1, x_2) plane. This comes from the asymptotic form of Eq. (6.5) in the limit $I \to \infty$, namely $\dot{I} = -2I$, which shows that trajectories with a large intensity I are restored towards the origin. Consequently, the only asymptotic behaviour of Eqs. (6.3 – 6.4) can be either a fixed point or a periodic orbit. As Eqs. (6.3 – 6.4) are written in the reference frame that rotates with frequency $-\eta$, a fixed point solution represents a situation in which the frequency of the laser electric field E equals that of the injected field. We are interested in finding the *locking range*, i.e. the set of parameters (ρ, η) for the injected field such that there exist *stable* fixed point solutions, also called *locking* solutions.

6.2.1 The fixed point solutions

The intensity I_s and phase ϕ_s of the fixed points are found by setting $\dot{I} = \dot{\phi} = 0$ in (6.5 – 6.6). The resulting equations can be rewritten as

$$\rho^2 = I_s \left[\frac{a}{b + I_s} - 1\right]^2 (1 + \alpha^2) + 2\alpha\eta I_s \left[\frac{a}{b + I_s} - 1\right] + I_s\eta^2, \tag{6.7}$$

$$\eta = \frac{\rho}{\sqrt{I_s}}\sqrt{1 + \alpha^2}\sin(\phi_s + \arctan(\alpha)). \tag{6.8}$$

We consider henceforth the case $a > b$ (corresponding to the lasing mode of operation $\Gamma > \kappa$). For given (ρ, η), the third degree–polynomial equation (6.7) can have either one or three real (always nonnegative) solutions for the intensity I_s, see Fig. 6.1. Particularly, in the case $\rho = 0$, the two fixed solutions for the intensity suffer a transcritical bifurcation, Fig. 3.2, at $a = b$. By multiplying Eq. (6.7) by $(1 + \alpha^2)$, one gets

$$\frac{\rho^2(1 + \alpha^2)}{I_s} = \left[\left(\frac{a}{b + I_s} - 1\right)(1 + \alpha^2) + \eta\alpha\right]^2 + \eta^2. \tag{6.9}$$

From this equation, it is straightforward to show that for any point of those solutions the condition

$$|\eta| \leq \frac{\rho}{\sqrt{I_s}}\sqrt{1 + \alpha^2} \tag{6.10}$$

is always satisfied, hence ensuring that there will be the corresponding solution for ϕ_s obtained from Eq. (6.8).

The lines separating the one fixed point solution region from the three fixed point solutions region can be found by using standard methods of algebra. These lines form the so–called *saddle–node* curve (solid line in Figs. 6.2 (a), 6.2 (b) and 6.3).

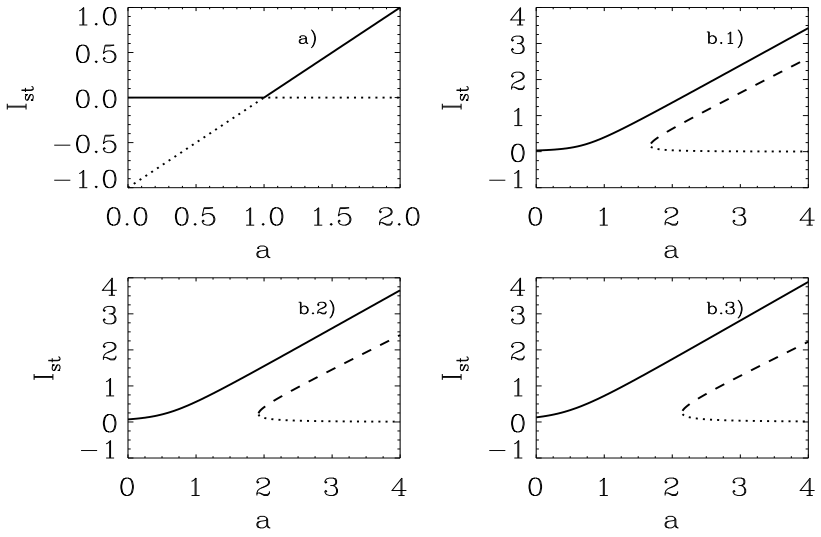

Figure 6.1: Fixed points for the intensity for a class A laser with injected signal, Eq. (6.7), versus a. Solid line: stable fixed point, dashed line: saddle point, dotted line: unstable point. $\alpha = 2$. $b = 1$. (a) $\rho = 0$, (b.1) $\rho = 0.4$, (b.2) $\rho = 0.6$, (b.3) $\rho = 0.8$.

It turns out that the three fixed points region is a connected set enclosing region labelled 2, 3, 4, 5, 8, 10 shown in Fig. 6.2 (a) for a typical case $a = 2$, $b = 1$, $\alpha = 2$. In regions 1, 6, 7, 9 only one fixed point exists. For moderate values of the intensity ρ, there is a range of values for the frequency $\eta \in (\eta_1, \eta_2)$ for which three fixed points exist, whereas for very large intensity, only one fixed point exists for all values of η. A similar scenario occurs for $\alpha = 0$, see Fig. 6.3 where the three fixed points region is labelled as 5, and only one fixed point appears in regions 1, 7, 9.

6.2.2 The periodic orbit solutions

At the saddle–node curve, a saddle point and another fixed point merge and disappear. In some cases this gives rise to a periodic orbit through an Andronov–Leontovich bifurcation. Near the bifurcation, it is possible to obtain approximately the evolution equation for the angle variable $\phi(t)$ by assuming that the intensity of the periodic orbit is constant. This approximation, which can be obtained via perturbation theory on the laser equations to lowest order [Zimmermann *et al.*, 2001], is derived here heuristically by neglecting fluctuations in the intensity, setting $\dot{I} = 0$ in Eq. (6.5), but allowing for a time dependent phase in Eq. (6.6) for ϕ. Setting $I = I_o$ constant in Eq. (6.5) and replacing in Eq. (6.6) we obtain

$$\dot{\phi} = \eta - \frac{\rho\sqrt{1+\alpha^2}}{\sqrt{I_o}} \sin(\phi + \arctan(\alpha)). \tag{6.11}$$

The next approximation is to consider that I_o is the intensity of the field at the nearest point (ρ, η) in the saddle–node curve with the same value of the external field amplitude ρ. Hence, I_o is computed as the double root of Eq. (6.7) taking the adequate value $\eta = \eta_1$ or $\eta = \eta_2$.

Eq. (6.11) is known as Adler's equation [Adler, 1946] and it can be easily analyzed by writing it as

$$\dot{\phi} = -\frac{dU}{d\phi}, \tag{6.12}$$

using the potential function

$$U(\psi) = -\eta_L \cos(\phi + \arctan(\alpha)) - \eta\phi, \tag{6.13}$$

where we have introduced

$$\eta_L = \frac{\rho\sqrt{(1+\alpha^2}}{\sqrt{I_o}}. \tag{6.14}$$

The dynamics of ϕ can be explained in terms of relaxation in the potential U. For $|\eta| < \eta_L$ the potential has local minima and the phase eventually stops in one of them. This is a fixed point solution which has been discussed in the previous subsection. A periodic orbit solution is obtained only in the case $|\eta| \geq \eta_L$ where the phase ϕ varies monotonically with time. The explicit solution is

$$\phi(t) = 2\arctan\left[\frac{\eta_{ef}}{\eta}\tan\left(\frac{\eta_{ef}}{2}t\right) + \frac{\eta_L}{\eta}\right] - \arctan(\alpha) - \eta t, \tag{6.15}$$

where $\eta_{ef} = \sqrt{\eta^2 - \eta_L^2}$.

Therefore, within this approximation, the line separating a fixed point from a periodic orbit solution is given by $|\eta| = \eta_L$. Notice that our derivation of this relation is different from the usual one in which one derives it by demanding that Eq. (6.10) is satisfied. We have shown that Eq. (6.10) is indeed satisfied for all values of η and ρ and that the condition $|\eta| = \eta_L$ determining the locking range is an approximated one. By using Eq. (6.7) this condition can be rewritten as

$$\rho = |\eta|\sqrt{\frac{a}{1+\alpha^2-\alpha\eta} - \frac{b}{1+\alpha^2}}. \tag{6.16}$$

The range of validity of this approximation has to be checked numerically. In Fig. 6.2 (c) we compare the exact result with the approximate one in the typical case $a = 2$, $b = 1$, $\alpha = 2$. It can be seen that the approximation is quite good for small values of ρ but it worsens as the intensity ρ is increased.

When crossing the saddle–node curve, for example crossing from region 9 or 1 to region 5 in Fig. 6.2 (a), the periodic orbit disappears. As a precursor of this disappearance, the period of the periodic orbit, T, grows in regions 1, 9 until it finally diverges at the saddle–node curve. The divergence can be fitted, for a fixed value of η to the law $T \sim (\rho_r - \rho)^{-1/2}$ [Strogatz, 1994], being ρ_r the value of ρ where the bifurcation occurs, see Fig. 6.4.

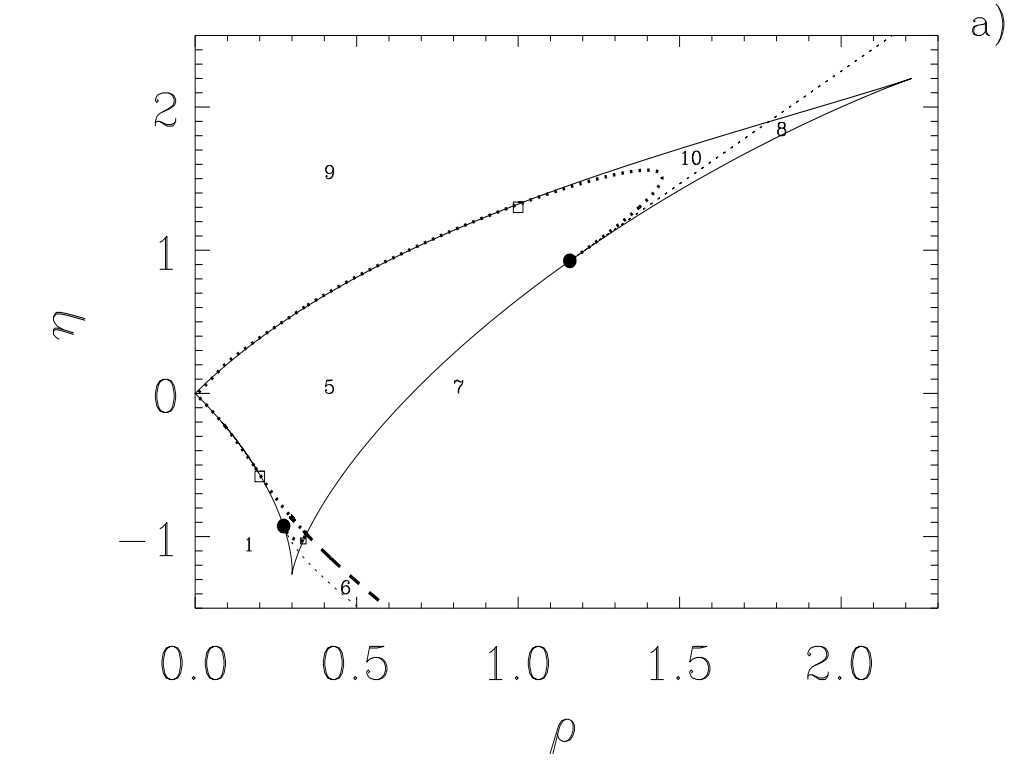
a)
2
1
0
−1
η
9
10
8
5
7
1
6
0.0
0.5
1.0
1.5
2.0
ρ

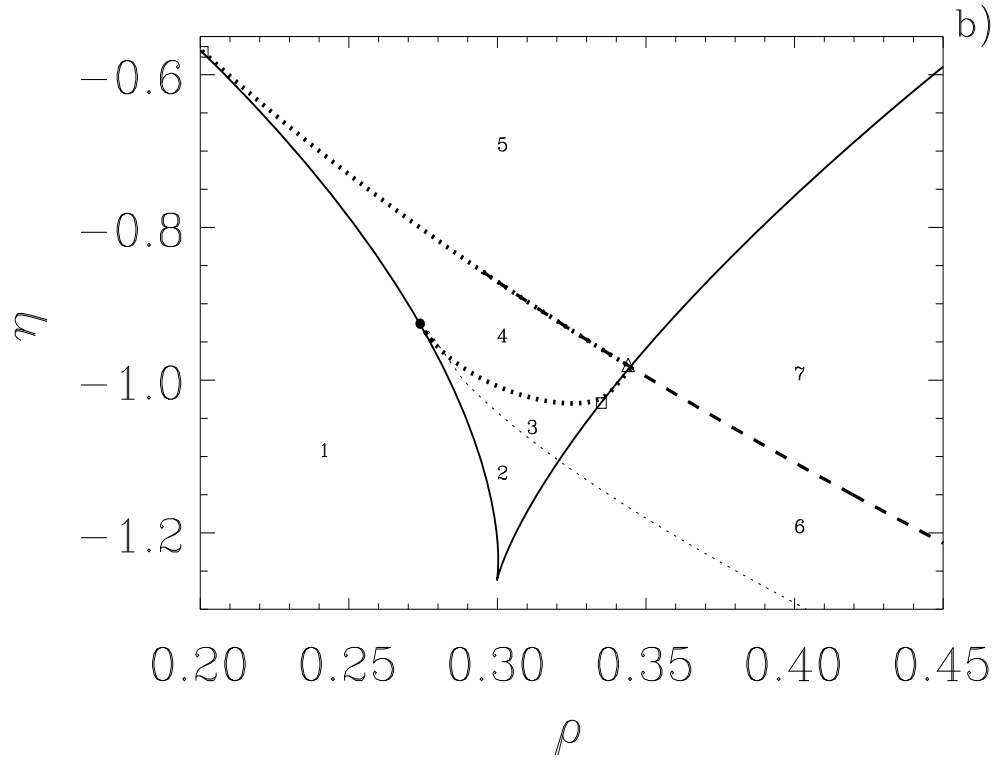
b)
−0.6
−0.8
−1.0
−1.2
η
5
4
7
3
1
2
6
0.20
0.25
0.30
0.35
0.40
0.45
ρ

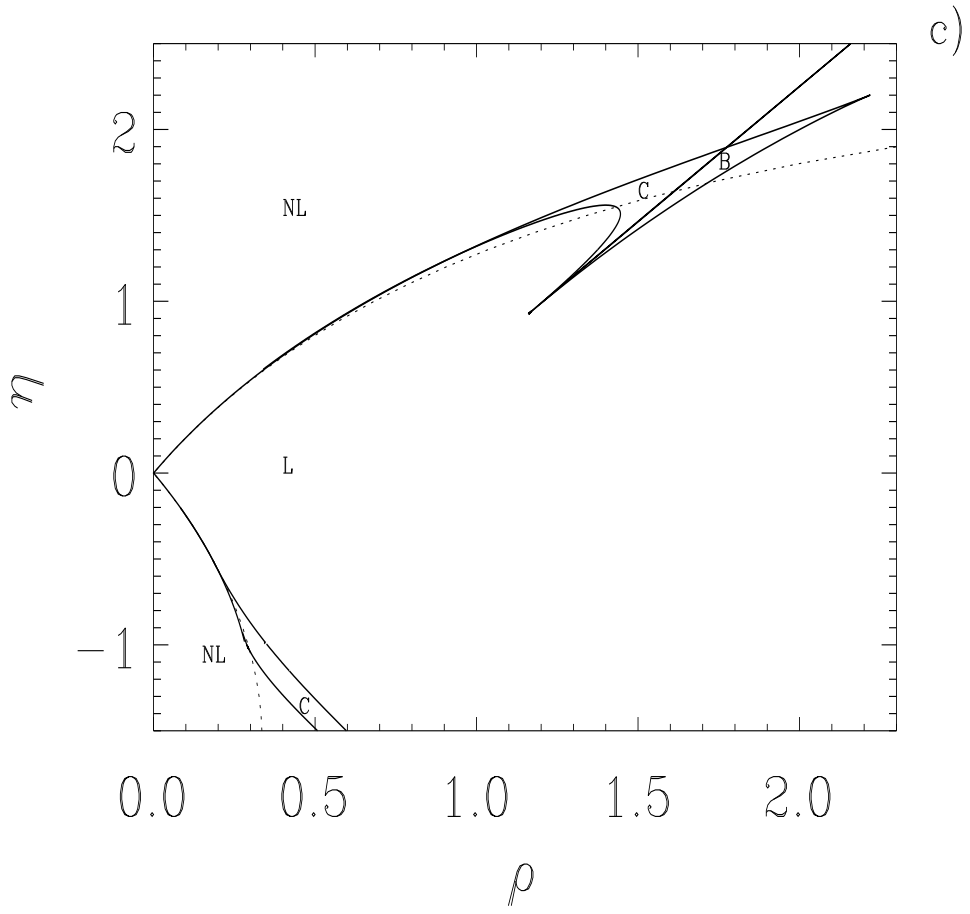

Figure 6.2: Bifurcation set for a class A laser with an injected signal for $a = 2$, $b = 1$ and $\alpha = 2$. In (a) and (b) the solid line is the saddle–node curve separating regions 1, 6, 7, 9 with one fixed point solution from regions 2, 3, 4, 5, 8, 10 with three fixed point solutions; the short–dashed lines separating the pairs of regions $8 - 10$, $2 - 3$, $7 - 9$ and $1 - 6$, are Hopf bifurcation, as given by Eq. (6.20), where a periodic orbit is created; the dotted lines are homoclinic bifurcation where the periodic orbits of regions 4 and 10 disappear when going to region 5, and one periodic orbit in 3 disappears when going to region 4; the coincidence of the curve of homoclinic orbits with the saddle–node curve mark the existence of Andronov–Leontovich bifurcation where the periodic orbit of 9 and 1 disappears when crossing to 5; the long–dashed line is a saddle–node bifurcation of periodic orbits and going from 7 to 6 two periodic orbits of different stability are created; the two big solid dots are Takens–Bogdanov points. There also exist homoclinic saddle–node codimension–2 points, in the intersection between the saddle-node curves and the homoclinic orbits (squares and triangle). In (c) we indicate the different regions of stability: in L, one fixed point is the stable solution; in NL, one periodic orbit is the stable solution; in C there is coexistence of a stable fixed point and a periodic orbit; finally, in B there are two stable fixed points. The dotted line is the approximate locking range given by Eq. (6.16).

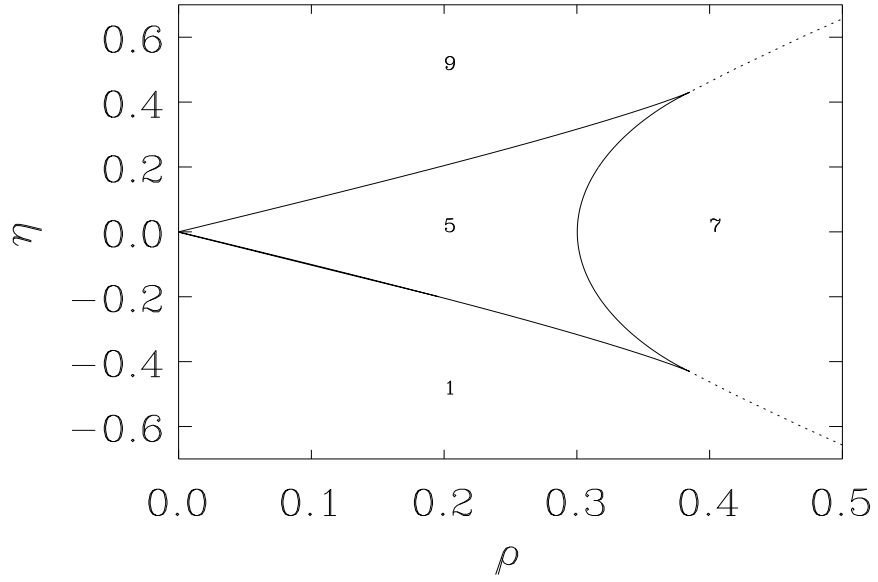

Figure 6.3: Bifurcation set for a class A laser with an injected signal for $a = 2$, $b = 1$ and $\alpha = 0$. The solid line is the saddle–node curve separating regions 1, 7, 9 with one fixed point solution from region 5 with three fixed point solutions. The dotted lines separating the pairs of regions $7-9$ and $7-1$, are Hopf bifurcation, as given by Eq. (6.20), where a periodic orbit is created. The locking range is formed by regions 5, 7 where a single fixed point is the only stable solution. In 1 and 9 the stable solution is a periodic orbit.

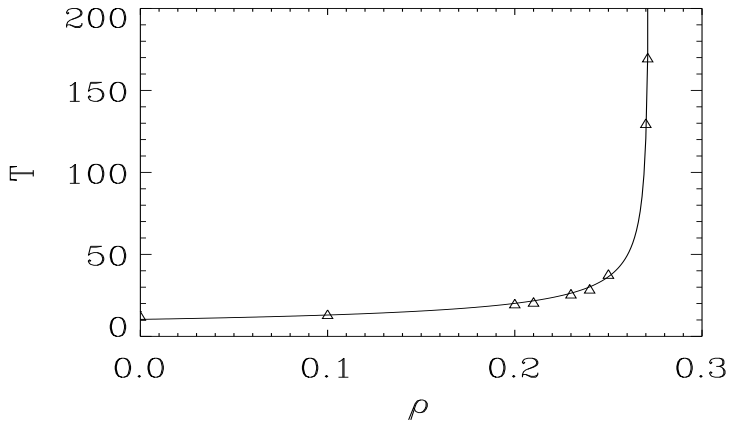

Figure 6.4: Period of the stable periodic orbit of region 9 of diagram of Fig. 6.2 versus ρ. $\eta = 0.5$ (diamonds). Solid line: $5.4/\sqrt{\rho_r - \rho}$, with $\rho_r = 0.272$.

6.2.3 Unfolding the bifurcation set

In the following we will perform the stability analysis of the different fixed points and the periodic orbit solutions. The fixed points for I are given by (6.7) and an equation that can have either one or three real roots depending on ρ and η. The stability of these fixed points defines the different regions of interest. Stability properties can be established in terms of the eigenvalues of the linearization matrix (Jacobian) of Eqs. (6.3 – 6.4) at the fixed points, see chapter 3. The local bifurcation takes place when the real part of some eigenvalue crosses zero.

The results of the stability analysis depend on the value of the parameter α. For $\alpha = 0$, the only possibility is to have regions in which either a stable fixed point or a stable periodic orbit exist, see Fig. 6.3. However, for $\alpha > 0$ a much richer behaviour appears. We summarize the results for the typical case $a = 2$, $b = 1$, $\alpha = 2$ shown in Fig. 6.2: In regions 5, 7 there exists only one locking (stable fixed point) solution. In region 8 there exist two locking solutions with different intensity. In regions 1, 2, 9 there exists one stable periodic orbit solution. Finally, in regions 3, 4, 6 and 10 one locking solution coexists with a stable periodic orbit solution. While some of the lines of this bifurcation set shown in Fig. 6.2 can be evaluated analytically, others have to be obtained numerically. We now give details of the calculations of those lines.

6.2.3.a Saddle–node bifurcation

A saddle–node bifurcation occurs when two fixed points are created/annihilated. The saddle–node curve separates, in this case, a region with one fixed point from another with three fixed points. On the saddle–node curve, two fixed points coincide (or equivalently, one of the eigenvalues of the Jacobian is zero). From another point of view, the saddle–node bifurcation curve can be obtained as the lines in the (ρ, η) plane in which the third degree equation (6.7) has a double root. In this case, the equation for the fixed points can be written in the form

$$\mu(I - I_1)(I - I_2)^2 = 0. \tag{6.17}$$

Comparing this expression with the one for the fixed points (6.7) and equating the different orders of I, a system of equations is obtained

$$\left[\begin{array}{rcl} \mu & = & (1+\alpha^2) - 2\alpha\eta + \eta^2, \\ -\mu(I_1 + 2I_2) & = & -2\alpha\eta b + 2b\eta^2 - 2(1+\alpha^)(a-b) + 2\alpha\eta(a-b) - \rho^2, \\ \mu(I_2^2 + 2I_1I_2) & = & (a-b)^2(1+\alpha^2) + 2\alpha\eta b(a-b) + b^2\eta^2 - 2b\rho^2, \\ \mu I_1 I_2^2 & = & b^2\rho^2. \end{array}\right. \tag{6.18}$$

From this system, the variables μ, I_1 and I_2 can be obtained, and an expression that relates ρ to η can be found. The resulting saddle–node bifurcation curve is indicated by a solid line in Figs. 6.2 (a), 6.2 (b) and 6.3.

6.2.3.b Hopf bifurcation

In a Hopf bifurcation of a two–dimensional system such as ours, a fixed point changes its stability (from stable to unstable, or vice versa) and a periodic orbit with opposite stability to the coexistent fixed point is born/disappears. At the bifurcation point, the eigenvalues of the Jacobian matrix J associated to the deterministic system (6.3) and (6.4) [or equivalently and somewhat easier (6.5) and (6.6)] are complex conjugated and pure imaginary. This condition can be written as $Tr(J) = 0$, $Det(J) > 0$. Hence,

$$(b + I)(a - b - I) - aI = 0. \tag{6.19}$$

This equation combined with the one for the fixed points (6.7) leads to the Hopf bifurcation curve,

$$\eta^2 + 2\alpha\eta\left(\sqrt{\frac{a}{b}} - 1\right) + \left(\sqrt{\frac{a}{b}} - 1\right)^2 (1 + \alpha^2) = \frac{\rho^2}{-b + \sqrt{ba}}, \tag{6.20}$$

also shown in Fig. 6.2 (a), 6.2 (b) (short–dashed line). From regions 8 to 10, 7 to 9, 1 to 6 and from 2 to 3 a periodic orbit is born and a fixed point changes its stability. The disappearance of those periodic orbits will be explained in the following subsections.

6.2.3.c Takens–Bogdanov singularities

At the points (ρ_{Hs}, η_{Hs}) where the Hopf and the saddle–node bifurcation curves intersect the eigenvalues of the Jacobian matrix are strictly equal to zero. This condition gives

$$\eta_{Hs} = \pm\left(\sqrt{\frac{a}{b}} - 1\right)\sqrt{1 + \alpha^2}, \tag{6.21}$$

$$\rho_{Hs} = \sqrt{2b\left(\sqrt{\frac{a}{b}} - 1\right)^3 \sqrt{1 + \alpha^2}(\sqrt{1 + \alpha^2} \pm \alpha)}. \tag{6.22}$$

For the parameters considered in Fig. 6.2 ($a = 2$, $b = 1$ and $\alpha = 2$), it is $(\rho_{Hs}, \eta_{Hs}) = (0.274, -0.926)$ and $(\rho_{Hs}, \eta_{Hs}) = (1.160, 0.926)$. At these intersection points, the Jacobian matrix is different from zero, and its normal form is

$$\begin{pmatrix} 0 & 1 \\ 0 & 0 \end{pmatrix}. \tag{6.23}$$

These points correspond to Takens–Bogdanov singularities [Kuznetsov, 1997]. At these intersection points, indicated in the figure, a homoclinic orbit is also born. These orbits have been found numerically and they are discussed in the next subsection.

6.2.3.d Homoclinic orbits

When (some branch of) the stable and unstable manifolds of a saddle point coincide we are in the presence of a homoclinic orbit. Homoclinic orbits have been obtained numerically using the program AUTO97 [Doedel *et al.*, 1997] as the "infinite-period limit" of periodic orbits. The resulting curves of homoclinic orbits are displayed as dotted lines in Fig. 6.2 (a), 6.2 (b). Their location in parameter space coincides partially with the saddle–node curve.

The intersections of the saddle–node curve and a homoclinic bifurcation occur at codimension–2 points. There exist intersection homoclinic saddle–node codimension–2 points (SH) at each of the saddle–node branches, see Fig. 6.2 and 6.6. The bifurcation structure near to these points was described in [Schecter, 1987]. Note that the location of these codimension–2 points cannot be completely exact due to the fact that the homoclinic orbits are obtained numerically (considering an orbit of large period but not infinite). The bifurcation branch emerging from these points with coincidence of the curve of homoclinic orbits with the saddle–node curve is an Andronov–Leontovich bifurcation.

6.2.3.e Saddle–node of periodic orbits

Besides the bifurcation curves described so far, there exists yet another curve of saddle–node bifurcations of periodic orbits. This is indicated by the the long–dashed curve in Fig. 6.2 (a), 6.2 (b) which has been obtained also numerically. When crossing this curve, the two periodic orbits of region 6 disappear. The point were the saddle–node of periodic orbits, the homoclinic and the neutral saddle curve intersect is a codimension–2 point, labelled as F, in Fig. 6.6. This point is not found exactly at Fig. 6.2 (b) due to numerical evaluation. The presence of this point gives rise to a small region, labelled as 11, where two periodic orbits, and three fixed points exist, see Fig. 6.6 and 6.7. For $\omega \approx -5$ [not shown in the scale of Fig. 6.2 (a)] the Hopf bifurcation and the saddle–node of periodic orbits collide and regions 1 and 7 are directly separated by the Hopf bifurcation.

6.2.3.f Different regions separated by the bifurcation set

We summarize in Table 6.1 the results of the previous subsections concerning the different regions separated by the bifurcation lines. In Fig. 6.5, the phase portrait of different regions is shown, namely regions $3 - 4 - 5 - 6$. In the first line, from left to right the transition from region 4 to 5 is shown. In the first column, one can observe the transition form region 4 to 3 through an homoclinic orbit. The transition from region 3 to 6, as a saddle–node bifurcation, appears in the last line. In the diagonal [Figs. 6.5 (a), 6.5 (e) and 6.5 (i)] one can observe the transition through an Andronov bifurcation. The saddle–node of periodic orbits is reflected in Fig. 6.5 (f). In Fig. 6.7, appears the phase portraits in region 11.

Many of the bifurcation features found in this system are present in other studies, as in the book by Kuznetsov [Kuznetsov, 1997] where a bifurcation diagram

topologically equivalent to ours is displayed in connection with the analysis of a predator–prey model by Bazykin.

These results allow us to identify the stability regions indicated in Fig. 6.2 (c): in **L**, one fixed point is the only stable solution; in **NL**, one periodic orbit is the only stable solution; in **C** there is coexistence of a stable fixed point and a periodic orbit; finally, in **B** there are two stable fixed points.

Table 6.1: Different regions in the bifurcation set for a class A laser with injected signal. We use the notation: f.p. = fixed point, p.o. = periodic orbit, St. = stable and Unst. = unstable.

$1 \rightarrow$	1 f.p. Unst., 1 p.o. St.
$2 \rightarrow$	2 f.p. Unst., 1 f.p. Saddle, 1. p.o. St.
$3 \rightarrow$	1 f.p. Unst., 1 f.p. Saddle, 1 f.p. St., 1 p.o. St., 1 p.o. Unst.
$4 \rightarrow$	1 f.p. Unst., 1 f.p. Saddle, 1 f.p. St., 1 p.o St.
$5 \rightarrow$	1 f.p. Unst., 1 f.p. Saddle, 1 f.p. St.
$6 \rightarrow$	1 f.p. St., 1 p.o. St., 1 p.o. Unst.
$7 \rightarrow$	1 f.p. St.
$8 \rightarrow$	2 f.p. St., 1 f.p. Saddle
$9 \rightarrow$	1 f.p. Unst., 1 p.o. St.
$10 \rightarrow$	1 f.p. Unst., 1 f.p. Saddle, 1 f.p. St., 1 p.o. St.
$11 \rightarrow$	1 f.p. Unst., 1 f.p. Saddle, 1 f.p. St., 1 p.o. St., 1 p.o. Unst.

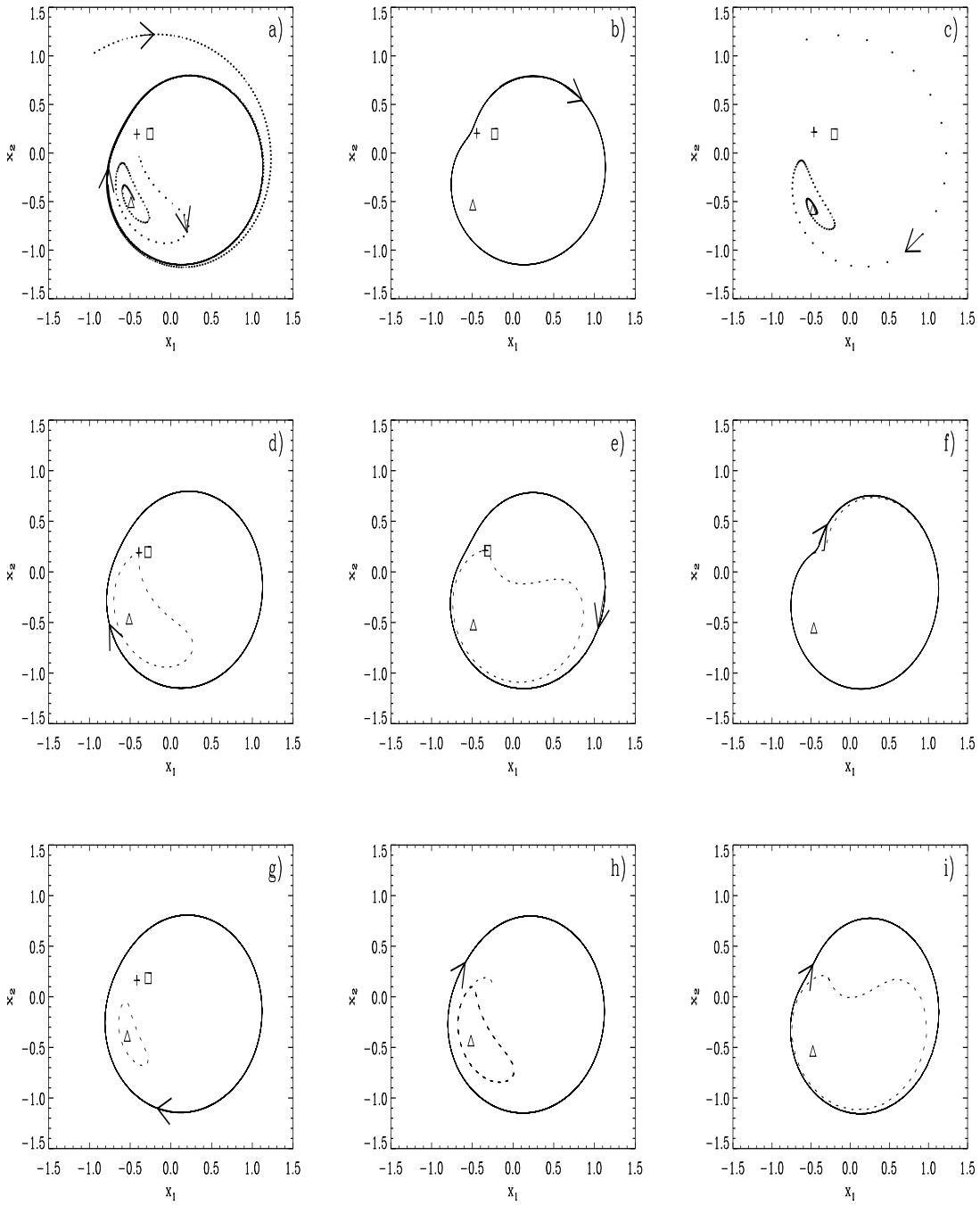

Figure 6.5: Phase portraits in different regions. Triangle: stable fixed point, square: unstable fixed point, cross: saddle point. Solid line: stable orbit, dashed line: unstable orbit. Points: trajectories. (a) Region 4: $(\rho, \eta) = (0.33, -1)$; (b) Near homoclinic $4-5$: $(\rho, \eta) = (0.33, -0.95)$; (c) Region 5: $(\rho, \eta) = (0.33, -0.9)$; (d) Close to homoclinic $3-4$: $(\rho, \eta) = (0.33, -1.03)$; (e) Close to Andronov bifurcation $4-6$: $(\rho, \eta) = (0.34, -1)$; (f) Close to the saddle–node of periodic orbits $6-7$: $(\rho, \eta) = (0.352, -1)$; (g) Region 3: $(\rho, \eta) = (0.33, -1.05)$; (h) Close to the saddle–node $3-6$: $(\rho, \eta) = (0.33, -1.065,)$; (i) Region 6: $(\rho, \eta) = (0.345, -1)$.

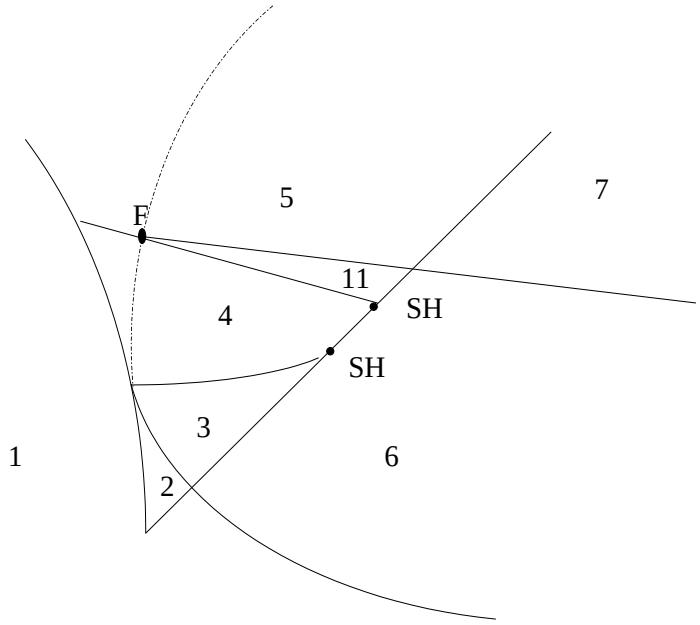

Figure 6.6: Sketch of the partial bifurcation set for a class A laser with injected signal. Different regions and intersection points detailed in Fig. 6.2 and Table 6.1. SH: homoclinic saddle–node codimension–2 points. F: intersection of the saddle–node bifurcation of periodic orbits, the homoclinic orbit and the continuation of the Hopf bifurcation (dotted line, which is not a bifurcation).

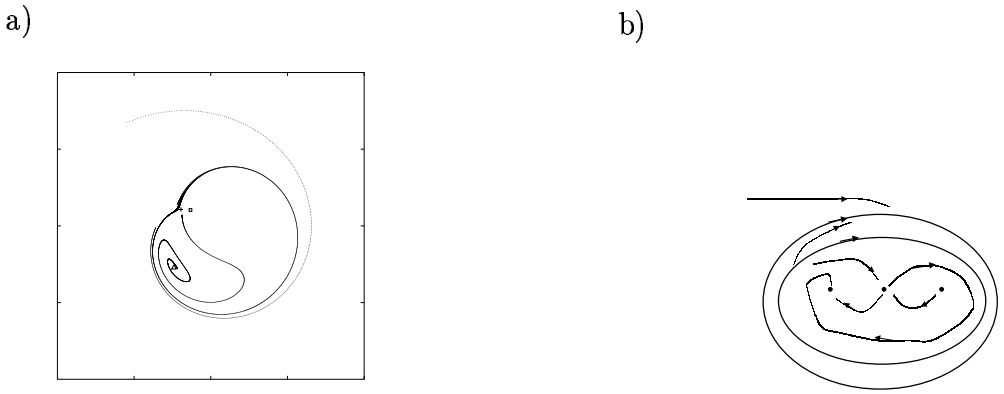

Figure 6.7: Phase portrait at region 11 of the bifurcation set. a) $(\rho, \omega) = (0.34, -0.9713)$, Triangle: stable fixed point, square: unstable fixed point, cross: saddle point. b) Sketch of the phase portrait: arrows indicate the sense of the flow.

6.3 Lyapunov potential

We now look for a description of the dynamical equations in terms of a Lyapunov potential, see Sec. 2.2. Equations (6.3) and (6.4) can be written as

$$\dot{x_i} = -\sum_{j=1}^{2} D_{ij}\frac{\partial V}{\partial x_j} + v_i + \sum_{j=1}^{2} g_{ij}\xi_j, \qquad i = 1, 2, \tag{6.24}$$

where the function V is [Haken, 1983]

$$V(x_1, x_2) = \frac{1}{2}\left[x_1^2 + x_2^2 - a\ln(b + x_1^2 + x_2^2)\right] - \frac{\rho}{(1+\alpha^2)}(x_1 - \alpha x_2), \tag{6.25}$$

or, written in terms of intensity and phase,

$$V(I, \phi) = \frac{1}{2}\left[I - a\ \ln(b + I)\right] - \frac{\rho\sqrt{I}}{\sqrt{1+\alpha^2}}\cos\left(\phi + \arctan\alpha\right). \tag{6.26}$$

The matrices D and g, and the vector $\mathbf{v}$ are

$$D = S + A = \begin{pmatrix} 1 & 0 \\ 0 & 1 \end{pmatrix} + \begin{pmatrix} 0 & -\alpha \\ \alpha & 0 \end{pmatrix}, \quad g = \begin{pmatrix} 1 & 0 \\ 0 & 1 \end{pmatrix}, \quad \mathbf{v} = \begin{pmatrix} -\eta x_2 \\ \eta x_1 \end{pmatrix}. \tag{6.27}$$

6.3.1 Deterministic Dynamics

In the deterministic dynamics ($\epsilon = 0$), Eqs. (6.24) show that $V(x_1, x_2)$ is a Lyapunov potential, i.e. a function that monotonically decreases along trajectories, $\dot{V} \leq 0$, provided that the *residual terms* (v_1, v_2) satisfy the *orthogonality condition* (2.30)

$$v_1\frac{\partial V}{\partial x_1} + v_2\frac{\partial V}{\partial x_2} = 0. \tag{6.28}$$

It turns out that this orthogonality condition is satisfied if $\eta\rho = 0$. This means that a Lyapunov function description of the dynamics using (6.25) is valid along the coordinate axis $\eta = 0$ and $\rho = 0$. Notice that the case $\rho = 0$, $\eta \neq 0$ corresponds to a situation in which there is no applied field but the reference system rotates at an arbitrary frequency η.

The equation for the intensity (6.7) can have one or three (positive) real roots depending on the parameters. In Fig. 6.8, the stationary solutions are plotted for a case in which $a > b$. The stability of these solutions follows immediately from the analysis in terms of the potential and it is described in the figure caption. The value at which the saddle and unstable solutions disappear corresponds to the saddle–node bifurcation value for $\eta = 0$ (see Fig. 6.2).

In the transient dynamics towards the stationary states, the combined effects of S and A produce in general a spiral–like trajectory in the (x_1, x_2) plane. The angular velocity of this movement is proportional to α. Finally, the residual term (v_1, v_2) induces a movement which does not decrease the value of the potential and

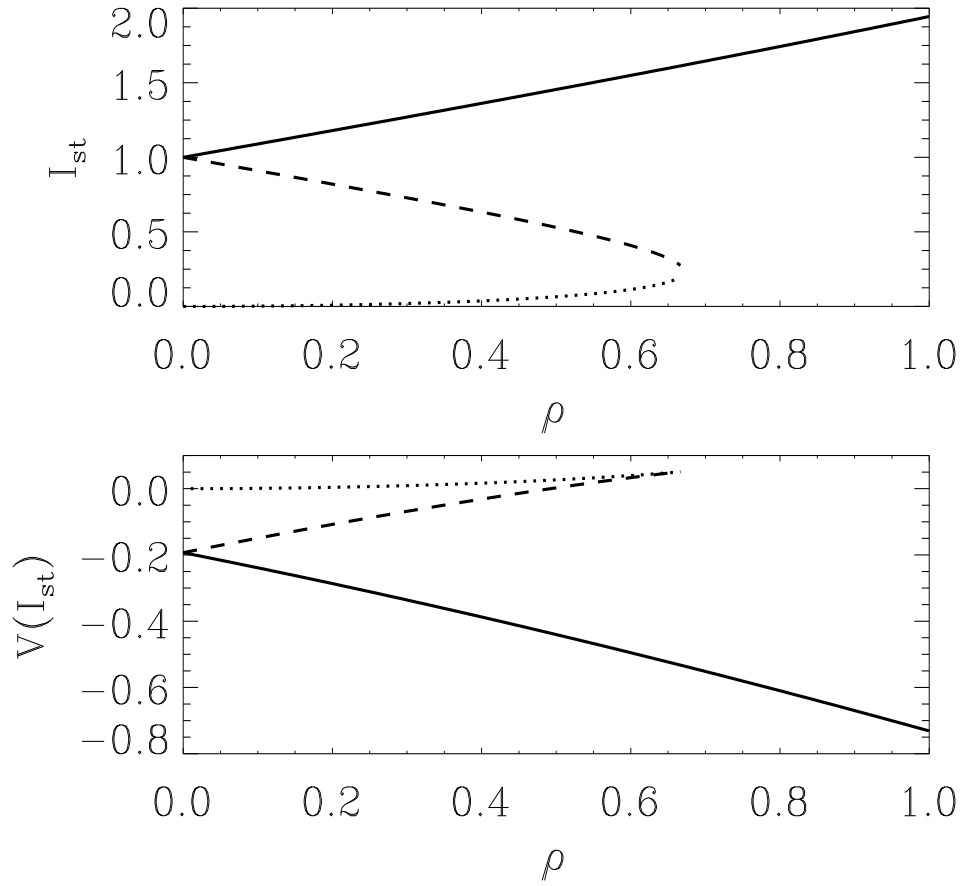

Figure 6.8: Upper figure: Fixed points of Eq. (6.7) versus ρ. Lower figure: Value of the potential, Eq. (6.25), evaluated at the different fixed points versus ρ. $\eta = 0$. $a = 2$, $b = 1$ and $\alpha = 2$. Dimensionless units.

it is responsible for any dynamics after the line of minima of the potential has been reached. We now analyze the different possibilities for the extrema of V.

In the case $\rho = 0$, the potential function was given in chapter 5. The potential does not depend on the phase ϕ of the electric field and it can adopt two qualitatively different shapes:
(i) For $a < b$ the potential has a single minimum at $x_1 = x_2 = 0$ and no maxima. Therefore, the only fixed point is the *off* state $I = 0$, which is stable.
(ii) For $a > b$, the potential has the shape of a *Mexican hat*, see Fig. 6.9 (a). The residual dynamics $\dot{x}_i = v_i$ gives a periodic harmonic movement in the minima of the potential with frequency η. This corresponds to the periodic orbits represented in Fig. 6.2.

In the case of zero–detuning injected signal, i.e. $\rho > 0$, $\eta = 0$, the potential,

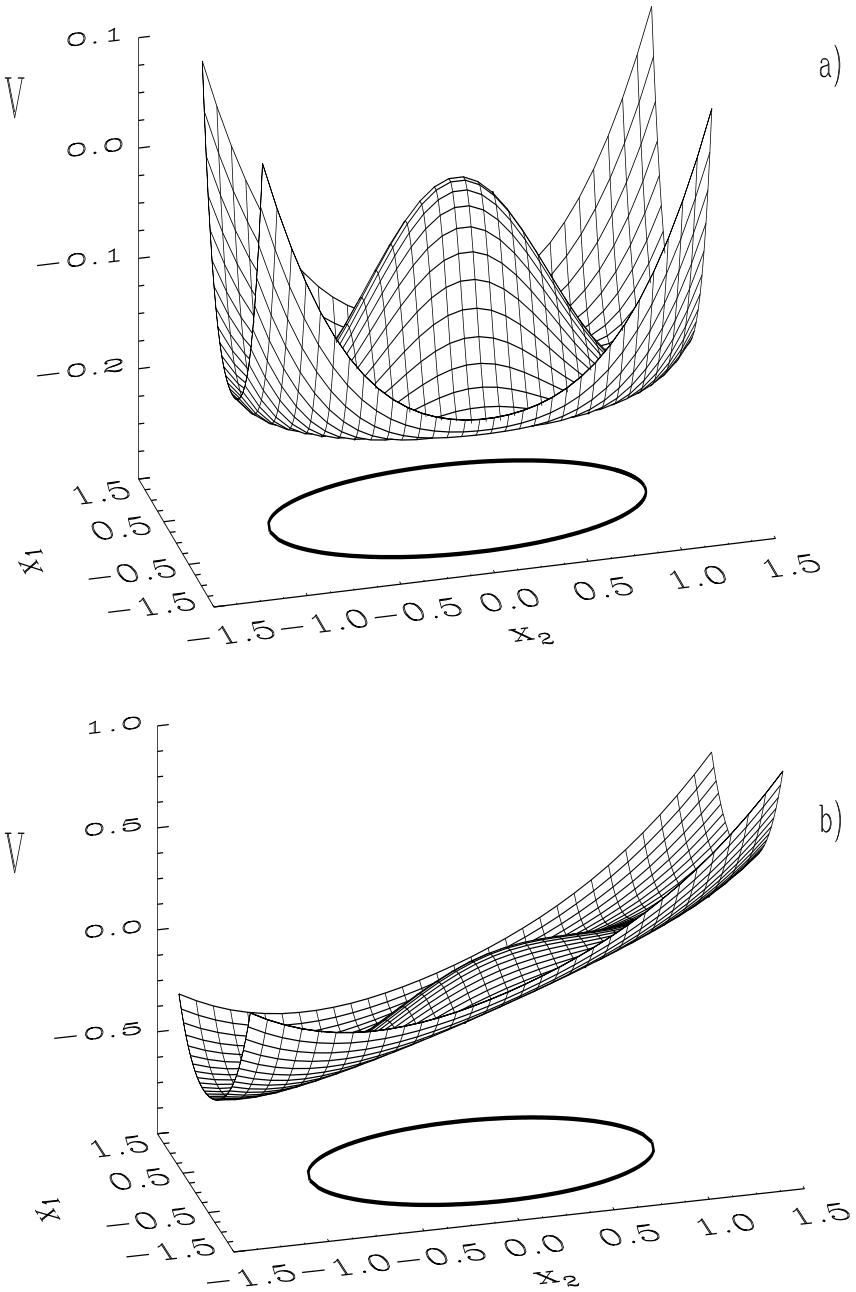

Figure 6.9: Potential for a class A laser with an injected signal with the same frequency of the unperturbed laser, Eq. (6.25), with the parameters $a = 2$, $b = 1$, $\alpha = 2$. Dimensionless units. (a) $\rho = 0$, (b) $\rho = 0.8$. In (a) we also indicate the projection of the line of minima of V and the corresponding line is plotted in (b).

which depends now explicitly on the phase ϕ, is tilted in a preferred direction. In the case $a < b$ the location of the minimum changes and the asymptotic state has a nonzero light intensity, that is proportional to ρ. In the case $a > b$, the Mexican hat is tilted as well in a preferred direction. For small ρ the inclination is small and the effect is that the maximum still remains a maximum, although its location varies slightly. The tilt breaks the symmetry amongst the line of degenerate minima and an absolute minimum is selected. At the same time, one of the previous minima becomes a maximum in the direction orthogonal to the tilt and a saddle point is born. Increasing ρ, the maximum of the Mexican hat and the saddle point disappear (corresponding to the saddle–node curve of figure 6.2) and the potential has only one minimum at a preferred phase direction, see Fig. 6.9 (b). Therefore, the asymptotically stable situation, in this case of $\rho > 0$, $\eta = 0$ and $a > b$ is that the laser switches to an *on* state with a well defined intensity and phase, in agreement with the results shown in Fig. 6.2.

It is an open question the validity of a Lyapunov potential description in the general case, $\rho\eta \neq 0$, and we have not been able to find an analytical expression for the potential V in this general case. However, since we do not expect qualitative changes in the dynamical features near the coordinate axis, we speculate that a Lyapunov potential description continues to be valid, at least for small values of $\eta\rho$.

Assuming the validity of this Lyapunov potential description we can understand the transition from locking to non–locking states. Let us consider a given value of $\rho > 0$ and increase the detuning frequency starting from $\eta = 0$. For $\eta = 0$, the potential is tilted and there are no residual terms, see Fig. 6.9 (b). As η increases, the shape of the potential deforms, the minimum of the potential and the saddle point approach through the deterministic circumference of minima of the system without optical injection, $\rho = 0$ (region 5 of Fig. 6.2). Moreover, the residual terms, proportional to η increase, but they are not big enough to overcome the tilt of the potential and to induce a rotation movement. For a value of η (corresponding to the saddle–node bifurcation) these two points (minimum and saddle) collapse and a periodic motion appear induced by the residual terms (corresponding to region 9 of Fig. 6.2).

Similarly, starting at a point $\eta > 0$ and increasing the intensity of the applied fields, ρ, a similar scenario appears. For $\rho = 0$, the potential has a line of degenerate minima, $I = a - b$, and trajectories are circumferences in the (x_1, x_2) plane induced by the residual terms. Increasing ρ, the line of minima deviate from the circumference due to the change of shape of the potential and it becomes an ellipse, the periodic orbit solution is also induced by the residual terms of the dynamics, which are proportional to η. In fact, it can be shown that the solution in the steady state for very small values of ρ has the form

$$I(t) = \frac{\mathcal{A}}{1 + \rho\sqrt{\mathcal{D}^2 + \mathcal{F}^2}\sin(\phi(t) + \gamma_1)}, \tag{6.29}$$

which represents an ellipse with a time dependent phase. This dependence is of the form

$$\phi(t) = \eta t - \rho\sqrt{\mathcal{B}^2 + \mathcal{C}^2}\sin(\phi(t) + \gamma_2). \tag{6.30}$$

The values of $\mathcal{A}$, $\mathcal{B}$, $\mathcal{C}$, $\mathcal{D}$, $\mathcal{E}$ have been obtained by using equations (6.5) and (6.6) and small values of ρ. The resulting expressions are

$$\begin{aligned}
\mathcal{A} &= a-b, \\
\mathcal{B} &= -\frac{[4(a-b)^2+\eta^2a^2+2\alpha a\eta(a-b)]}{\eta\sqrt{a-b}[4(a-b)^2+\eta^2a^2]}, \\
\mathcal{C} &= -4\frac{\alpha}{\eta}\frac{(a-b)^{3/2}}{[4(a-b)^2+\eta^2a^2]}, \\
\mathcal{D} &= \frac{4a\sqrt{a-b}}{4(a-b)^2+\eta^2a^2}, \\
\mathcal{F} &= \frac{2\sqrt{a-b}a^2\eta}{4(a-b)^3+\eta^2a^2(a-b)}, \\
\gamma_1 &= \arctan(-\mathcal{D}/\mathcal{F}), \\
\gamma_2 &= \arctan(-\mathcal{B}/\mathcal{C}).
\end{aligned} \tag{6.31}$$

Increasing ρ even further, the potential deforms continuously until arriving to the saddle–node bifurcation.

6.3.2 Stochastic effects

In the presence of low–to–moderate levels of noise, $\epsilon > 0$, the qualitative features of the transient dynamics remain the same as in the deterministic case. The most important differences appear near the stationary situation and show up as fluctuations of the intensity and phase of the electric field. While the intensity simply oscillates around its mean value, one can observe in some cases an additional phase drift which shows up as a variation in the frequency of the emitted light. The potential picture developed in the previous section helps us to understand the origin of this noise–induced frequency shift, as well as to compute its magnitude.

Let us look at the potentials depicted in Fig. 6.9. First consider the case $\rho = 0$. The deterministic movement is such that the line of minima (shown as a projection in the (x_1, x_2) plane) is ran at a constant frequency η. On top of that movement there are fluctuations which allow frequent excursions beyond the minima of the potential V. Away from the minima, the antisymmetric part of the dynamics (governed by the matrix A in equation (6.27) and proportional to α) gives a nonzero contribution of the rotation terms producing the observed phase drift. For $\eta = 0$, $\rho \neq 0$, when only one minimum of the potential exists, the fluctuations make the system to explore regions outside this minimum allowing the rotation terms to act again, see Fig. 6.10. Depending on the value of ρ and ϵ the rotation term can be strong enough to produce the phase flow.

After these qualitative arguments, we now turn to a more quantitative calculation. In those cases in which a Lyapunov potential $V(x_1, x_2)$ exists and the matrices D and g of (6.24) satisfy the fluctuation–dissipation relation (2.35), the stationary probability distribution is given by equation (2.38). This relation is exact if the

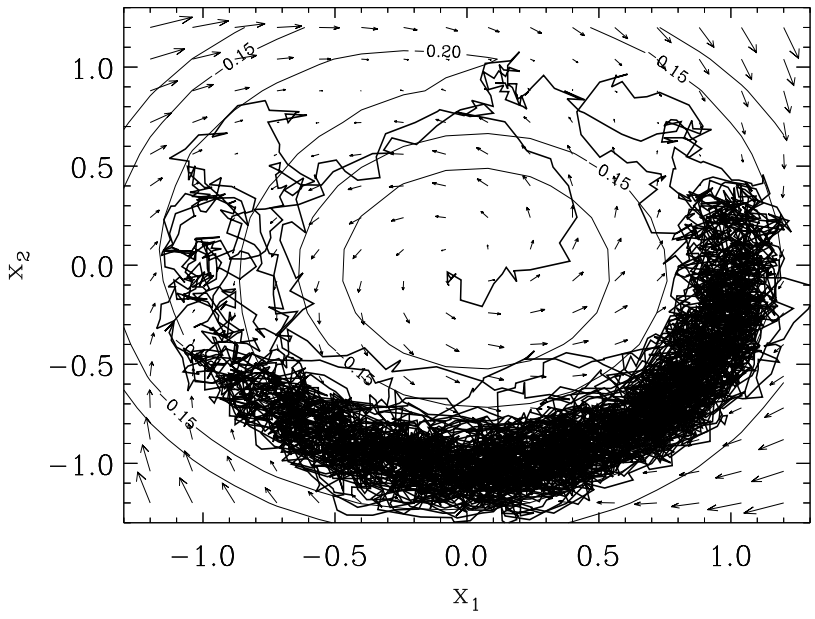

Figure 6.10: Vector field for a class A lasers with injected signal. Thick solid line: simulation of Eqs. (6.3) and (6.4). Thin lines are the equipotential curves of Eq. (6.25) and the arrows indicate the sense of the flow. Parameters: $a = 2$, $b = 1$, $\alpha = 2$, $\eta = 0$, $\rho = 0.05$. $\epsilon = 0.01$. Initial conditions: $x_1 = 0$, $x_2 = 0$. Dimensionless units.

residual terms $\mathbf{v}$ satisfy the orthogonality condition (6.28) and if they are divergence–free (2.37) (as they are in our case). In other cases, it has to be understood as an approximation valid in the limit of small noise $\epsilon \to 0$.

By changing variables to intensity and phase, we find that the probability density function is

$$P_{st}(I,\phi) = Z^{-1}\, e^{-I/2\epsilon}\, (b+I)^{a/2\epsilon}\, \exp\left(\frac{\rho\sqrt{I}}{\epsilon\sqrt{1+\alpha^2}}\cos(\phi+\arctan(\alpha))\right), \qquad (6.32)$$

and the marginal probability density function for I is

$$P_{st}(I) = Z^{-1} e^{-I/2\epsilon}(b+I)^{a/2\epsilon}\, \mathcal{I}_0\left(\frac{\rho\sqrt{I}}{\epsilon\sqrt{1+\alpha^2}}\right), \qquad (6.33)$$

where $\mathcal{I}_0$ is the Bessel function of the first kind and order 0. Expression (6.33) reduces to (5.17) for $\rho = 0$.

The maximum of the probability density function, I_m, is given by

$$b + I_m = a + \frac{(b+I_m)\rho}{\sqrt{I_m}\sqrt{1+\alpha^2}}\frac{\mathcal{I}_1(\bar{\rho})}{\mathcal{I}_0(\bar{\rho})}, \qquad (6.34)$$

where $\bar{\rho} \equiv \rho\sqrt{I_m}/(\epsilon\sqrt{1+\alpha^2})$ and $\mathcal{I}_1$ is the Bessel function of the first kind and order 1. For $\epsilon = 0$, deterministic case, $\mathcal{I}_1(\bar{\rho})/\mathcal{I}_0(\bar{\rho}) = 1$ and the equation is reduced to (6.7) with $\eta = 0$.

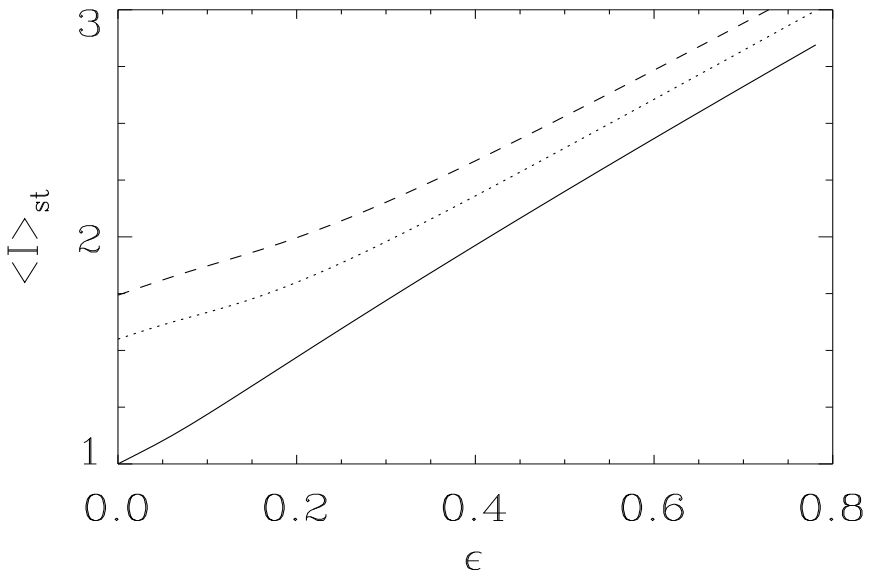

Figure 6.11: Mean value of the intensity in the steady state in a class A laser with zero–detuning ($\eta = 0$) injected signal for $a = 2$, $b = 1$ and $\alpha = 2$. The solid line corresponds to $\rho = 0$ and has been computed using the analytical result Eq. (5.19), the dotted line ($\rho = 0.6$) and the dashed line ($\rho = 0.8$) have been computed numerically using Eq. (6.33).

The steady state average value for the intensity $\langle I \rangle_{st} = \int dI\, I P_{st}(I)$ can be analytically computed in the case $\rho = 0$ with the result (5.19). In the most general case, for $\rho \neq 0$, the mean value can be computed numerically by using (6.33). In Fig. 6.11, this mean value is plotted versus ϵ, for fixed value of ρ. The mean value is always larger than the deterministic ($\epsilon = 0$) case.

As mentioned before, in the steady state of the stochastic dynamics, the phase of the electric field ϕ fluctuates around a mean value that changes linearly with time. This is clearly seen in the numerical simulations (see Fig. 6.12) and it physically corresponds to a change $\Delta\omega$ in the emission frequency of the laser.

This frequency shift can be computed as the average value of the phase derivative $\langle \dot{\phi} \rangle$. In the case that the steady state is a periodic orbit of period T, one needs to subtract from this value the intrinsic frequency $2\pi/T$. By taking the average value of Eq. (6.6) and using the rules of the stochastic calculus, one arrives to

$$\Delta\omega = Z^{-1}\alpha \int_0^\infty e^{-I/2\epsilon}(b+I)^{a/2\epsilon}\left[\frac{(a-b-I)}{b+I} I_o\left(\frac{\rho\sqrt{I}}{\epsilon\sqrt{1+\alpha^2}}\right) + \sqrt{I}\, I_1\left(\frac{\rho\sqrt{I}}{\epsilon\sqrt{1+\alpha^2}}\right)\right] dI. \tag{6.35}$$

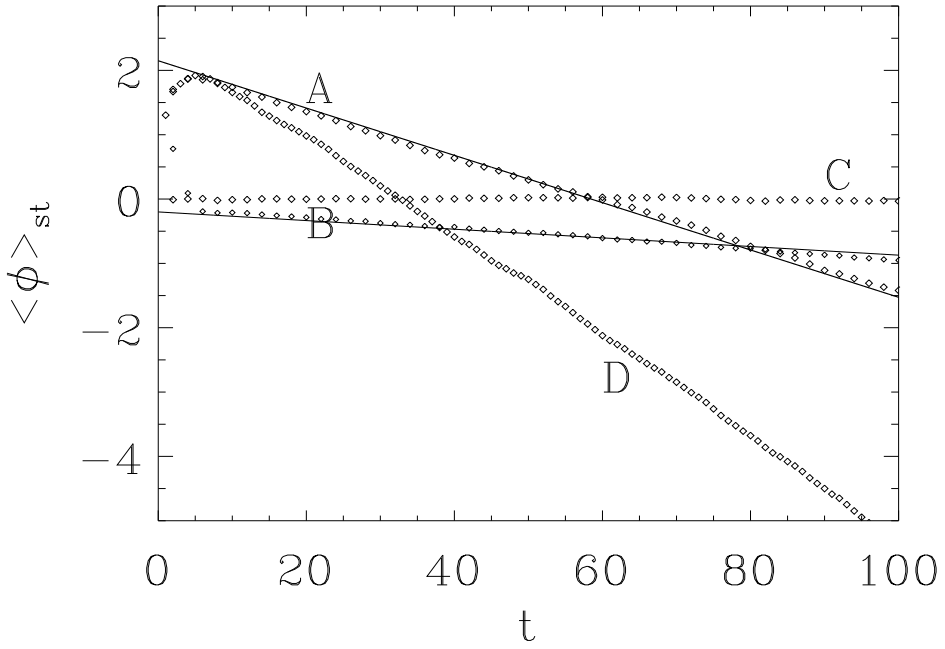

Figure 6.12: Time evolution of the mean value of the phase ϕ in a class A laser without injected signal $\rho = 0$ (line A) and zero–detuning injected signal $\rho = 0.6$, $\eta = 0$ (line B), in the case $\alpha = 2$ there is a linear variation of the mean value of the phase at late times. For $\alpha = 0$ (line C) there is only phase diffusion and the average value is 0 for all times. The solid lines have the slope given by the theoretical prediction Eq. (6.35). Line D: time evolution of $< \phi >_{st} -2\pi t/T$, being T the period of the periodic orbit in the deterministic case, for $\rho = 0.5$, $\eta = 1$. In all the curves: $a = 2$, $b = 1$ and $\epsilon = 0.1$.

Notice that this stochastic frequency shift is zero in the case $\alpha = 0$ or for the deterministic dynamics ($\epsilon = 0$). In the case $\rho = 0$ this expression analytically reduces to (5.23).

For $\rho \neq 0$, one needs to evaluate the expression (6.35) numerically. In all cases, the results are in excellent agreement with numerical simulations of the rate equations in the presence of noise. In Fig. 6.13, we plot the stochastic frequency shift as a function of the noise intensity for several values of ρ. For a fixed value of ρ, $|\Delta\omega|$ increases as ϵ increases, since a larger value of ϵ can induce larger fluctuations and larger excursions in phase space (x_1, x_2) away from the minima of the potential. For fixed ϵ, $|\Delta\omega|$ decreases as ρ increases. This result can be understood by noticing that when ρ is increased, the inclination of the potential increases and the trajectory becomes more confined around a fixed value.

In the case $\rho \neq 0$ and $\eta \neq 0$, the stochastic frequency shift is also present, see Fig. 6.12 (line D), although it is not possible to compute its magnitude because we do not have an explicit expression for the Lyapunov potential.

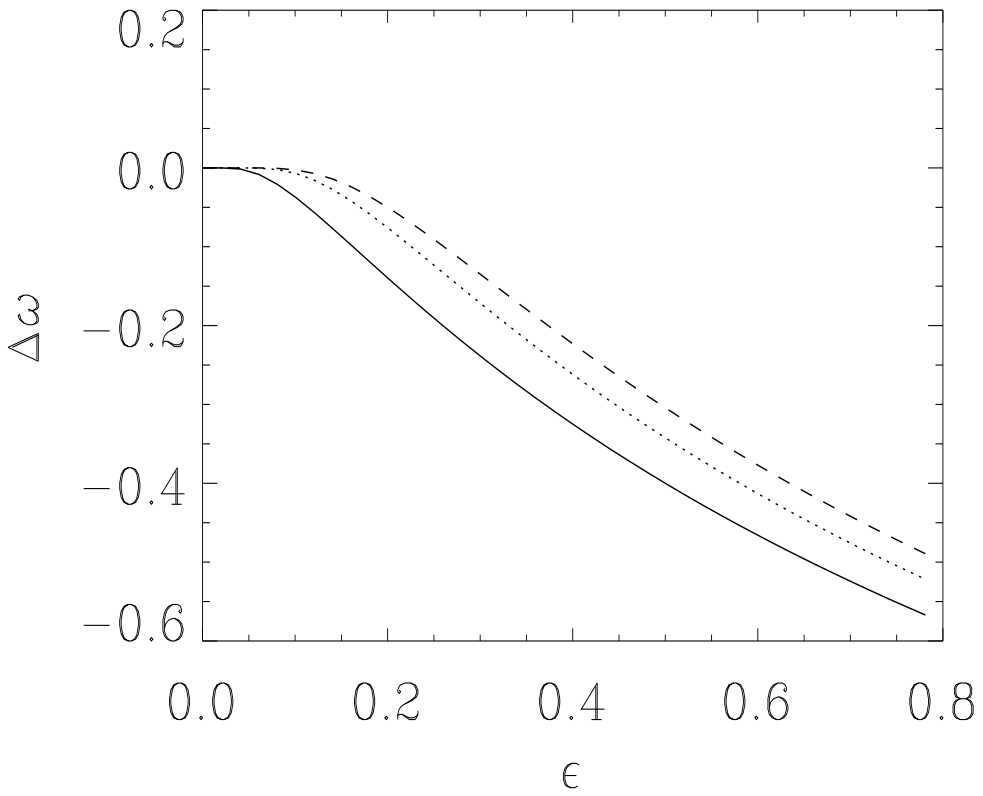

Figure 6.13: Stochastic frequency shift $\Delta\omega \equiv \langle\dot{\phi}\rangle$ in a class A laser for $a = 2$, $b = 1$ and $\alpha = 2$. For $\rho = 0$ (solid line) the explicit result Eq. (5.23) is used, whereas for $\rho = 0.6$ (dotted line) and $\rho = 0.8$ (dashed line) (6.35) has been numerically evaluated.